https://www.mdc-berlin.de/de/veroeffentlichungstypen/clinical-journal-club

Als gemeinsame Einrichtung von MDC und Charité fördert das Experimental and Clinical Research Center die Zusammenarbeit zwischen Grundlagenwissenschaftlern und klinischen Forschern. Hier werden neue Ansätze für Diagnose, Prävention und Therapie von Herz-Kreislauf- und Stoffwechselerkrankungen, Krebs sowie neurologischen Erkrankungen entwickelt und zeitnah am Patienten eingesetzt. Sie sind eingeladen, uns beizutreten. Bewerben Sie sich!

spherules

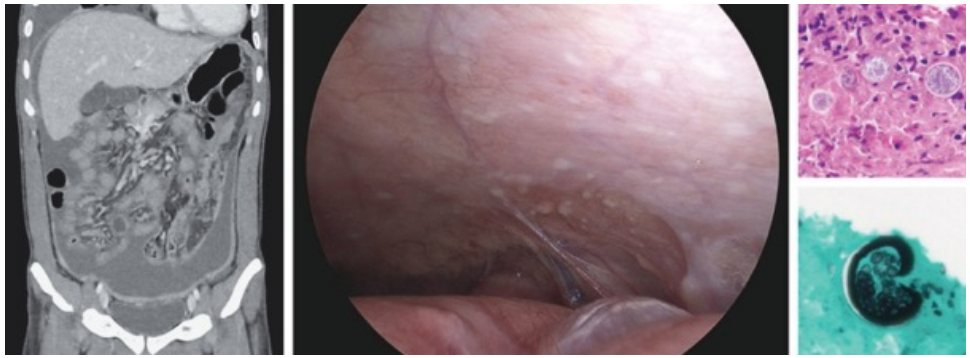

A 23-year-old man presented to the emergency department with a 2-month history of unintentional weight loss and worsening abdominal pain and distension. The patient had recently moved to Arizona from a remote Pacific Island. Physical examination was notable for a firm abdomen with diffuse tenderness to palpation. A diagnostic laparoscopy revealed peritoneal nodules and inflammatory adhesions. A peritoneal biopsy and computed tomography of the chest, abdomen, and pelvis are shown. Which of the following is the most likely etiology of the peritoneal nodules?

Carcinomatosis from intraabdominal malignancy

Coccidioidomycosis

Mesothelioma

Sarcoidosis

Tuberculosis

Histopathological analysis of the peritoneal biopsy showed necrotizing granulomas with large, thick-walled spherules, and a fungal culture of peritoneal tissue grew coccidioides. A diagnosis of peritoneal coccidioidomycosis was made. Treatment with a prolonged course of fluconazole was initiated. At 1-month follow-up after discharge, the patient's symptoms had resolved.

IgA nephropathy (IgAN) wird durch die Ansammlung veränderter Immunglobuline vom Typ A1 (IgA1) verursacht, denen die normalen Zucker-/Galaktosepartikel fehlen. Dieses IgA1 mit Galaktosemangel kann „klebriger“ sein als normales IgA1 und kommt im Blut bei IgAN häufig in Paaren, Dreiergruppen oder sogar Aggregaten vor. Dies allein kann ausreichen, um Ablagerungen und Entzündungen in Glomeruli zu verursachen, wie viele Tierstämme mit IgA-Überproduktion zeigen, die eine IgAN-ähnliche Krankheit entwickeln. Darüber hinaus wird IgA ohne Galaktose als „fremd“ angesehen, und der Körper produziert Anti-körper gegen defektes IgA (Anti-IgA-Auto-antikörper). Diese Antikörper binden sich an die veränderten IgA1-Proteine und bilden Immunkomplexe, die sich in den Glomeruli – genauer gesagt im Mesangium – ansammeln.

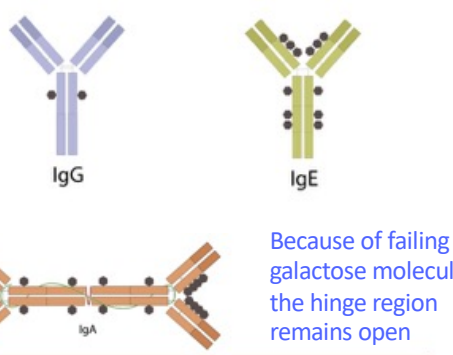

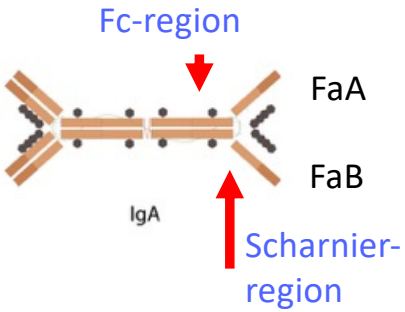

Infektionen der oberen Atemwege (Mund, Nase, Rachen und Kehlkopf) oder des Magen-Darm-Trakts führen zu einer erhöhten Produktion von IgA, einschließlich defektem IgA, das sich ansammelt und die Bildung von Autoantikörpern erhöhen kann, was zu IgA-IgA und IgA-IgG Immunkomplexen führt, die sich im Mesangium ablagern. Dies erklärt, warum Infektionsepisoden die Symptome von IgAN verschlimmern können.

Die **Galaktosylierung** ist ein entscheidender Prozess in der Glykosylierung von Antikörpern, insbesondere bei **Immunglobulin G (IgG)**. Dabei wird der Zuckerbaustein **Galaktose** an die Kohlenhydratketten im Fc-Teil (dem konstanten Teil) des Antikörpers angehängt.

Warum ist das wichtig?
Die Galaktosylierung fungiert als molekularer "Schalter", der die Effektorfunktionen des Immunsystems steuert:

- **Entzündungshemmung:** Ein hoher Galaktosylierungsgrad korreliert oft mit einem **anti-inflammatorischen** (entzündungshemmenden) Zustand. In der Schwangerschaft steigt beispielsweise die Galaktosylierung von IgG stark an, was Entzündungsschübe bei Krankheiten wie rheumatoider Arthritis lindern kann.
- **Immunaktivierung:** Eine Abnahme der Galaktose (Agalaktosylierung, "G0"-Glykane) führt hingegen zu einem **pro-inflammatorischen** Milieu und wird häufig bei chronisch-entzündlichen Erkrankungen beobachtet.
- **Zerstörung von Zielzellen:** Die Galaktosylierung beeinflusst die Bindungsstärke an Fc-Rezeptoren auf Immunzellen. Dies verstärkt die **antikörperabhängige zellvermittelte Zytotoxizität (ADCC)** und die Phagozytose (Fressen von Fremdkörpern).

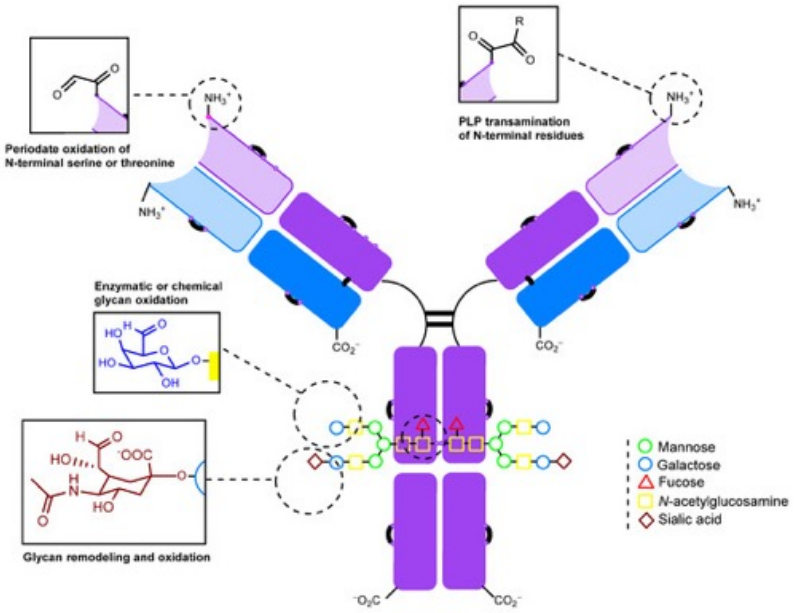

Die IgA-Nephropathie (IgAN, Morbus Berger) ist eine chronische Autoimmunerkrankung, bei der sich Immunglobulin A-Ablagerungen in den Nierenkörperchen (Glomeruli) festsetzen, Entzündungen verursachen und die Filterfunktion stören. Sie ist die weltweit häufigste Glomerulonephritis, tritt oft zwischen 20 und 30 Jahren auf und führt über Jahre zu Blut/Eiweiß im Urin. 25-30% der Betroffenen entwickeln eine terminale Niereninsuffizienz.

Wichtige Aspekte der IgA-Nephropathie:

- **Symptome & Diagnose:** Oft symptomlos, wird sie häufig zufällig durch Urinuntersuchungen (rotes Blutbild, Eiweiß) entdeckt. Typisch sind wiederkehrende Makro- oder Mikrohämaturie (sichtbares oder mikroskopisches Blut im Urin), oft nach Infekten der Schleimhäute (Atemwege, Darm). Diagnose erfolgt durch Nierenbiopsie.
- **Verlauf:** Die Erkrankung verläuft oft langsam schleichend, kann aber bei einigen Patienten zu einem raschen Funktionsverlust führen. Symptome im fortgeschrittenen Stadium sind Bluthochdruck, Ödeme (Wassereinlagerungen) und Niereninsuffizienz.
- **Ursachen:** Ursprung ist vermutlich eine Fehlregulation des Immunsystems, häufig ausgehend vom Darm, bei der sich bestimmte IgA-Immunkomplexe in der Niere ablagern.
- **Behandlung:** Das Ziel ist die Verlangsamung des Fortschreitens. Therapieoptionen umfassen eine optimierte Blutdruckeinstellung (ACE-Hemmer, Sartane), gegebenenfalls Kortikosteroide oder andere Immunsuppressiva.
- **Prognose:** Bei vielen Patienten ist der Verlauf über Jahrzehnte gutartig, jedoch benötigen ca. 25–30 % der Betroffenen innerhalb von 20–25 Jahren eine Dialyse oder Nierentransplantation.

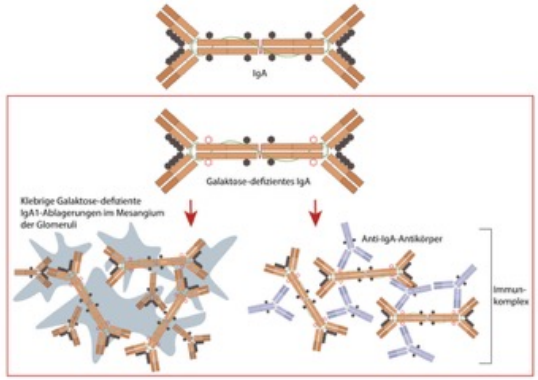

Galaktose-defizient (Gd)

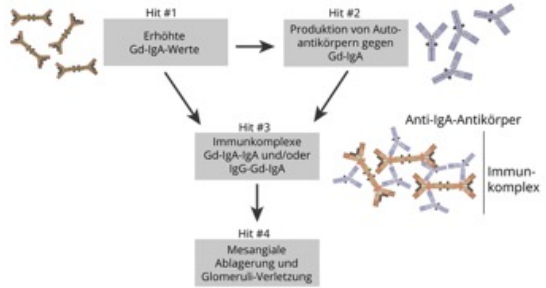

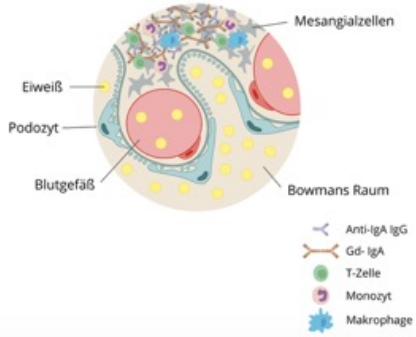

Der **A Proliferation-Inducing Ligand (APRIL)**, auch bekannt als **TNFSF13** oder **CD256**, ist ein körpereigenes Zytokin aus der Tumornekrosefaktor-Superfamilie. Es spielt eine zentrale Rolle bei der Steuerung des Immunsystems und dem Überleben bestimmter Zellen.

Biologische Funktion

- **B-Zell-Entwicklung:** APRIL ist entscheidend für das Überleben von **Plasmazellen** (antikörperproduzierende Zellen) im Knochenmark und in der Schleimhaut.
- **Antikörper-Klassenwechsel:** Es fördert den Wechsel von B-Zellen zur Produktion von **Immunglobulin A (IgA)**, was besonders für die Immunabwehr an Schleimhäuten (Darm, Atemwege) wichtig ist.
- **Zellwachstum:** Wie der Name sagt, kann es die **Vermehrung** (Proliferation) von Zellen anregen – ursprünglich wurde es für seine Fähigkeit entdeckt, das Wachstum von Tumorzellen zu stimulieren.

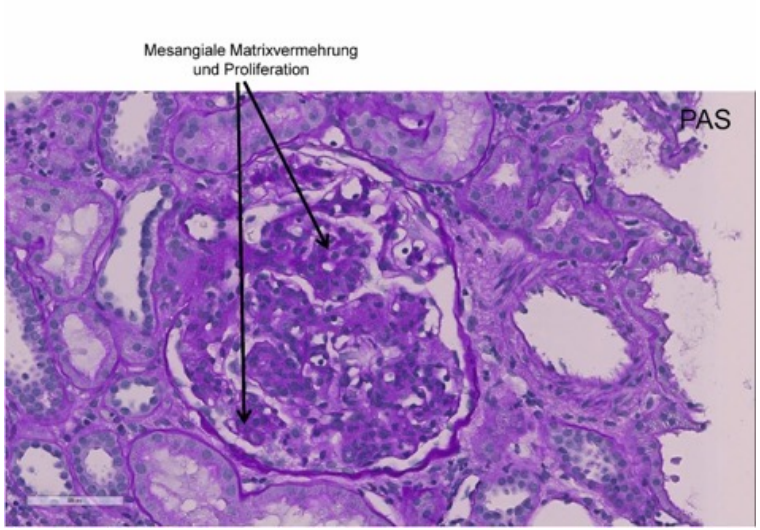

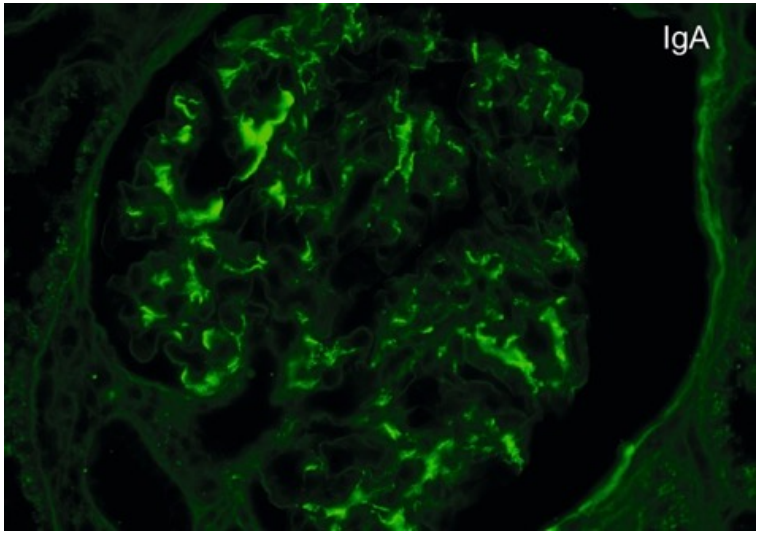

Sibeprenlimab in IgA Nephropathy — Interim Analysis of a Phase 3 Trial

The cytokine A proliferation-inducing ligand (APRIL) is considered a key driver of the pathogenesis of IgA nephropathy. Sibeprenlimab, a humanized IgG2 monoclonal antibody, selectively binds to and inhibits APRIL.

In this phase 3, multicenter, double-blind, randomized, placebo-controlled trial, we assigned adults with biopsy-confirmed IgA nephropathy in a 1:1 ratio to receive either subcutaneous sibeprenlimab at a dose of 400 mg or placebo administered every 4 weeks for 100 weeks. The primary end point for this interim analysis was the 24-hour urinary protein-to-creatinine ratio at 9 months as compared with baseline. The key secondary end point, to be reported at trial completion, is the annualized slope of estimated glomerular filtration rate over 24 months. Other secondary end points included the change in the level of serum immunoglobulin and safety. Exploratory end points included the change in galactose-deficient IgA1 and APRIL concentrations, the spot 24-hour urinary protein-to-creatinine ratio, hematuria, and remission of proteinuria.

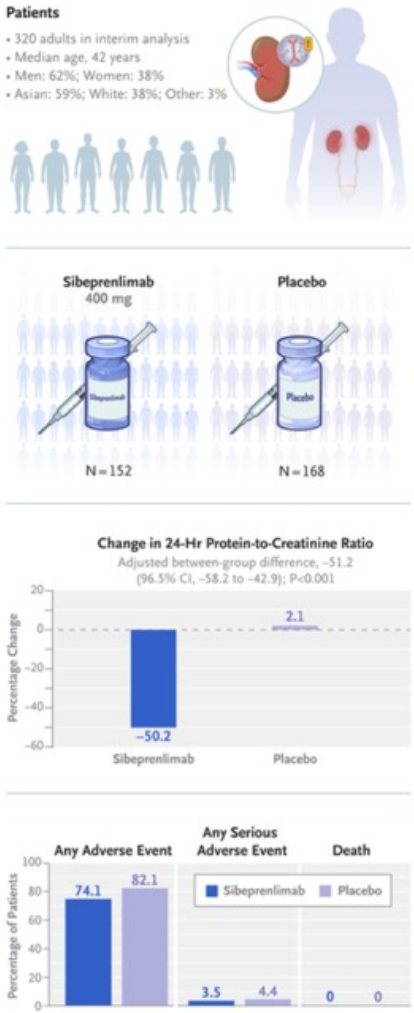

Sibeprenlimab is a humanized IgG2 monoclonal antibody that selectively inhibits the cytokine A proliferation-inducing ligand (APRIL) by preventing it from binding to its receptors. APRIL, considered to be a key driver of the pathogenesis of IgA nephropathy, mediates antibody class switching in mature B cells and plasma-cell survival, leading to the production of IgA and pathogenic galactose-deficient IgA1.

In the phase 2 ENVISION trial, intravenous sibeprenlimab administered every 4 weeks for 12 months reduced proteinuria, stabilized the estimated glomerular filtration rate (eGFR), suppressed serum levels of APRIL, and decreased levels of galactose-deficient IgA1, with an acceptable safety profile. The VISIONARY trial is an ongoing phase 3 trial evaluating the efficacy and safety of subcutaneous sibeprenlimab at a dose of 400 mg administered every 4 weeks in combination with supportive care in order to assess its ability to preserve kidney function in patients with IgA nephropathy. Dose selection was based on the clinical effects of intravenous sibeprenlimab at a dose of 4 mg per kilogram of body weight shown in the phase 2 trial as well as modeling that showed that subcutaneous sibeprenlimab at a dose of 400 mg resulted in levels of exposure and IgA reduction that were similar to those with intravenous administration. Here, we report the prespecified interim analysis of this phase 3 trial.

Patients

Adults with biopsy-confirmed IgA nephropathy, a 24-hour urinary protein-to-creatinine ratio of 0.75 or higher or 24-hour urinary protein excretion of 1.0 g per day or higher, and eGFR of 30 ml or more per minute per 1.73 m^2 at screening were eligible for the main trial cohort. Treatment with a stable and maximally tolerated dose of an angiotensin-converting–enzyme (ACE) inhibitor or angiotensin-receptor blocker (ARB) for at least 3 months before screening was generally required. Patients in whom therapy with an ACE inhibitor or ARB caused unacceptable side effects were eligible if they were otherwise receiving care that was concordant with applicable IgA nephropathy guidelines. Patients who were receiving stable sodium–glucose cotransporter 2 inhibitor therapy that began at least 3 months before screening were eligible.

End Points and Assessments

The primary efficacy end point in this interim analysis was the 24-hour urinary protein-to-creatinine ratio at 9 months as compared with baseline. The key secondary end point of annualized eGFR slope estimated over 24 months currently remains blinded to preserve ongoing trial integrity and is not reported here. The secondary end points presented here include safety (adverse events that emerged during the treatment period) and pharmacodynamic markers.

Characteristic	Sibeprenlimab (N=152)	Placebo (N=168)
Median age (range) — yr	42.0 (18–75)	43.0 (18–83)
Sex — no. (%)		
Male	100 (65.8)	100 (59.5)
Female	52 (34.2)	68 (40.5)
Race — no. (%)†		
Asian	94 (61.8)	95 (56.5)
White	55 (36.2)	66 (39.3)
Other	3 (2.0)	7 (4.2)
Ethnic group — no. (%)†		
Hispanic or Latinx	16 (10.5)	22 (13.1)
Not Hispanic or Latinx	132 (86.8)	141 (83.9)
Other (including unknown)	4 (2.6)	5 (3.0)
Region — no. (%)‡		
North America	22 (14.5)	21 (12.5)
South America	11 (7.2)	15 (8.9)
Europe	30 (19.7)	36 (21.4)
East Asia	43 (28.3)	48 (28.6)
South Asia or Southeast Asia	46 (30.3)	48 (28.6)
Mean body-mass index§	28.0±6.1	26.7±4.9
Mean blood pressure — mm Hg		
Systolic blood pressure	124.5±11.3	123.1±11.4
Diastolic blood pressure	77.8±8.1	78.7±8.0
Median time from initial biopsy to randomization (range) — yr	1.30 (0.10–23.70)	1.85 (0.00–34.00)
24-Hr urinary protein-to-creatinine ratio¶‖		
Geometric mean	1.33±1.74	1.32±1.63
Median (range)	1.22 (0.49–6.69)	1.28 (0.50–5.46)
eGFR — ml/min/1.73 m^2¶		
Mean	63.49±24.40	63.36±25.34
Median (range)	57.5 (25.0–131.0)	60.0 (27.0–129.0)
Hematuria — no. (%)**		
Negative	33 (21.7)	49 (29.2)
Positive	119 (78.3)	119 (70.8)
Previous use of immunosuppressive drugs — no. (%)††	6 (3.9)	6 (3.6)
Background regimen — no. (%)		
ACE inhibitor or ARB or both	149 (98.0)	163 (97.0)
Sodium–glucose cotransporter 2 inhibitor	56 (36.8)	72 (42.9)

Adverse Events Occurring during the Treatment Period in the Safety Population.

Event	Sibeprenlimab (N=259)	Placebo (N=251)
	no. of patients (%)	
Any adverse event occurring during treatment period†	192 (74.1)	206 (82.1)
Adverse event related to sibeprenlimab or placebo	75 (29.0)	67 (26.7)
Event occurring in ≥5% of patients in either trial group		
Injection-site erythema	34 (13.1)	30 (12.0)
Injection-site pain	26 (10.0)	23 (9.2)
Injection-site swelling	16 (6.2)	13 (5.2)
Pyrexia	14 (5.4)	10 (4.0)
Coronavirus disease 2019	25 (9.7)	17 (6.8)
Influenza	21 (8.1)	16 (6.4)
Nasopharyngitis	32 (12.4)	25 (10.0)
Upper respiratory tract infection	38 (14.7)	35 (13.9)
Back pain	17 (6.6)	14 (5.6)
Any serious adverse event occurring during treatment period‡	9 (3.5)	11 (4.4)
Any serious adverse event related to sibeprenlimab or placebo	1 (0.4)	1 (0.4)
Any severe adverse event occurring during treatment period	4 (1.5)	8 (3.2)
Any adverse event leading to discontinuation of sibeprenlimab or placebo	1 (0.4)	4 (1.6)
Death	0	0

A Change in 24-Hr UPCR at Month 9

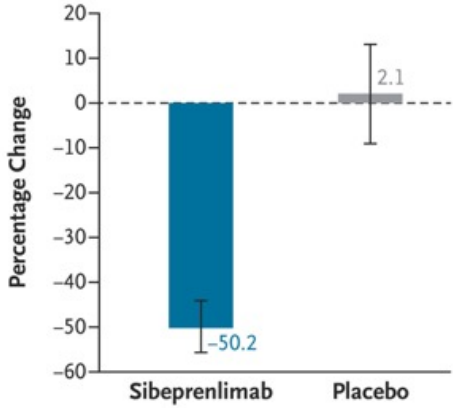

	Sibeprenlimab	Placebo
Baseline		
No. of patients	152	168
24-Hr UPCR — GM (GSD)	1.33 (1.74)	1.32 (1.62)
Month 9 (week 40)		
No. of patients	145	161
24-Hr UPCR — GM (GSD)	0.65 (2.34)	1.31 (2.03)

B Least-Squares Geometric Mean Change in Spot UPCR from Baseline

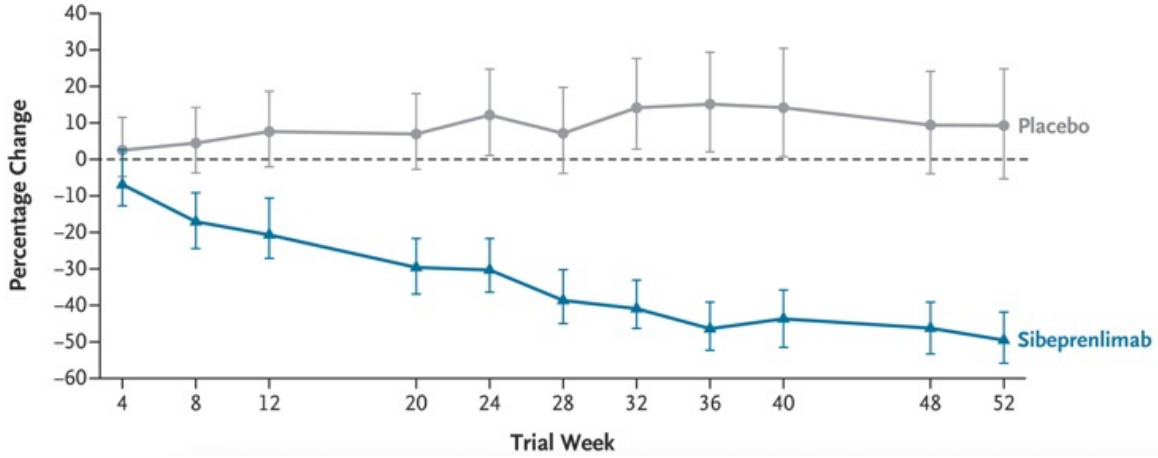

Change from Baseline in Urinary Protein-to-Creatinine Ratio.

The full-analysis population comprises patients who were in the interim-analysis population (the first 62.5% of patients who underwent randomization, had a baseline 24-hour urinary protein-to-creatinine ratio [UPCR] evaluation, and had the opportunity to complete the 9-month [40-week] 24-hour UPCR evaluation). In Panel A, the percentage reduction of 24-hour UPCR at month 9 is compared to baseline with the use of analysis of covariance (ANCOVA). The percentage reduction was calculated using the following formula: (−1) × (1−the geometric mean [GM] of the 24-hour UPCR estimated from the ANCOVA model) × 100%. The error bars indicate the 95% confidence interval (CI) of the GM. The placebo-adjusted treatment effect is 51.2% (96.5% CI, 42.9–58.2; P<0.001). The 95% confidence intervals shown in Panels A and B correspond to the treatment-specific reductions, whereas the 96.5% confidence interval shown in Panel A corresponds to the between-group difference aligned with the predefined split alpha of 0.035 used for testing the 24-hour UPCR end point in the interim analysis. For the 24-hour UPCR, both protein and creatinine are measured in grams. Panel B shows a line plot (generated from a mixed model for repeated measures) of spot UPCR results by visit as compared with baseline. Error bars indicate 95% confidence intervals. The widths of the confidence intervals have not been adjusted for multiplicity and should not be used in place of hypothesis testing. GSD denotes geometric standard deviation.

A Change in 24-Hour UPCR from Baseline at 9 Months, According to Demographic Characteristics

Subgroup	Sibeprenlimab	Placebo	Percentage Change, Sibeprenlimab vs. Placebo (95% CI)
	no. of patients		
Ethnic group			
Hispanic or Latinx	16	22	−49.3 (−65.9 to −24.4)
Not Hispanic or Latinx	132	141	−50.9 (−57.9 to −42.7)
Sex at birth			
Male	100	100	−51.9 (−60.4 to −41.6)
Female	52	68	−50.3 (−59.8 to −38.5)
Age			
≤40 yr	69	68	−51.8 (−60.3 to −41.5)
>40 yr	83	100	−51.8 (−60.7 to −40.9)
Race			
Asian	94	95	−53.8 (−61.8 to −44.2)
White	55	66	−45.8 (−56.6 to −32.4)
Geographic region			
North America	22	21	−25.6 (−48.6 to 7.5)
South America	11	15	−37.1 (−60.8 to 1.2)
Europe	30	36	−54.1 (−66.2 to −37.7)
East Asia	43	48	−56.5 (−66.7 to −43.3)
South and Southeast Asia	46	48	−56.5 (−67.7 to −41.4)

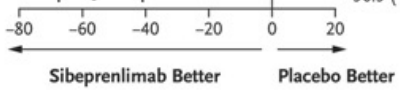

B Change in 24-Hour UPCR from Baseline over 9 Months, According to Stratification Factors

Subgroup	Sibeprenlimab	Placebo	Percentage Change, Sibeprenlimab vs. Placebo (95% CI)
	no. of patients		
24-Hr UPCR based on IRT record			
≤2.0 g/g	116	130	−45.9 (−53.9 to −36.6)
>2.0 g/g	36	38	−64.7 (−74.4 to −51.3)
Estimated GFR based on IRT record			
30–44 ml/min/1.73 m^2	37	43	−44.7 (−59.4 to −24.5)
≥45 ml/min/1.73 m^2	115	125	−52.6 (−59.8 to −44.2)
Screening SGLT2i based on IRT record			
No	98	96	−50.0 (−59.0 to −39.1)
Yes	54	72	−52.9 (−61.8 to −42.0)

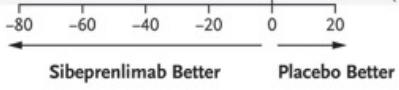

Interim Subgroup Analyses of 24-Hr UPCR at 9 Months (Full Analysis Population).

Panel A shows a forest plot for the subgroup analysis of the 24-hour UPCR at month 9 as compared with baseline according to demographic characteristics (including ethnic group, sex at birth, age group, and region). Panel B shows a forest plot for the subgroup analysis of the 24-hour UPCR at month 9 as compared with baseline according to stratification factors (including 24-hour UPCR, estimated glomerular filtration rate [eGFR], and sodium–glucose cotransporter 2 inhibitor [SGLT2i]). The percentage change is based on the ratio of sibeprenlimab to placebo. The widths of the confidence intervals have not been adjusted for multiplicity and should not be used in place of hypothesis testing. IRT denotes interactive response technology.

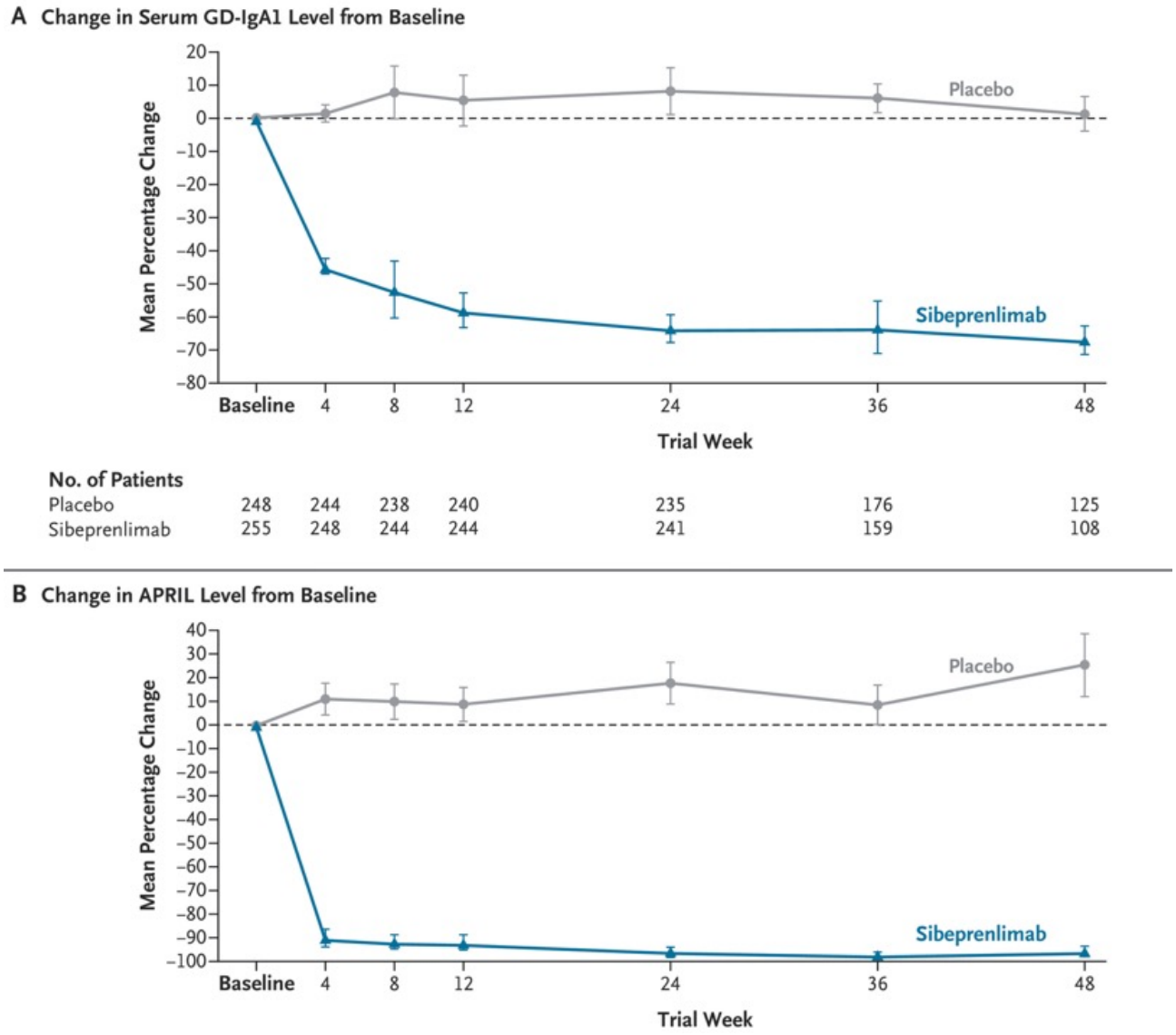

Change in Serum GD-IgA1 and Serum APRIL Levels in the Pharmacodynamic Population over Time.

The pharmacodynamic population consisted of all the participants who received at least one dose of sibeprenlimab or placebo and who had a baseline and at least one postbaseline evaluable (nonmissing and interpretable) pharmacodynamic measurement. The widths of the confidence intervals have not been adjusted for multiplicity and should not be used in place of hypothesis testing. APRIL denotes the cytokine A proliferation-inducing ligand.

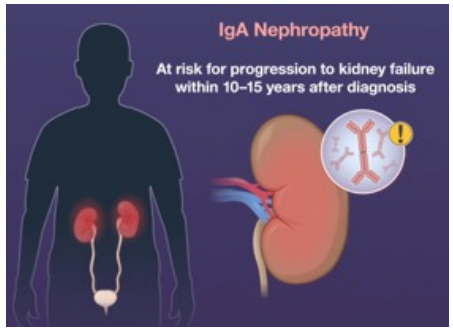
IgA Nephropathy
At risk for progression to kidney failure within 10–15 years after diagnosis

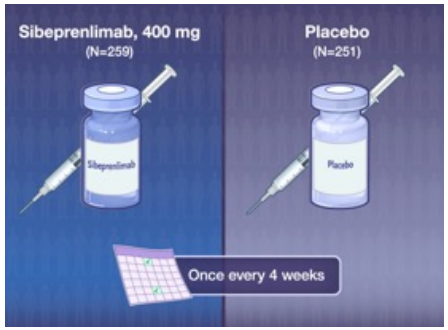
Sibeprenlimab, 400 mg
(N=259)
Placebo
(N=251)
Once every 4 weeks


SAFETY
Any Adverse Event
Any Serious Adverse Event
Death
Percentage of Patients
100
80
60
40
20
0
74%
82%
4%
4%
0%
0%
(percentages are rounded)
Sibeprenlimab
Placebo


Intravenous Sibeprenlimab
Humanized IgG2 monoclonal antibody
Has shown promise in phase 2 studies

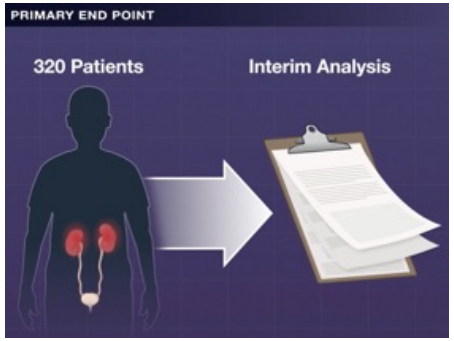
PRIMARY END POINT
320 Patients
Interim Analysis

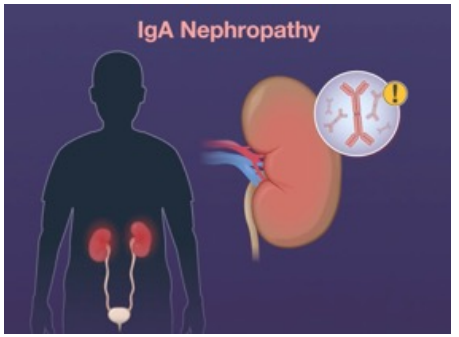
IgA Nephropathy

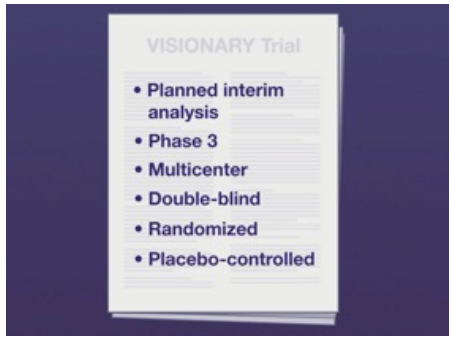
VISIONARY Trial
• Planned interim analysis
• Phase 3
• Multicenter
• Double-blind
• Randomized
• Placebo-controlled

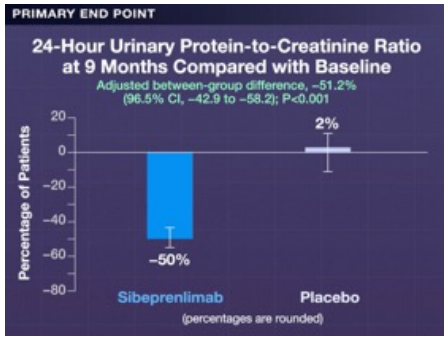
PRIMARY END POINT
24-Hour Urinary Protein-to-Creatinine Ratio at 9 Months Compared with Baseline
Adjusted between-group difference, −51.2%
(96.5% CI, −42.9 to −58.2); P<0.001
Percentage of Patients
20
0
−20
−40
−60
−80
2%
−50%
Sibeprenlimab
Placebo
(percentages are rounded)

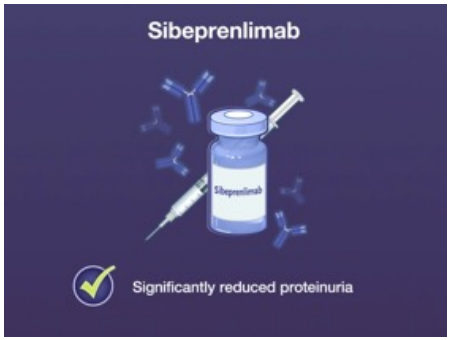
Sibeprenlimab
Significantly reduced proteinuria

Proposed pathogenesis of IgA nephropathy (IgAN) and potential treatments

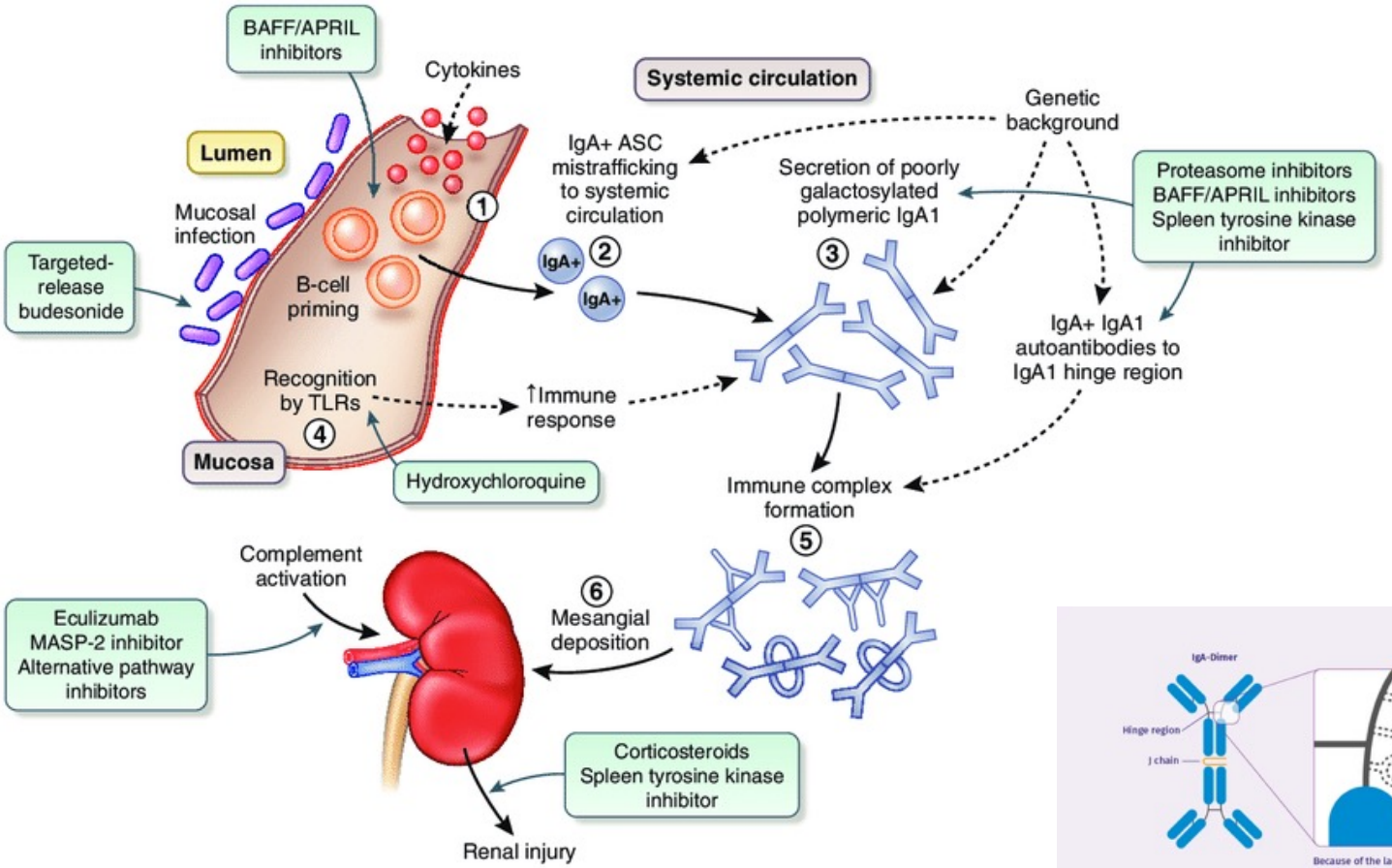

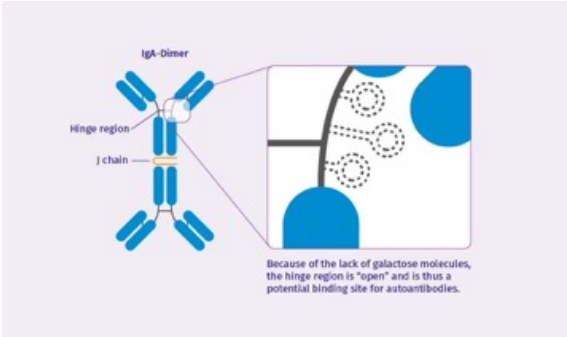

Atacicept ist ein in der klinischen Prüfung befindliches, rekombinantes Fusionsprotein, das zur Behandlung von Autoimmunerkrankungen, insbesondere der IgA-Nephropathie, entwickelt wird. Es bindet und neutralisiert die Zytokine BAFF und APRIL, wodurch B-Zellen gehemmt, die Autoantikörperbildung reduziert und Entzündungen sowie Nierenschäden verringert werden.

Wichtige Fakten zu Atacicept:

•**Wirkmechanismus:** Atacicept ist ein TACI-Ig-Fusionsprotein, das die für das Überleben von B-Lymphozyten und Plasmazellen entscheidenden Zytokine BAFF (B-cell activating factor) und APRIL (A proliferation-inducing ligand) blockiert.

•**Hauptindikationen (in Entwicklung):** Der Schwerpunkt liegt auf der Behandlung der **IgA-Nephropathie**
(Morbus Berger), wo es die Proteinurie (Eiweiß im Urin) und Hämaturie (Blut im Urin) signifikant reduzieren konnte
. Weitere untersuchte Indikationen umfassten den systemischen Lupus erythematodes (SLE) und andere Autoimmunerkrankungen.

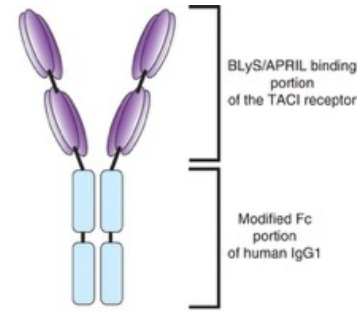

Atacicept

•**Studienlage:** In Phase-II-Studien (wie JANUS und ORIGIN) zeigte Atacicept ein Potenzial zur Reduktion von Serum-Gd-IgA1 und Proteinurie. Eine Phase-3-Studie (ORIGIN 3) untersucht derzeit die Wirksamkeit und Sicherheit bei 150 mg subkutaner Dosierung.

•**Verabreichung:** Der Wirkstoff wird subkutan (unter die Haut) verabreicht.

•**Entwicklungsstatus:** Die Rechte liegen aktuell bei Vera Therapeutics, nachdem sie ursprünglich von ZymoGenetics und Merck Serono entwickelt wurden.

•**Sicherheit:** In Studien zur IgA-Nephropathie wurde Atacicept generally als gut verträglich beschrieben.

BLyS and APRIL are **not the same**, although they are very closely related, belong to the same family (TNF superfamily), share similar functions in B-cell survival, and share receptors. Here are the key differences: **Definition: BLyS** (B-lymphocyte stimulator) is also commonly known as **BAFF** (B-cell activating factor). **APRIL** stands for **A PR**oliferation-**I**nducing **L**igand.

Atacicept: targeting B cells

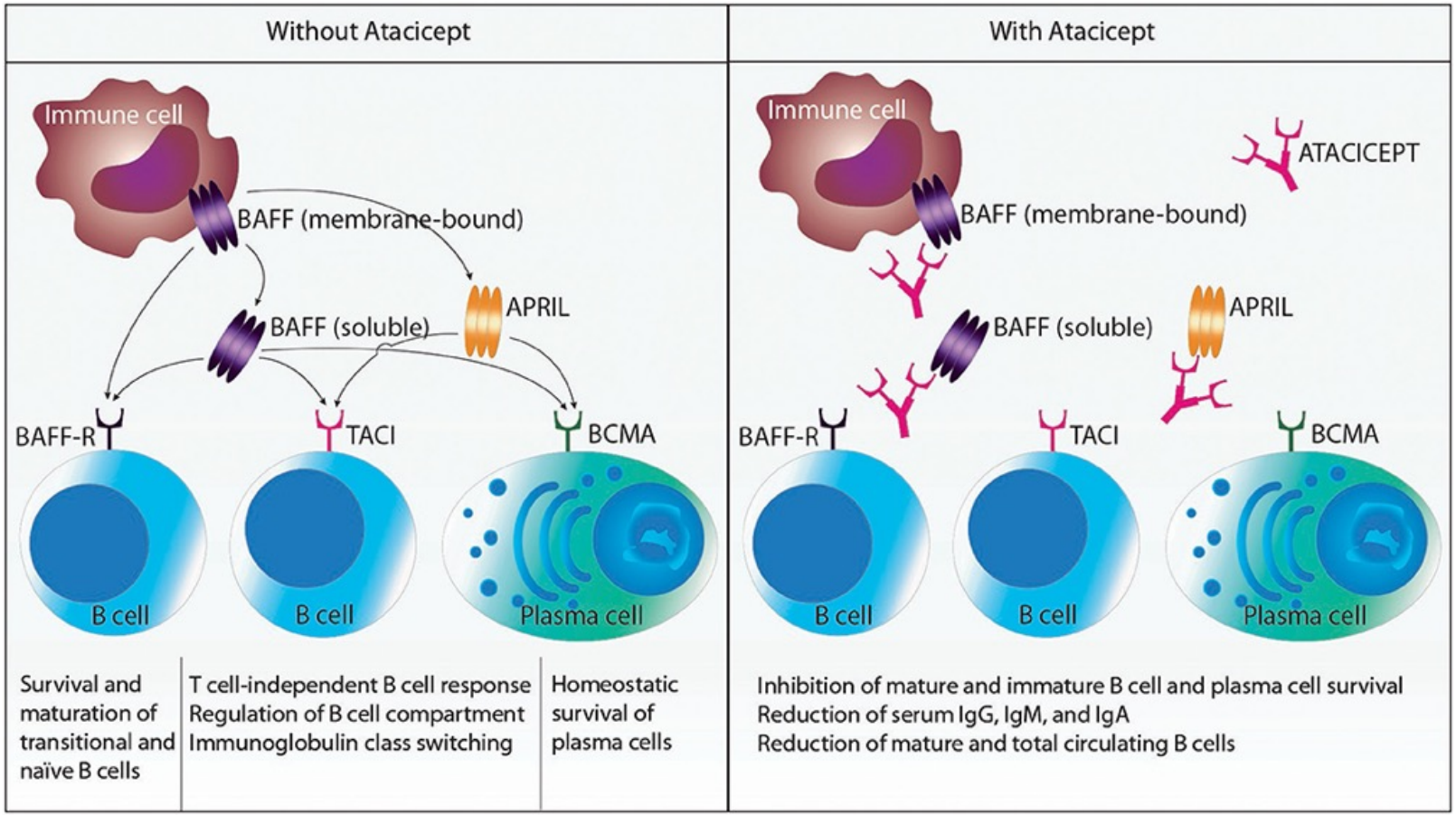

Definition: BLyS (B-lymphocyte stimulator) is also commonly known as **BAFF** (B-cell activating factor).

TACI=*Transmembrane Activator and CAML Interactor*, der vor allem auf B-Zellen vorkommt und Signale für das Überleben und die Aktivierung verarbeitet.

A Phase 3 Trial of Atacicept in Patients with IgA Nephropathy

IgA nephropathy, the most common primary glomerulopathy worldwide, is a kidney disorder of B-cell origin characterized by mesangial accumulation of IgA-containing immune complexes. In at least 50% of patients, IgA nephropathy leads to kidney failure or death within 10 to 20 years after diagnosis. Atacicept is a native human transmembrane activator and calcium-modulator and cyclophilin-ligand interactor (TACI)–Fc fusion protein that inhibits two key immunoregulatory cytokines — B-cell activating factor (BAFF) and a proliferation-inducing ligand (APRIL) — that are thought to be central to the pathophysiology of IgA nephropathy.

In this ongoing, phase 3, multicenter, double-blind, randomized, placebo-controlled trial, we assigned patients with IgA nephropathy in a 1:1 ratio to receive atacicept at a dose of 150 mg once weekly, administered subcutaneously by patients at home, or matching placebo. The primary end point was the percentage change from baseline in the 24-hour urinary protein-to-creatinine ratio at week 36. Safety was also evaluated.

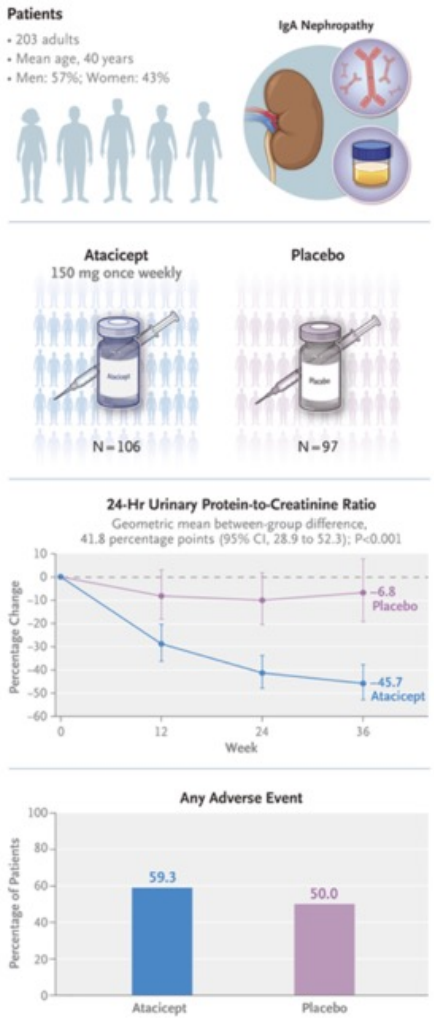

Atacicept is a native human TACI–Fc fusion protein with picomolar binding affinity for BAFF and APRIL that modulates B-cell activity, which reduces circulating levels of galactose-deficient IgA1, anti–galactose-deficient IgA1 autoantibodies, and immune complexes. The ability of atacicept to decrease BAFF and APRIL signaling of B cells directly targets the upstream pathophysiology of IgA nephropathy.

A phase 2b trial (ORIGIN 2b) evaluated the safety and efficacy of atacicept in patients with IgA nephropathy that had been confirmed by biopsy and showed a significant treatment benefit as compared with placebo with respect to the mean percentage change in the 24-hour urinary protein-to-creatinine ratio at 24 weeks (the primary end point). In addition, at 36 weeks, the reduction in the galactose-deficient IgA1 level, resolution of hematuria, and stabilization of the eGFR favored the atacicept group over the placebo group. In an open-label, 60-week extension period, the patients in the atacicept group had further reductions in proteinuria and the level of galactose-deficient IgA1, as well as resolution of hematuria. Through 96 weeks of atacicept treatment, eGFR was stabilized at the mean (±SE) annualized slope of −0.6±0.5 ml per minute per 1.73 m^2 of body-surface area, a rate similar to that in the general population without kidney disease. These results suggest that atacicept may offer a long-term, disease-modifying treatment for IgA nephropathy.

Patients

Eligible patients were adults 18 years of age or older with IgA nephropathy confirmed by biopsy. Other key inclusion criteria included a 24-hour urinary protein-to-creatinine ratio of at least 1.0 (with protein and creatinine both measured in grams) or proteinuria (defined as a urinary excretion of protein of ≥1.0 g per day), an eGFR of at least 30 ml per minute per 1.73 m^2, treatment with a stable renin–angiotensin system (RAS) inhibitor at the maximum labeled or tolerated dose for at least 12 weeks, and a blood pressure of 150/90 mm Hg or lower. Patients who were undergoing treatment with SGLT2 inhibitors at the time of enrollment had to have been receiving a stable dose for at least 12 weeks before screening and were expected to maintain a stable dose during the trial period. Patients were excluded from the trial if they had IgA nephropathy secondary to another condition, if nephrotic syndrome developed within 6 months before screening, or if evidence of rapidly progressive glomerulonephritis was found. The population in this trial was representative of the general population of patients with IgA nephropathy and was consistent with the patients involved in other IgA nephropathy trials.

End Points

The primary efficacy end point was the change from baseline at week 36 in the urinary protein-to-creatinine ratio (computed on the natural log scale and derived from a 24-hour urine collection). The secondary end points assessed at the interim analysis at week 36 included the change from baseline in the natural log–transformed serum galactose-deficient IgA1 levels and resolution of hematuria.

Characteristic	Atacicept (N=106)	Placebo (N=97)
Age — yr	40.1±11.1	40.9±11.6
Sex — no. (%)		
Male	57 (54)	58 (60)
Female	49 (46)	39 (40)
Race or ethnic group — no. (%)†		
American Indian or Alaska Native	0	0
Asian	59 (56)	52 (54)
Black or African American	0	1 (1)
Native Hawaiian or other Pacific Islander	0	1 (1)
White	46 (43)	42 (43)
Other	1 (1)	1 (1)
Hispanic or Latino	14 (13)	6 (6)
Non-Hispanic or non-Latino	92 (87)	91 (94)
Hematuria — no. (%)‡		
Negative or trace amount of blood	42 (40)	39 (40)
1+	21 (20)	16 (16)
2+	25 (24)	20 (21)
3+	18 (17)	22 (23)
Urinary protein-to-creatinine ratio§	1.7±0.9	1.8±1.2
Estimated glomerular filtration rate — ml/min/1.73 m^2	65.3±27.7	64.9±29.0
Urinary protein excretion — g/day	2.2±1.0	2.3±1.4
Urinary albumin-to-creatinine ratio§	1.3±0.7	1.3±0.9
Galactose-deficient IgA1 — μg/liter	5248.2±4192.5	4671.8±2411.7
IgA — mg/dl	336.7±119.1	332.5±109.8
IgG — mg/dl	1165.9±278.7	1150.1±277.0
IgM — mg/dl	111.8±57.1	99.1±54.8
Stable use of SGLT2 inhibitor — no. (%)	59 (56)	49 (51)
Use of RAS inhibitor — no. (%)	105 (99)	97 (100)
Time since biopsy — yr	2.5±2.6	2.5±2.4

Adverse Events (Safety Analysis).

Event	Atacicept (N=214)	Placebo (N=214)
	no. of patients (%)	
Any adverse event	127 (59.3)	107 (50.0)
Mild	90 (42.1)	74 (34.6)
Moderate	34 (15.9)	24 (11.2)
Severe	3 (1.4)	9 (4.2)
Adverse events occurring in >5% of the patients in either group		
Injection-site reaction	41 (19.2)	4 (1.9)
Upper respiratory tract infection	26 (12.1)	19 (8.9)
Nasopharyngitis	17 (7.9)	13 (6.1)
Injection-site erythema	12 (5.6)	1 (0.5)
Any adverse event related to the trial regimen	63 (29.4)	22 (10.3)
Mild	55 (25.7)	15 (7.0)
Moderate	8 (3.7)	5 (2.3)
Severe	0	2 (0.9)
Any serious adverse event	1 (0.5)†	11 (5.1)
Any adverse event related to infection or infestation	68 (31.8)	60 (28.0)
Mild	55 (25.7)	48 (22.4)
Moderate	13 (6.1)	10 (4.7)
Severe	0	2 (0.9)
Any serious adverse event related to infection or infestation	0	3 (1.4)
Any adverse event associated with injection-site reactions‡	62 (29.0)	11 (5.1)
Mild	56 (26.2)	10 (4.7)
Moderate	6 (2.8)	1 (0.5)
Severe	0	0
Any adverse event related to the trial regimen and associated with injection-site reactions	51 (23.8)	11 (5.1)
Any adverse event leading to interruption of the trial regimen	5 (2.3)	5 (2.3)
Any adverse event leading to discontinuation of the trial regimen	2 (0.9)	8 (3.7)
Any adverse event leading to death	0	0

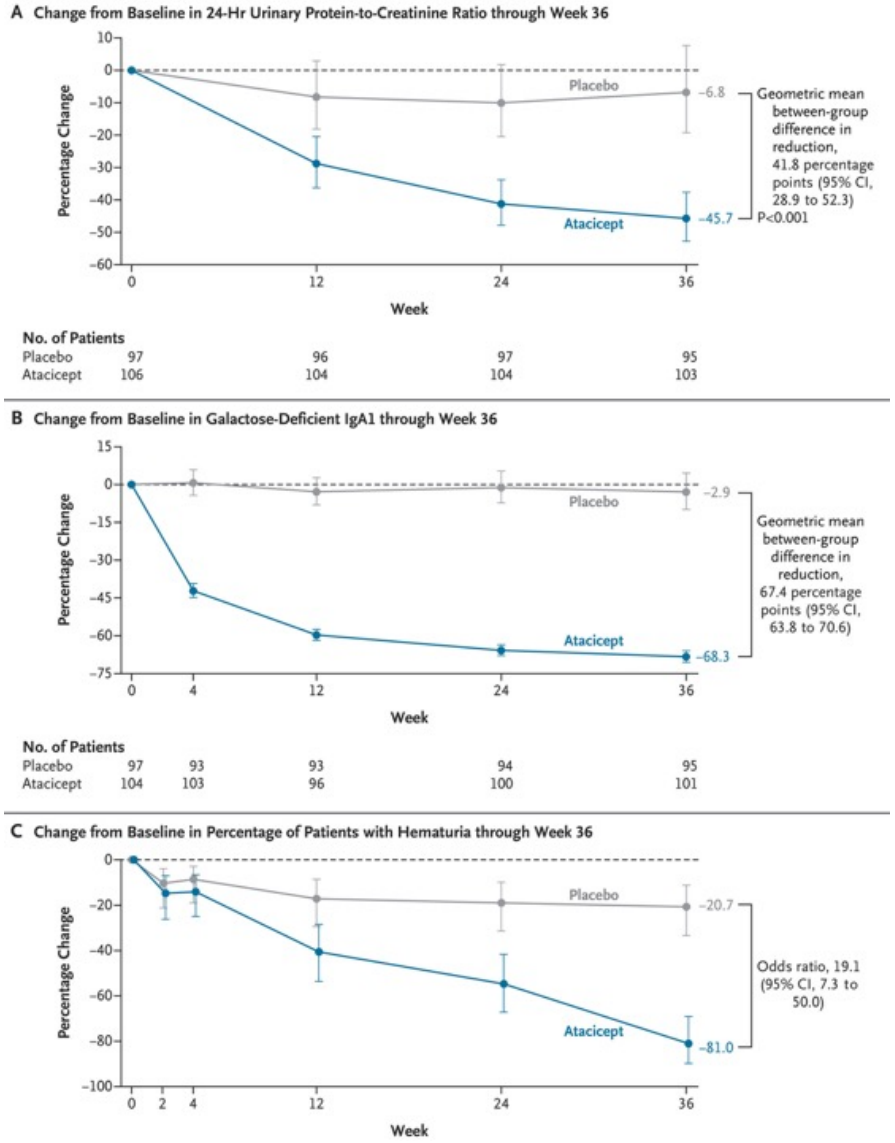

Percentage Change in Urinary Protein-to-Creatinine Ratio, Galactose-Deficient IgA1 Level, and Hematuria.

Panel A shows the mean percentage change from baseline through week 36 in the 24-hour urinary protein-to-creatinine ratio (primary end point). At week 36, data were available for 103 patients in the atacicept group and 95 patients in the placebo group. Panel B shows the mean percentage change from baseline through week 36 in the galactose-deficient IgA1 level. Panel C shows the change from baseline through week 36 in the percentage of patients with hematuria; the number of patients at each visit is the number of patients with baseline hematuria (≥1+), determined on the basis of dipstick testing, and nonmissing values. I bars indicate 95% confidence intervals. The between-group difference in the geometric mean percentage reduction in the 24-hour urinary protein-to-creatinine ratio at week 36 was calculated as $[1-(1-0.457)\div(1-0.068)]\times100=41.8\%$, which represents the atacicept treatment effect; the between-group difference in the geometric mean percentage reduction in the galactose-deficient IgA1 level at week 36 was computed with the use of the same method. The 95% confidence intervals for the percentage of patients with hematuria at each postbaseline visit were computed with the use of the Clopper–Pearson method. The analyses of the galactose-deficient IgA1 level and percentage of patients with hematuria were not adjusted for multiplicity and should not be used in place of hypothesis testing.

Subgroup	Atacicept	Placebo	Mean Change from Baseline		Mean Reduction vs. Placebo (95% CI)
			Atacicept	Placebo	
	no. of patients (%)		*percent*		*percentage points*
Overall	106 (100)	97 (100)	−45.7	−6.8	41.8 (28.9–52.3)
Age					
<40 yr	48 (45)	49 (51)	−44.5	0.5	44.7 (22.7–60.4)
≥40 yr	58 (55)	48 (49)	−46.4	−14.1	37.6 (21.2–50.6)
Sex					
Male	57 (54)	58 (60)	−41.1	−9.3	35.1 (13.5–51.2)
Female	49 (46)	39 (40)	−50.8	−2.4	49.6 (33.7–61.7)
Geographic region					
Asia	50 (47)	48 (49)	−49.5	−13.7	41.5 (18.1–58.2)
Other	56 (53)	49 (51)	−42.5	1.4	43.2 (29.0–54.6)
Race					
White	46 (43)	42 (43)	−42.4	0.1	42.5 (25.9–55.4)
Non-White	60 (57)	55 (57)	−48.4	−11.1	42.0 (22.1–56.9)
Urinary protein-to-creatinine ratio at baseline					
<1.5	53 (50)	47 (48)	−44.0	3.3	45.8 (27.7–59.4)
≥1.5	53 (50)	50 (52)	−48.5	−13.4	40.5 (21.2–55.1)
Estimated GFR at baseline					
<60 ml/min/1.73 m^2	50 (47)	52 (54)	−35.3	−1.3	34.5 (13.2–50.5)
≥60 ml/min/1.73 m^2	56 (53)	45 (46)	−53.0	−14.0	45.3 (27.0–59.1)
SGLT2 inhibitor use at baseline					
Yes	59 (56)	49 (51)	−48.2	−6.9	44.4 (26.4–57.9)
No	47 (44)	48 (49)	−42.9	−5.9	39.3 (19.1–54.4)

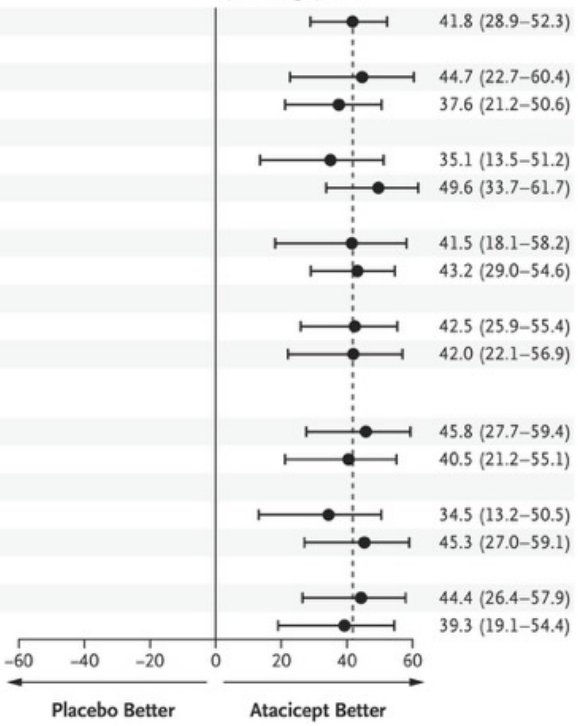

Subgroup Analyses of the Primary End Point.

Shown are prespecified subgroup analyses of the mean percentage change from baseline at week 36 in the 24-hour urinary protein-to-creatinine ratio. Separate analyses were conducted for each subgroup category with the use of the same imputed datasets and the same mixed-effects model with repeated measures (MMRM) model as for the primary analysis. If the subgroup was one of the covariates in the model, the covariate was removed from the model statement when the model was used for the particular subgroup. The number of patients per subgroup represents the sample size of the subgroup. The percentage of patients represents the number of patients per subgroup divided by the overall number of patients per trial group included in the analysis (patients with nonmissing baseline data and nonmissing covariates). The analyses were not adjusted for multiplicity and should not be used in place of hypothesis testing. The urinary protein-to-creatinine ratio was calculated with protein and creatinine both measured in grams. GFR denotes glomerular filtration rate, and SGLT2i sodium–glucose cotransporter 2 inhibitor.

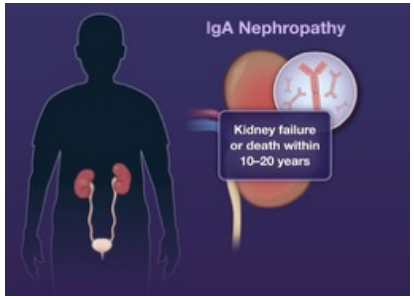
IgA Nephropathy
Kidney failure or death within 10–20 years


203 Adults
IgA nephropathy and persistent proteinuria despite standard treatment


SAFETY
Adverse Events
Percentage of Patients
100
80
60
40
20
0
59.3%
50.0%
Atacicept (N=214)
Placebo (N=214)

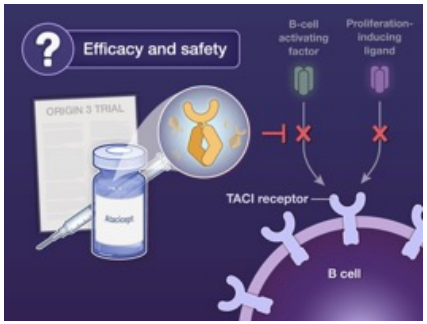
Efficacy and safety
B-cell activating factor
Proliferation-inducing ligand
ORIGIN 3 TRIAL
Atacicept
TACI receptor
B cell

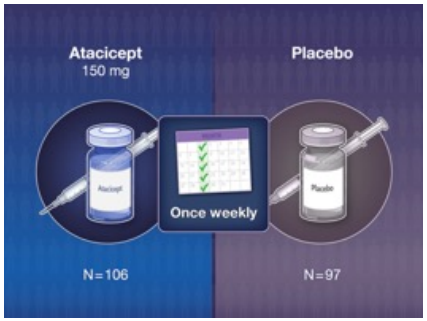
Atacicept 150 mg
Placebo
Once weekly
N=106
N=97

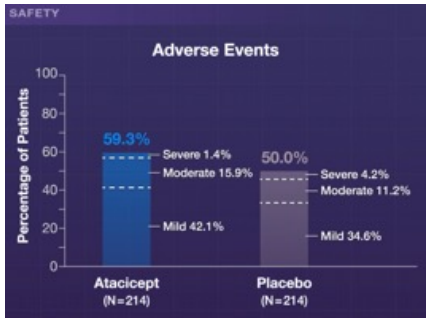
SAFETY
Adverse Events
Percentage of Patients
100
80
60
40
20
0
59.3%
Severe 1.4%
Moderate 15.9%
Mild 42.1%
50.0%
Severe 4.2%
Moderate 11.2%
Mild 34.6%
Atacicept (N=214)
Placebo (N=214)

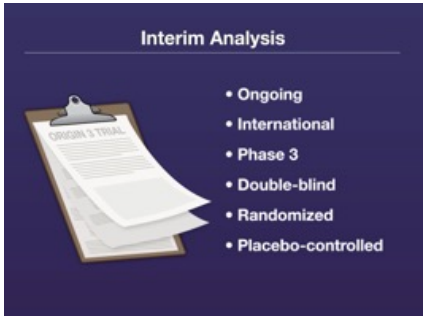
Interim Analysis
ORIGIN 5 TRIAL
• Ongoing
• International
• Phase 3
• Double-blind
• Randomized
• Placebo-controlled

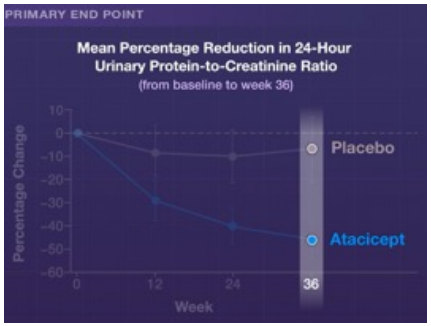
PRIMARY END POINT
Mean Percentage Reduction in 24-Hour Urinary Protein-to-Creatinine Ratio
(from baseline to week 36)
Percentage Change
10
0
−10
−20
−30
−40
−50
−60
0
12
24
36
Week
Placebo
Atacicept

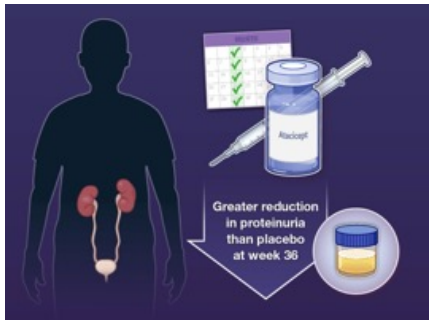
Atacicept
Greater reduction in proteinuria than placebo at week 36

Managing atrial fibrillation (AF) in patients with a new coronary stent requires balancing high stroke/stent-thrombosis risk against bleeding risk. Standard care involves a brief period of triple therapy—an oral anticoagulant (preferably a DOAC) plus clopidogrel and aspirin—followed by dual or mono-therapy to reduce bleeding risks.

Key Treatment Strategies

- **Triple Therapy (Short-Term):** For the first 1-4 weeks to 3 months, combine an oral anticoagulant (OAC) with a P2Y12 inhibitor (usually clopidogrel) and aspirin.
- **Dual Therapy (Intermediate):** After the initial period (often 1-6 months), discontinue aspirin and continue OAC plus a P2Y12 inhibitor (usually clopidogrel) for up to 12 months.
- **Monotherapy (Long-Term):** After 12 months, manage with an OAC alone, as prolonged antiplatelet therapy may increase bleeding risks.

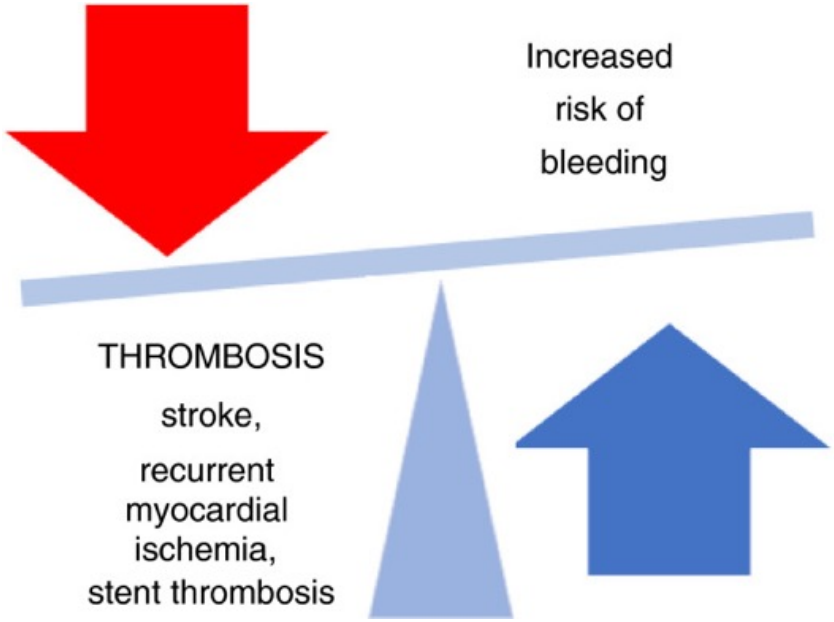

Therapy for Atrial Fibrillation in Patients with Drug-Eluting Stents

Despite guideline recommendations, evidence for the use of non–vitamin K antagonist oral anticoagulant (NOAC) monotherapy in patients with atrial fibrillation after implantation of a drug-eluting stent remains limited.

In this multicenter, randomized, open-label, noninferiority trial in South Korea, we assigned patients with atrial fibrillation who had undergone the implantation of a drug-eluting stent at least 1 year earlier in a 1:1 ratio to receive NOAC monotherapy or combination therapy (NOAC plus clopidogrel). The primary end point was net adverse clinical events, a composite of death from any cause, myocardial infarction, stent thrombosis, stroke, systemic embolism, or major bleeding or clinically relevant nonmajor bleeding at 12 months. The noninferiority margin was 3.0 percentage points.

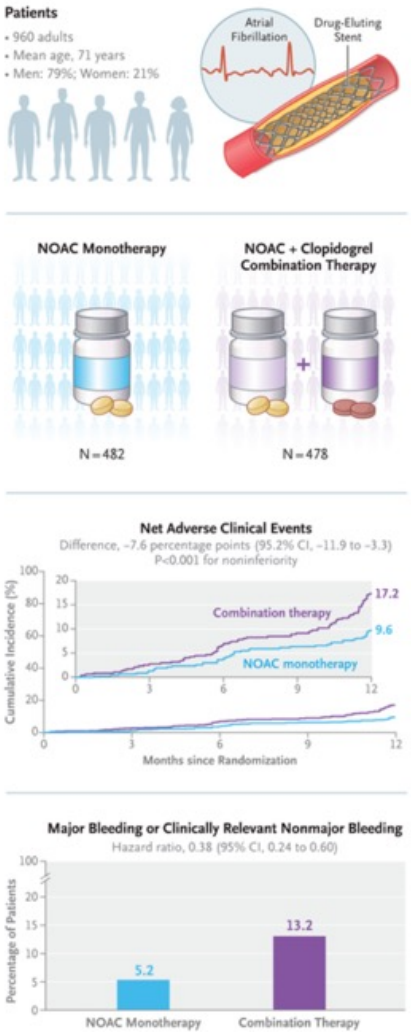

Patients with atrial fibrillation typically receive long-term anticoagulation therapy to prevent ischemic stroke and systemic embolism, whereas patients who are undergoing percutaneous coronary intervention (PCI) with implantation of drug-eluting stents are recommended to receive antiplatelet therapy to prevent stent thrombosis and further ischemic events. However, combining anticoagulation and antiplatelet therapies increases the risk of bleeding. Consequently, several randomized trials have investigated the most effective antithrombotic therapy for patients with atrial fibrillation immediately after PCI.

On the basis of these studies, current guidelines recommend early discontinuation of aspirin and continuation of combination therapy — preferably, the administration of a non–vitamin K antagonist oral anticoagulant (NOAC) with a $P2Y_{12}$ inhibitor — for 6 to 12 months after PCI. In contrast, these guidelines recommend monotherapy with oral anticoagulants beyond 1 year after PCI, when the patient's condition has been stabilized. However, evidence from randomized trials supporting this approach is limited.

Patients

Patients were eligible to participate in the trial if they were between the ages of 19 and 85 years and had received a diagnosis of atrial fibrillation and undergone PCI with implantation of second- or third-generation drug-eluting stents at least 1 year before enrollment.

We screened patients with atrial fibrillation using the CHA_2DS_2-VASc score, which indicates the risk of ischemic stroke among patients with atrial fibrillation on a scale ranging from 0 to 9, with higher scores indicating greater risk. Patients who were identified as being at high risk for thromboembolism (defined as a score of ≥2) were enrolled in the trial. The bleeding risk at baseline was assessed according to the patient's score on the HAS-BLED scale, which is a measure of the risk of bleeding among patients with atrial fibrillation who are receiving anticoagulant therapy, with scores ranging from 0 to 9 and higher scores indicating greater risk.

End Points

The primary end point was net adverse clinical events, defined as a composite of death from any cause, myocardial infarction, stent thrombosis, stroke, systemic embolism, or major bleeding or clinically relevant nonmajor bleeding at 12 months after randomization. Major bleeding or clinically relevant nonmajor bleeding were defined according to the criteria of the International Society on Thrombosis and Haemostasis.

The secondary end points were the individual components of the primary end point; a composite of major bleeding or clinically relevant nonmajor bleeding; a composite of death from any cause, myocardial infarction, stent thrombosis, stroke, systemic embolism, or major bleeding.

Characteristic	NOAC Monotherapy (N=482)	Combination Therapy (N=478)
Age — yr	71.0±8.4	71.2±8.7
Male sex — no. (%)	372 (77.2)	383 (80.1)
Body-mass index†	25.2±3.4	24.9±3.3
Medical history — no. (%)		
Hypertension	346 (71.8)	338 (70.7)
Diabetes mellitus	192 (39.8)	179 (37.4)
Chronic kidney disease	56 (11.6)	48 (10.0)
Heart failure	86 (17.8)	87 (18.2)
Dyslipidemia	281 (58.3)	264 (55.2)
Current smoker	76 (15.8)	95 (19.9)
CHA_2DS_2-VASc score‡		
Mean	4.1±1.4	4.1±1.3
Median (IQR)	4 (3–5)	4 (3–5)
HAS-BLED score§		
Mean	2.7±0.9	2.8±0.9
Median (IQR)	3 (2–3)	3 (2–3)
Acute coronary syndrome at index PCI — no. (%)	312 (64.7)	310 (64.9)
NOAC type		
Apixaban	294 (61.0)	299 (62.6)
Rivaroxaban	166 (34.4)	156 (32.6)
Edoxaban	19 (3.9)	23 (4.8)
Warfarin	3 (0.6)	0

Clinical Outcomes.

Outcome	NOAC Monotherapy (N=482)	Combination Therapy (N=478)	Difference (95% CI)†	Hazard Ratio (95% CI)	P Value‡
	no. of patients (%)§		*percentage points*		
Primary end point					
Net adverse clinical events¶	46 (9.6)	82 (17.2)	−7.6 (−11.9 to −3.3)	0.54 (0.37 to 0.77)	<0.001
Secondary end points‖					
Death from any cause	14 (2.9)	19 (4.0)	−1.1 (−3.4 to 1.2)	0.73 (0.37 to 1.46)	
Cardiovascular death	7 (1.5)	11 (2.3)	−0.9 (−2.6 to 0.9)	0.63 (0.24 to 1.63)	
Myocardial infarction	4 (0.8)	6 (1.3)	−0.4 (−1.7 to 0.9)	0.66 (0.19 to 2.34)	
Stent thrombosis**	2 (0.4)	2 (0.4)	0 (−0.8 to 0.8)	0.99 (0.14 to 7.02)	
Stroke	5 (1.0)	4 (0.8)	0.2 (−1.0 to 1.4)	1.24 (0.33 to 4.64)	
Ischemic event	5 (1.0)	2 (0.4)	0.6 (−0.5 to 1.7)	2.49 (0.48 to 12.85)	
Hemorrhagic event	0	2 (0.4)	−0.4 (−1.0 to 0.2)	ND	
Major bleeding or clinically relevant nonmajor bleeding††	25 (5.2)	63 (13.2)	−8.0 (−11.6 to -4.4)	0.38 (0.24 to 0.60)	
Major bleeding	11 (2.3)	29 (6.1)	−3.8 (−6.3 to −1.3)	0.37 (0.18 to 0.74)	
Clinically relevant nonmajor bleeding	14 (2.9)	34 (7.1)	−4.2 (−7.0 to −1.5)	0.40 (0.21 to 0.74)	
Composite of death from any cause, myocardial infarction, stent thrombosis, stroke, systemic embolism, or major bleeding	33 (6.8)	49 (10.3)	−3.4 (−6.9 to 0.1)	0.66 (0.42 to 1.03)	
Composite of cardiovascular death, myocardial infarction, stent thrombosis, stroke, or systemic embolism	16 (3.3)	19 (4.0)	−0.7 (−3.0 to 1.7)	0.84 (0.43 to 1.63)	

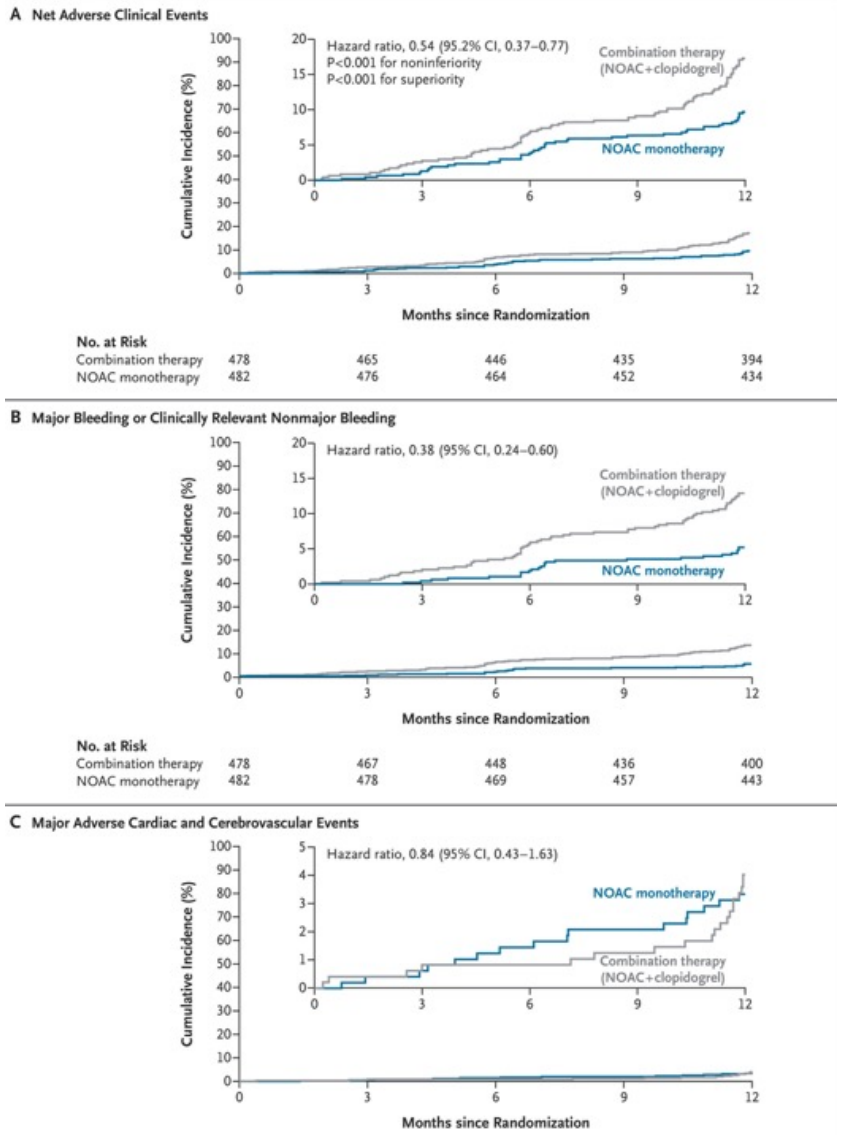

Cumulative Incidence of Trial End Points (Intention-to-Treat Population).

Shown is the incidence of net adverse clinical events (primary end point), defined as a composite of death from any cause, myocardial infarction, stent thrombosis, stroke, systemic embolism, or major bleeding or clinically relevant nonmajor bleeding at 12 months (Panel A); major bleeding or clinically relevant nonmajor bleeding, as defined by the International Society on Thrombosis and Haemostasis (Panel B); and a composite of cardiovascular death, myocardial infarction, stent thrombosis, ischemic stroke, or systemic embolism (a secondary end point) (Panel C). For secondary end points, the widths of the confidence intervals (CIs) have not been adjusted for multiplicity and should not be used to infer treatment effects. In each panel, the inset displays the same data on an expanded y axis.

Subgroup	NOAC Monotherapy	Combination Therapy	Hazard Ratio for Event or Death (95% CI)
	no. of events/total no. of patients (Kaplan–Meier estimate — %)		
All patients	46/482 (9.6)	82/478 (17.2)	0.54 (0.37–0.77)
Age			
<75 yr	28/299 (9.4)	39/285 (13.7)	0.67 (0.41–1.09)
≥75 yr	18/183 (9.8)	43/193 (22.3)	0.41 (0.24–0.71)
Sex			
Female	9/110 (8.2)	22/95 (23.2)	0.32 (0.15–0.70)
Male	37/372 (9.9)	60/383 (15.7)	0.62 (0.41–0.93)
Time of PCI before randomization			
<24 mo	20/184 (10.9)	31/199 (15.6)	0.69 (0.39–1.20)
≥24 mo	26/298 (8.7)	51/279 (18.3)	0.45 (0.28–0.73)
Clinical presentation at PCI			
Stable coronary artery disease	16/170 (9.4)	24/168 (14.3)	0.63 (0.33–1.18)
Acute coronary syndrome	30/312 (9.6)	58/310 (18.7)	0.50 (0.32–0.77)
Type of NOAC			
Apixaban	30/294 (10.2)	53/299 (17.7)	0.56 (0.36–0.87)
Rivaroxaban	16/166 (9.6)	27/156 (17.3)	0.53 (0.29–0.98)
Edoxaban or warfarin	0/22 (0)	2/23 (8.7)	—
CHA_2DS_2-VASc score			
<4	15/160 (9.4)	23/177 (13.0)	0.72 (0.38–1.38)
≥4	31/322 (9.6)	59/301 (19.6)	0.46 (0.30–0.72)
HAS-BLED score			
<3	16/168 (9.5)	28/160 (17.5)	0.53 (0.29–0.97)
≥3	30/314 (9.6)	54/318 (17.0)	0.54 (0.35–0.84)
Complex PCI			
Yes	12/126 (9.5)	26/121 (21.5)	0.42 (0.21–0.83)
No	34/356 (9.6)	56/357 (15.7)	0.59 (0.39–0.90)
Drug-eluting stent generation			
Second generation	21/205 (10.3)	36/214 (16.8)	0.59 (0.34–1.01)
Third generation	25/277 (9.0)	46/264 (17.4)	0.50 (0.31–0.81)

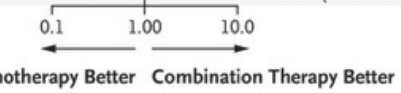

Subgroup Analyses of the Primary End Point.

Hazard ratios for the comparison between NOAC monotherapy and combination therapy for a primary end-point event according to prespecified subgroups are shown. On the basis of the results of the interim analysis, a 95.2% confidence interval was adopted for the primary end point. Analyses for complex PCI and generation of the implanted drug-eluting stent were performed post hoc. CHA_2DS_2-VASc scores range from 0 to 9, with higher scores indicating a greater risk of stroke. HAS-BLED scores range from 0 to 9, with higher scores indicating a greater bleeding risk. The cumulative incidence of a primary end-point event at 12 months was estimated with the Kaplan–Meier method in the intention-to-treat population. Thus, the percentages may not reflect the crude ratio of the numerator to the denominator. The widths of the confidence intervals have not been adjusted for multiplicity and should not be used to infer treatment effect.

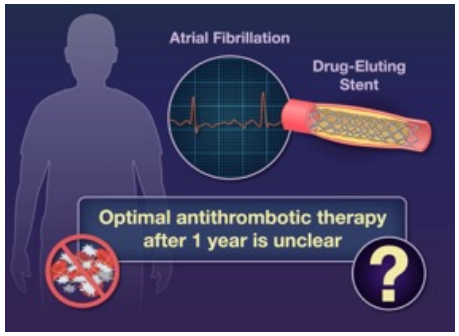
Atrial Fibrillation
Drug-Eluting Stent
Optimal antithrombotic therapy after 1 year is unclear

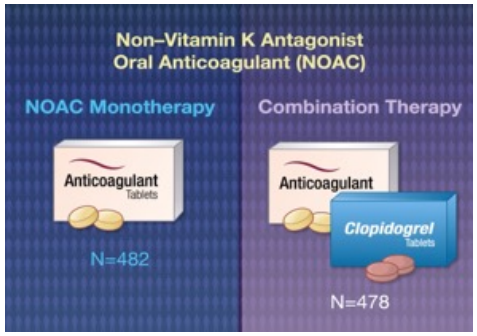
Non–Vitamin K Antagonist Oral Anticoagulant (NOAC)
NOAC Monotherapy
Combination Therapy
Anticoagulant
Tablets
N=482
Anticoagulant
Clopidogrel
Tablets
N=478

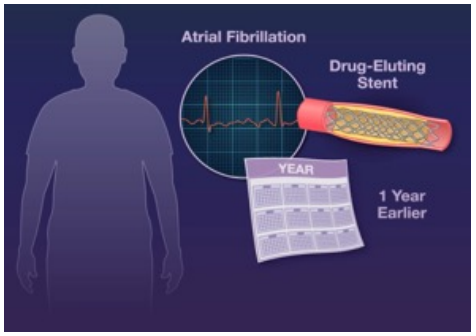
Atrial Fibrillation
Drug-Eluting Stent
YEAR
1 Year Earlier


Current Guidelines
Non–Vitamin K Antagonist Oral Anticoagulant Monotherapy
YEAR

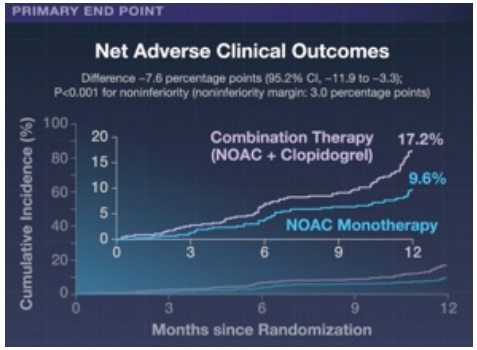
PRIMARY END POINT
Net Adverse Clinical Outcomes
Difference −7.6 percentage points (95.2% CI, −11.9 to −3.3);
P<0.001 for noninferiority (noninferiority margin: 3.0 percentage points)
Cumulative Incidence (%)
Combination Therapy (NOAC + Clopidogrel)
17.2%
9.6%
NOAC Monotherapy
Months since Randomization

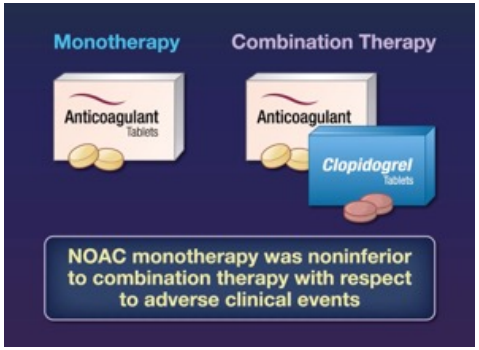
Monotherapy
Combination Therapy
Anticoagulant
Tablets
Anticoagulant
Clopidogrel
Tablets
NOAC monotherapy was noninferior to combination therapy with respect to adverse clinical events

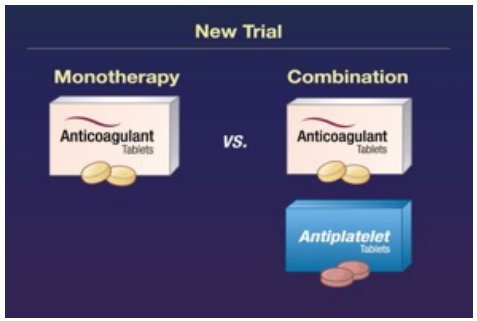
New Trial
Monotherapy
Combination
Anticoagulant
Tablets
vs.
Anticoagulant
Tablets
Antiplatelet
Tablets

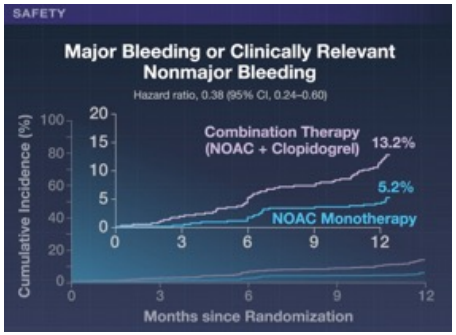
SAFETY
Major Bleeding or Clinically Relevant Nonmajor Bleeding
Hazard ratio, 0.38 (95% CI, 0.24–0.60)
Cumulative Incidence (%)
Combination Therapy (NOAC + Clopidogrel)
13.2%
5.2%
NOAC Monotherapy
Months since Randomization

Der **Plättchenfaktor 4 (PF4)** ist ein wichtiges Protein, das bei der Blutgerinnung und Entzündungsreaktionen eine Rolle spielt. Er wird bei der Aktivierung von Blutplättchen freigesetzt und ist vor allem für seine Beteiligung an der seltenen, aber schwerwiegenden **Heparin-induzierten Thrombozytopenie (HIT)** bekannt.

Ziemlich häufig

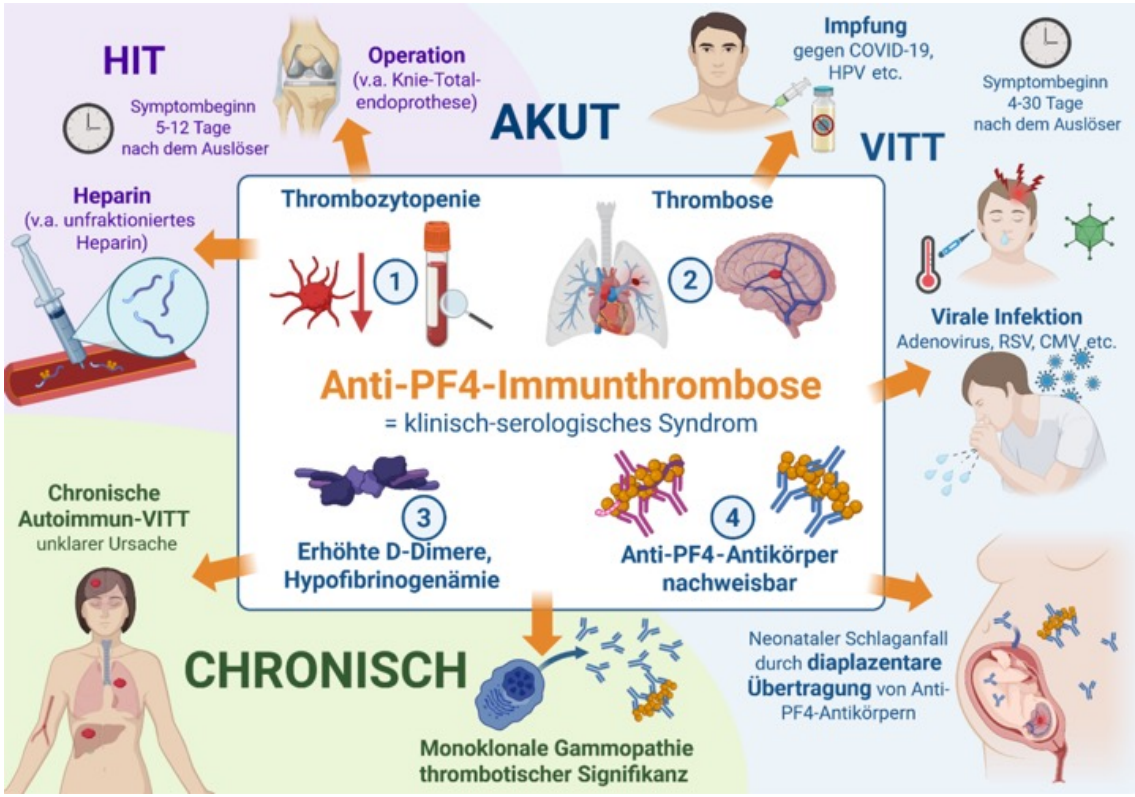

Sehr selten
(1:200 000)

Der Begriff **VITT** wird meist als Abkürzung für die **Vakzin-induzierte immunthrombotische Thrombozytopenie** (eine seltene Impfkomplikation) oder für das **Fischerdorf Vitt auf Rügen** verwendet.

Medizinische Bedeutung

VITT steht für **Vakzin-induzierte immunthrombotische Thrombozytopenie** (englisch: *vaccine-induced immune thrombotic thrombocytopenia*). Es handelt sich dabei um eine seltene, aber schwerwiegende Komplikation, die nach der Impfung mit bestimmten COVID-19-Impfstoffen, insbesondere denen auf Basis viraler Vektoren (wie AstraZeneca), beobachtet wurde.

- **Definition:** Die VITT ist ein Autoimmunsyndrom, das durch die Bildung von Antikörpern gegen Blutplättchen gekennzeichnet ist, was sowohl zu einer verminderten Blutplättchenzahl (Thrombozytopenie) als auch zur Bildung von Blutgerinnseln (Thrombosen, z.B. Hirnvenenthrombosen) führen kann.
- **Symptome:** Die Symptome treten meist innerhalb von 4 bis 28 Tagen nach der Impfung auf und umfassen oft neurologische Beschwerden wie starke Kopfschmerzen, Krampfanfälle, aber auch andere Thrombosen in verschiedenen Körperregionen.
- **Behandlung:** Eine frühzeitige Diagnose und spezifische, von der Standard-Heparin-Therapie abweichende Behandlung (z.B. mit Immunglobulinen oder Bivalirudin) sind entscheidend für die Prognose.

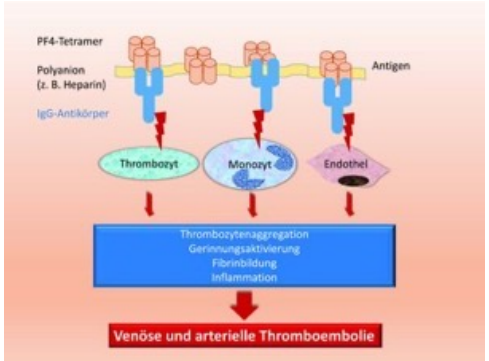

Heparin macht manchmal HIT
Was ist das Antigen bei VITT?

Adenoviral-basierte Impfstoffe nutzen modifizierte **Adenoviren** (die normalerweise Erkältungen verursachen) als "Vektoren" oder Transportmittel, um genetische Baupläne eines Erregers direkt in menschliche Zellen zu schleusen.

Funktionsweise

- **Der Vektor:** Wissenschaftler entfernen die Gene für die Vermehrung aus dem Adenovirus, sodass es im Körper **keine Infektion** auslösen kann.
- **Die Fracht:** Anstelle der Vermehrungs-Gene wird ein Gen-Abschnitt des Ziel-Erregers (z. B. der Bauplan für das Spike-Protein von SARS-CoV-2) in das Virusgenom eingefügt.
- **Die Reaktion:** Nach der Injektion dringt der Vektor in Körperzellen ein. Die Zelle liest den Bauplan und stellt das fremde Protein (Antigen) selbst her. Das Immunsystem erkennt dieses Protein als fremd und bildet daraufhin **Antikörper** sowie spezialisierte **T-Zellen**.

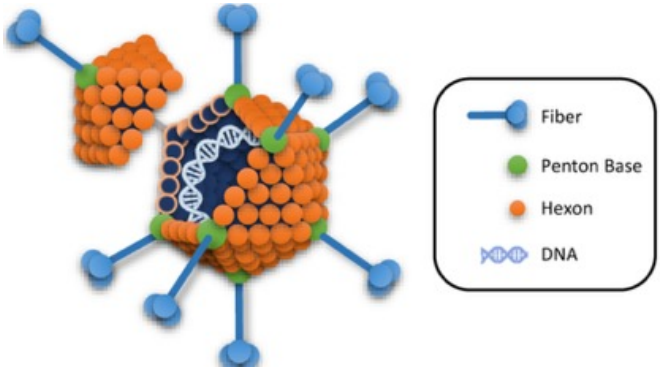

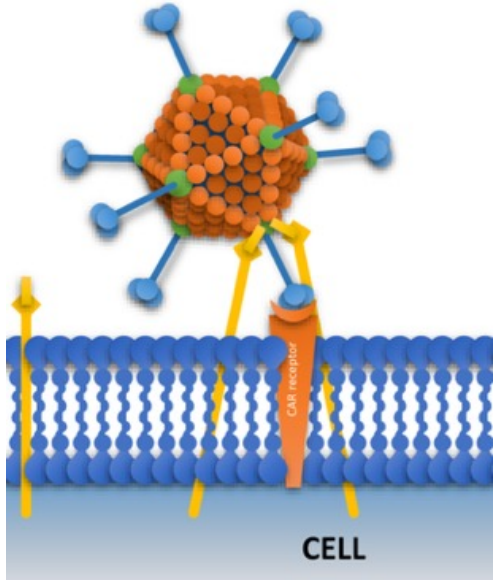

More cases of vaccine-induced immune thrombocytopenia and thrombosis (VITT), as the syndrome became known, soon emerged in Europe among AstraZeneca recipients and also in people in the United States who had received a similar COVID-19 vaccine produced by Johnson & Johnson (J&J). They, too, had PF4 antibodies. The condition turned out to be rare— occurring in roughly one in 200,000 people who received the vaccines—but Eichinger's worries were borne out. Many European countries restricted use of AstraZeneca's vaccine to older people, who were most at risk of dying from COVID-19, or dropped it completely. In the U.S., where AstraZeneca was never approved, the J&J vaccine was ultimately abandoned.

Molecular mimicry

Adenovirus-based vaccines against COVID-19 can cause B cells to produce antibodies carrying an excess of negative charge that miss their target, a viral protein, and instead bind to PF4, a human clotting factor. That sets off a potentially fatal chain reaction called vaccine-induced immune thrombocytopenia and thrombosis (VITT).

Molekulare Mimikry bezeichnet ein immunologisches Phänomen, bei dem Krankheitserreger (Viren, Bakterien) ihre Oberflächenmoleküle so gestalten, dass sie körpereigenen Strukturen ähneln. Diese "Tarnung" soll dem Erreger helfen, der Immunabwehr zu entgehen. Führt dies zu einer Immunantwort, kann das System irrtümlich eigene Zellen angreifen, was Autoimmunerkrankungen auslösen kann.

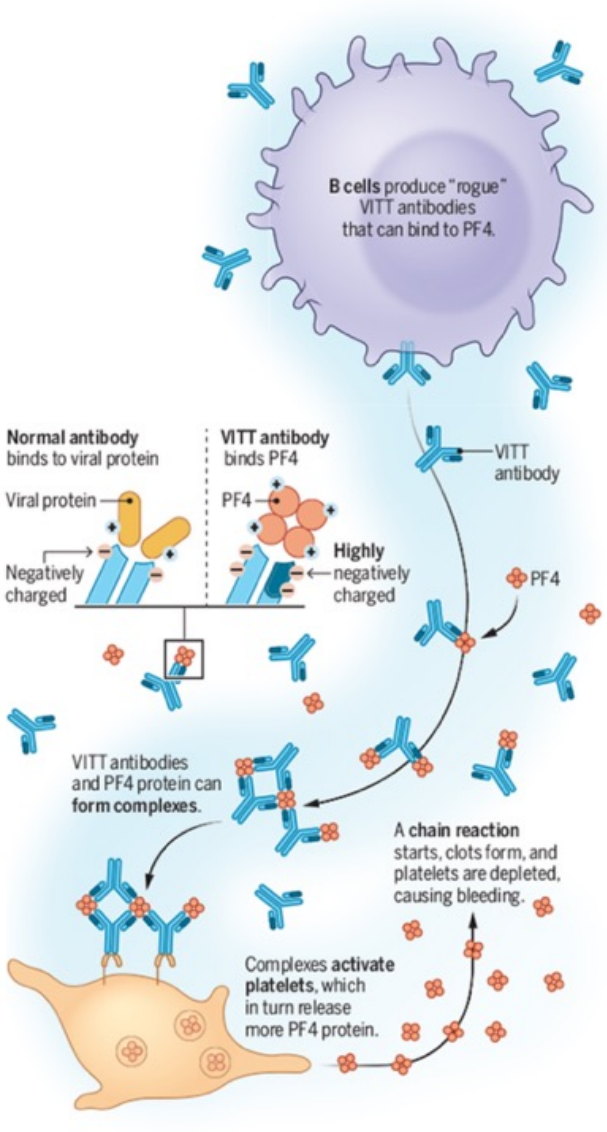

Adenoviral Inciting Antigen and Somatic Hypermutation in VITT

Background

Vaccine-induced immune thrombocytopenia and thrombosis (VITT) is a rare prothrombotic complication that occurs after adenoviral vector–based vaccination against coronavirus disease 2019; in rare cases, it can also occur after natural adenovirus infection. VITT is mediated by platelet-activating antibodies against the highly cationic protein platelet factor 4 (PF4). The underlying inciting antigen trigger and immunopathogenesis remain unknown.

Methods

We used antibody proteomics to determine the amino acid sequences of anti-PF4 antibodies from 21 patients with VITT and sequenced the genes encoding the immunoglobulin light-chain hypervariable region from 100 patients with VITT. To identify an adenoviral trigger, we used the antigen-binding fingerprints of anti-PF4 and anti–adenovirus protein antibodies to identify a shared serum clonotype and subsequently used adenovirus protein peptides and recombinant anti-PF4 VITT antibodies to map the mimicking linear epitope.

Conclusions

The results of our study indicate that VITT occurs when, in persons with immunoglobulin light-chain allele IGLV3-21*02 or *03, a specific somatic hypermutation develops that affects antibodies that recognize a specific epitope on the adenoviral core protein pVII, which results in misdirection of antibody targeting toward PF4. (Funded by Deutsche Forschungsgemeinschaft and others)

Anti–platelet factor 4 (PF4) antibodies cause the severe adverse reaction termed vaccine-induced immune thrombocytopenia and thrombosis (VITT; also known as vaccine-induced immune thrombotic thrombocytopenia). VITT specifically occurs after receipt of an adenovirus vector–based coronavirus disease 2019 (Covid-19) vaccine — ChAdOx1-S (Oxford–AstraZeneca) or Ad26.COV2.S (Johnson & Johnson–Janssen). The common feature of these two vaccines is the adenovirus particle, although it is derived from distinct adenovirus serotypes in the two vaccines: ChAdOx1 is a chimpanzee adenovirus, and Ad26 is a human adenovirus.

In rare cases, VITT also occurs after natural adenovirus infection, which suggests that a highly conserved structure within different adenovirus subtypes may induce the anti-PF4 response. This notion is corroborated by the uniform structure of the anti-PF4 antibodies that are induced in the VITT immune response. Anti-PF4 antibodies that are isolated from the serum of patients with VITT after vaccination or natural adenovirus infection are typically monoclonal or oligoclonal. These antibodies have light and heavy chains with molecular fingerprints that are nearly identical (“stereotyped”) among patients. This characteristic allowed us to generate recombinant versions of these antibodies, which made detailed in vitro and in vivo studies possible.

Clinical Characteristics, *IGLV3-21* Genotyping, and Mass-Spectrometric Sequencing of Serum Anti-PF4 Light Chains from 21 Patients with VITT.

All patients had platelet-activating anti-PF4 antibodies detected by anti–PF4–heparin enzyme-linked immunosorbent assay (ELISA), with strong reactivity against PF4 alone in a chemiluminescence assay, as well as by PF4-induced platelet activation assay (PIPA). Baseline repository plasma was also available from two patients who had donated blood several weeks before Covid-19 vaccination and subsequent development of VITT.

All contained a key similarity: At position 31 in the so-called light chain of the antibody, the amino acid lysine, which has a positive charge, had been replaced by glutamic acid or aspartic acid, which are both negatively charged. Other evidence showed the change must have occurred in the particular B cells that make the rogue antibodies.

Condition and Patient ID†	Phenotype‡	Anti-PF4–Heparin IgG ELISA Result	*IGLV3-21* Genotype§	Mass-Spectrometric Sequencing¶	
				Immunoglobulin Light-Chain Variable Region Subfamily	LCDR3 Amino Acid Sequence
		OD			
Classic VITT after ChAdOx1-S					
VITT1	CVST with secondary ICH	2.43	NA	IGLV3-21*02	QVWDSSSDHPVFGGGTKLTVL
VITT04	DVT, thrombosis of internal jugular vein	3.11	*03/*03	IGLV3-21*03	QVWDGSSDHPVFGGGTKLTVL
VITT05	PE, DVT, severe headache	3.41	*03/*01	IGLV3-21*03	QVWDGSRDHPVFGGGTKLTVL
VITT07	CVST with secondary bleeding	3.13	*02/*01	IGLV3-21*02	QVWDGSSDHPVFGGGTKLTVL
VITT08	Not provided	2.19	*03/*01	IGLV3-21*03	QVWDGSLDHPVFGGGTKLTVL
VITT09	PVT, headache	2.40	*03/*01	IGLV3-21*03	QVWDSSSDHPVFGGGTKLTVL
VITT12	PE, DVT	1.04	*02/*02	IGLV3-21*02	QVWDGSSDHPVFGGGTKLTVL
VITT13	CVST with secondary bleeding	1.19	*03/*01	IGLV3-21*03	QVWDSSSDHVVFGGGTKLTVL
VITT16	PVT	2.50	*03/*01	IGLV3-21*03	QAWDSSSDRPVFGGGTKLTVL
VITT19	CVST, PE	3.09	*02/*02	IGLV3-21*02	QVWDSSSDHPVFGGGTRLTVL
VITT25	CVST	1.57	NA	IGLV3-21*02	QVWDSSSDHVVFGGGTKLTVL
VITT81‖	DVT, PE, PVT	3.42	*02/*01	IGLV3-21*02	QVWDSSSDHPVFGGGTKLTVL
VITT86	Arterial stroke, CVST, DVT, PE, PVT	2.80	NA	IGLV3-21*02	QVWDGSDEHVVFGGGTKLTVL
Classic VITT after Ad26.COV2.S					
VITT15	DVT, PE, PVT	3.57	*02/*01	IGLV3-21*02	QVWDGSSDRPVFGGGTKLTVL
VITT38	DVT in both legs	3.20	*02/*01	IGLV3-21*02	QMWDGSSDLPVFGGGTKLTVL
VITT40	DVT, PE	3.24	*02/*02	IGLV3-21*02	QVWHSSRDRVLFGGGTKLTVL
Pre-VITT syndrome after ChAdOx1-S**					
VITT06	Pre-VITT syndrome	3.15	*02/*02	IGLV3-21*02	QVWDSSSDHPVFGGGTKLTVL
VITT17	Pre-VITT syndrome	1.69	*02/*02	IGLV3-21*02	QVWDGSSDHVLFGGGTKLTVL
VITT36‖	Pre-VITT syndrome	3.60	*02/*01	IGLV3-21*02	QVWDSGDDHVFFGGGTKLTVL
VITT39	Pre-VITT syndrome	3.26	*02/*01	IGLV3-21*02	QVWDGSTDHVLFGGGTKLTVL
VITT51	Pre-VITT syndrome	2.34	*02/*02	IGLV3-21*02	QAWESSSDHVVFGGGTKLTVL

Light-chain hypervariable region from 21 VITT patients

The immunoglobulin light-chain alleles **IGLV3-21*02** and **IGLV3-21*03** have been identified as key genetic factors in the pathogenesis of Vaccine-Induced Immune Thrombotic Thrombocytopenia (VITT). These specific germline alleles, which differ by a single amino acid (glutamine for *02, lysine for *03) at position 17, are associated with a specific somatic hypermutation (K31E) that allows for cross-reactivity with platelet factor 4 (PF4).

Antibody Proteomics and Production of Recombinant Anti-PF4 Antibodies

We affinity-purified antibodies from the serum of patients with VITT and used ChAdOx1 virion–coated magnetic beads to isolate antibodies binding to ChAdOx1 surface antigens. Next, we used PF4-coupled and pVII-coupled magnetic beads to purify anti-PF4 and anti-pVII antibodies from these serum samples; by the same approach, we also purified anti-penton, anti–protein IIIa (pIIIa), anti–protein V (pV), and anti–protein VI (pVI) antibodies (all adenovirus proteins). We separated the heavy and light chains of these affinity-purified antibodies by sodium dodecyl sulfate–polyacrylamide gel electrophoresis (SDS-PAGE) under reduced conditions, and used tandem mass spectrometry to determine the amino acid sequences of peptides without the use of an existing sequence database ("de novo sequencing") by means of mass spectrometry and International ImMunoGeneTics database matching with PEAKS Studio XPro software (Bioinformatics Solutions). Using the amino acid sequences of anti-PF4 antibodies obtained by mass spectrometry, we generated two recombinant anti-PF4 IgG1 antibodies (CR22046 and CR23004) by reverse engineering. In both recombinant antibodies, we also engineered back-mutations to the germline by changing the amino acid glutamic acid at position 31 of the light-chain hypervariable region to the germline amino acid, lysine (E31K-CR22046 and E31K-CR23004). For CR22046, we also generated a second antibody variant, changing the first aspartic acid at position 50 of the DDSD motif in the light chain complementarity-determining region 2 (LCDR2) encoded by alleles IGLV3-21*02 and *03 to the tyrosine encoded by alleles IGLV3-21*01 and *04 (D50Y-CR22046).

Assessment of Genes Encoding the Immunoglobulin Light-Chain Hypervariable Region

DNA purified from EDTA-anticoagulated peripheral blood was sequenced on an Illumina NovaSeq 6000 S4 Flowcell with 150-bp paired-end reads. The genes encoding the hypervariable region of the immunoglobulin light chain were retrieved from the genome.

Adenovirus and Adenovirus Domains

Microtiter plates were coated with the adenovirus vectors ChAdOx1-S and Ad26.COV2.S and with the recombinantly produced adenovirus proteins (GenScript) penton, pIIIa, pV, pVI, and pVII, and a peptide library of the ChAdOx1 pVII protein (Mimotopes; peptide sequences are provided in Fig. S2) to test binding of antibodies from the serum of patients with VITT, as well as binding of the recombinant anti-PF4 antibodies and their back-mutated counterparts.

Experiments in Animals

The recombinant antibody CR22046 or its back-mutated variant E31K-CR22046 was given intravenously (1.5 µg per gram of body weight per day) for 5 consecutive days to transgenic mice expressing human PF4 and FcγIIa receptors with an additional knockout of mouse PF4 on a C57BL/6J background (B6[Cg];SJL-Pf4tm1 Tg[PF4] Tg[FCGR2A]).

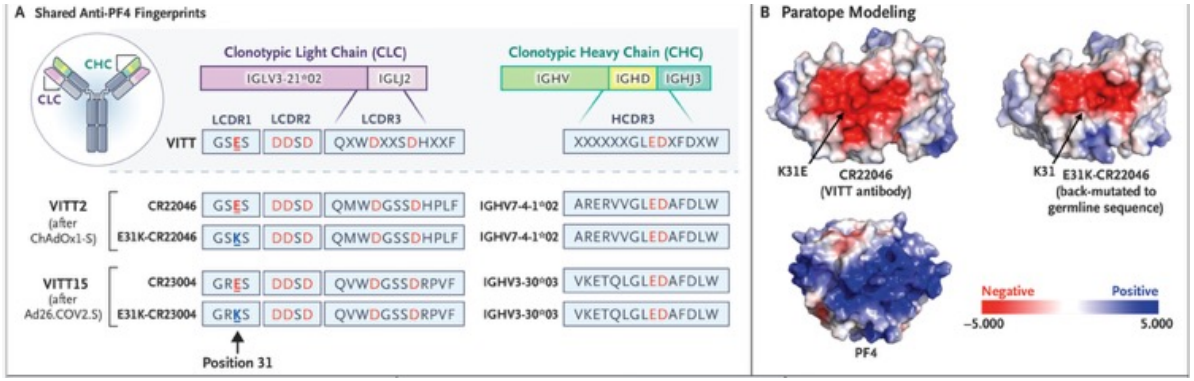

Characterization of Anti-PF4 Antibodies.

Panel A shows the anti–platelet factor 4 (PF4) fingerprints of the antibodies used in this study. The top of panel A shows consensus anti-PF4 antibody fingerprints from patients with classic vaccine-induced thrombocytopenia and thrombosis (VITT), specified by a single immunoglobulin lambda variable 3-21*02 (IGLV3-21*02) light chain paired with a single heavy chain that expresses a shared ED motif in the heavy-chain third complementarity-determining region (HCDR3). The bottom part of the panel (below the dashed line) shows the recombinant anti-PF4 antibody fingerprints derived from two patients with VITT after vaccination with ChAdOx1-S or Ad26.COV2.S. The upper sequence shows the fingerprint of the antibodies as derived from patient serum. Their anti-PF4 signatures are remarkably conserved; acidic (negatively charged) residues are shown in red. All the antibodies have a strongly acidic DDSD motif, a mutation resulting in a change from basic lysine to acidic glutamic acid at position 31 in light-chain complementarity-determining region 1 (LCDR1), and identical LCDR3 lengths with two equally spaced aspartic acid residues combined with an immunoglobulin lambda joining 2 (IGLJ2). Their heavy chains are of identical HCDR3 lengths (a marker of clonal sharing) with an acidic ED motif rearranged with an immunoglobulin heavy joining 3 (IGHJ3). Anti-PF4 antibodies are made up of distinct immunoglobulin heavy variable (IGHV) subfamilies. The lower sequence shows the fingerprint of the recombinant antibodies in which the somatic hypermutation of glutamic acid at position 31 of LCDR1 has been back-mutated to the germline lysine (E31K-CR22046 and E31K-CR23004). Data for Patient VITT2 were published previously. **Panel B** shows representative paratopes modeled with AlphaFold3. The structures represent the heavy- and light-chain variable domains of a VITT anti-PF4 antibody induced by adenoviral vector–based vaccination against coronavirus disease 2019 (Covid-19), along with its variant back-mutated to the germline sequence (IGLV3-21 with a lysine at position 31). The antibody variable domains and PF4 tetramer (Protein Data Bank code 1RHP [www.rcsb.org/structure/1RHP]) were visualized with PyMoL. The key indicates the surface electrostatic potential as calculated with APBS (Adaptive Poisson–Boltzmann Solver) software, which is expressed as the kinetic energy at a given temperature divided by the elementary charge (kT/e) and ranges from −5.000 to 5.000; the colors correspond to acidic (negatively charged; red) and basic (positively charged; blue) amino acid residues. The acidic amino acid residues from heavy and light chains form the PF4-binding paratopes. The exchange of glutamic acid with the germline-encoded lysine at position 31 (E31K) results in a major alteration of the paratope, disrupting its negative charge by removing an acidic residue that is predicted to bind to basic region of PF4.

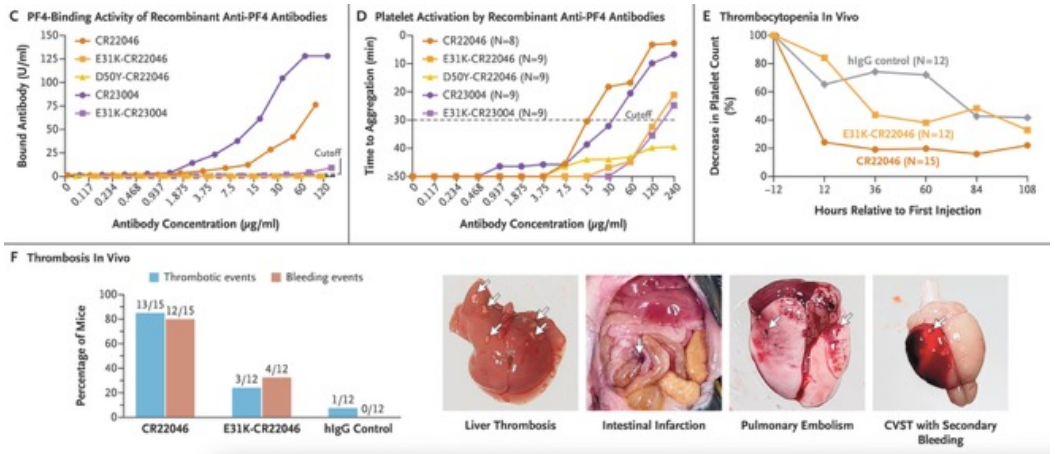

Panel C shows PF4-binding activity of the recombinant anti-PF4 antibodies derived from the two patients with VITT. CR22046 and CR23004 were found to bind in a concentration-dependent fashion to PF4 (anti-PF4 antibody chemiluminescence assay; Werfen) but not to PF4–heparin complexes (Fig. S3) in two chemiluminescence assays at concentrations of 0.117 to 120 µg per milliliter. Antibody concentrations are plotted on a $\log_2$ scale. In contrast, their back-mutated counterparts, E31K-CR22046 and E31K-CR23004, in which the glutamic acid at position 31 of the hypervariable region of the light chain was back-mutated to lysine (germline DNA sequence), lost their PF4-binding capacity. This was also observed for the D50Y-CR22046 variant, in which we changed the allele sequence from IGLV3-21*02 or *03 to IGLV3-21*01 or *04 by targeted mutation. Symbols below the cutoff (2.6 U per milliliter) might partially overlap. **Panel D** shows platelet activation by recombinant anti-PF4 antibodies. When incubated with washed platelets, CR22046 and CR23004 activated platelets in a dose-dependent manner, whereas their back-mutated counterparts E31K-CR22046 and E31K-CR23004, as well the D50Y-CR22046 variant, did not, up to a concentration of 120 µg per milliliter. The dashed line shows the cutoff of the functional assay. The mean values of eight or nine different donor platelets are shown to enable readability. Antibody concentrations diluted in serum (x axis) are plotted on a $\log_2$ scale. Individual data points are shown in Figure S6. **Panel E** shows the mean percent decrease in platelet counts in mice transgenic for human PF4 and FcγIIa receptors with knockout of mouse PF4 on a C57BL/6J background; mice received 1.5 µg per gram of body weight per day for 5 consecutive days of CR22046, its back-mutated variant E31K-CR22046, or human IgG (hIgG) control. Because euthanasia was performed during the course of the experiments, data were not measured for all mice at later time points. An overview of the exact numbers of mice in each group contributing to the different measurement time points is provided in Figure S7. The delayed decrease in the platelet count in the control animals was caused by frequent blood sampling and also occurred if only saline was given in the experiment. The graph in **Panel F** shows the percentage of mice with macroscopic thrombosis or bleeding and representative images of liver, intestines, lung, and brain. Of the 15 mice that received CR22046, 13 (87%) had thrombotic complications (8 mice had thromboses at multiple sites). Secondary cerebral hemorrhage was caused by cerebral venous sinus thrombosis. Of the 12 mice that received the back-mutated E31K-CR22046 variant, only 3 had thrombotic complications (1 mouse had multiple thromboses in the liver and cerebral venous sinus, and 2 had pulmonary embolism). CVST denotes cerebral venous sinus thrombosis.

VITT antibodies are monoclonal
pVII antibodies are polyclonal

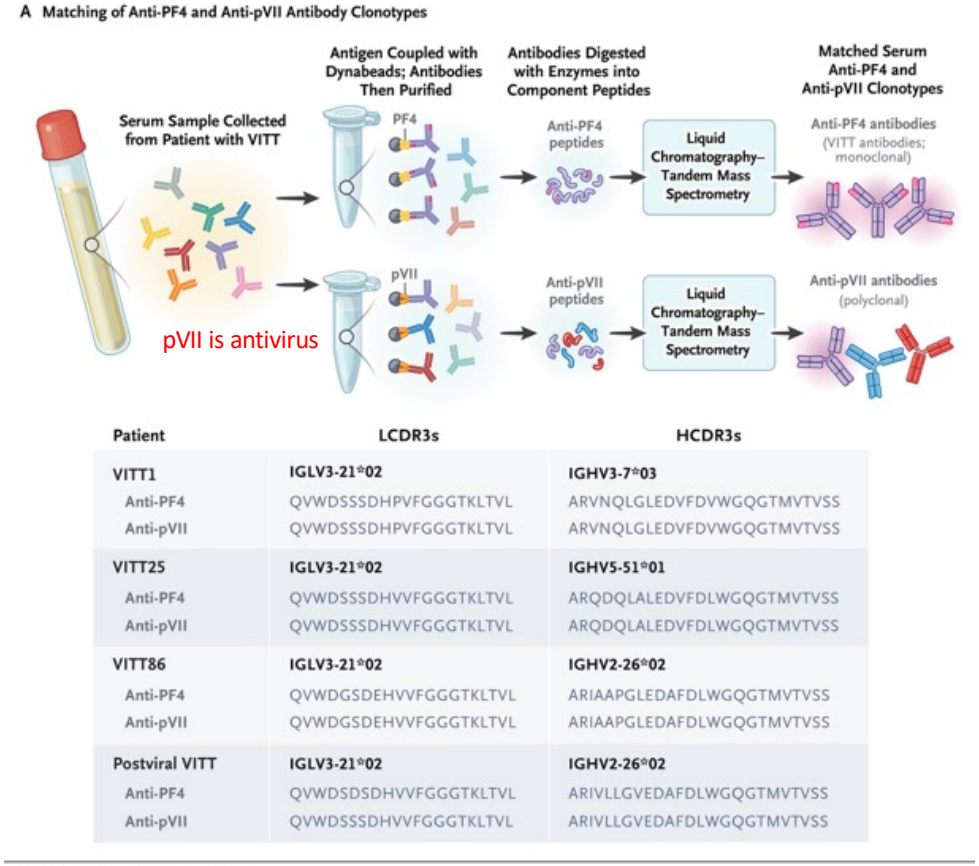

Patient	LCDR3s	HCDR3s
VITT1	IGLV3-21*02	IGHV3-7*03
Anti-PF4	QVWDSSSDHPVFGGGTKLTVL	ARVNQLGLEDVFDVWGQGTMVTVSS
Anti-pVII	QVWDSSSDHPVFGGGTKLTVL	ARVNQLGLEDVFDVWGQGTMVTVSS
VITT25	IGLV3-21*02	IGHV5-51*01
Anti-PF4	QVWDSSSDHVVFGGGTKLTVL	ARQDQLALEDVFDLWGQGTMVTVSS
Anti-pVII	QVWDSSSDHVVFGGGTKLTVL	ARQDQLALEDVFDLWGQGTMVTVSS
VITT86	IGLV3-21*02	IGHV2-26*02
Anti-PF4	QVWDGSDEHVVFGGGTKLTVL	ARIAAPGLEDAFDLWGQGTMVTVSS
Anti-pVII	QVWDGSDEHVVFGGGTKLTVL	ARIAAPGLEDAFDLWGQGTMVTVSS
Postviral VITT	IGLV3-21*02	IGHV2-26*02
Anti-PF4	QVWDSDSDHVVFGGGTKLTVL	ARIVLLGVEDAFDLWGQGTMVTVSS
Anti-pVII	QVWDSSSDHVVFGGGTKLTVL	ARIVLLGVEDAFDLWGQGTMVTVSS

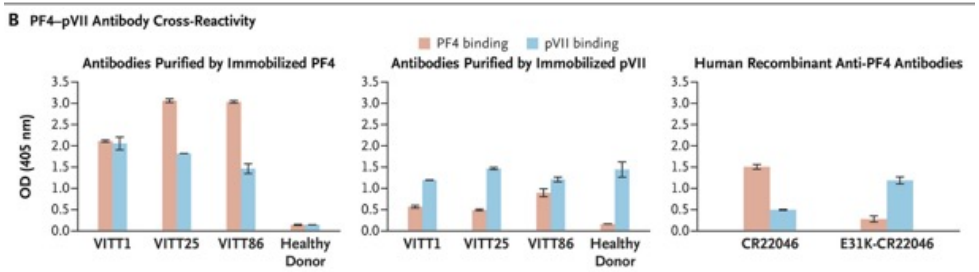

Serum Anti-PF4 and Anti-pVII Clonotype Analyses and Immune Cross-Reactivity.

Panel A shows matching of anti-PF4 and anti–adenovirus protein VII (pVII) antibody clonotypes. Specific antibodies purified from serum obtained from patients with VITT with PF4- or pVII-coupled Dynabeads were digested with enzymes to generate peptides for liquid chromatography–tandem mass spectrometry. The matched serum anti-PF4 and anti-pVII clonotypes were identified by heavy- and light-chain complementarity determining region 3 (HCDR3 and LCDR3, respectively) clonotypic barcodes. Data on the patient with postviral VITT were published previously (Patient 1 in Wang et al.[9]). Panel B shows two-way immune cross-reactivity of bead-purified anti-PF4 IgGs, anti-pVII IgGs, or human recombinant anti-PF4 antibodies derived from serum from patients with VITT with pVII and PF4 antigens by enzyme-linked immunosorbent assay. Serum from a healthy recipient of the ChAdOx1-S vaccine was included as the healthy donor sample. Boxes indicate the means, and I bars indicate the standard deviations. OD denotes optical density.

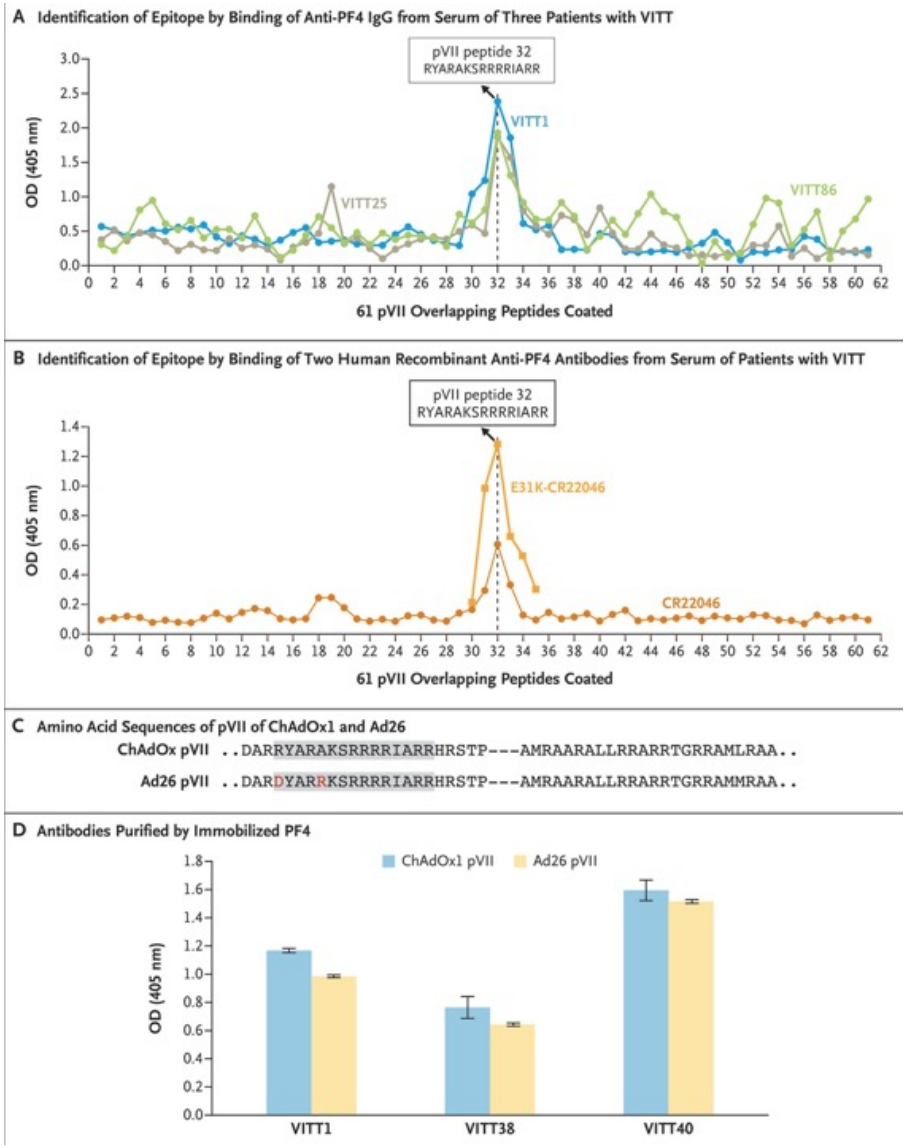

Identification of the pVII Epitope.

A set of 15-mer overlapping peptides (61 in total) with an offset every 3 amino acids relative to the ChAdOx1 pVII sequence was produced and coated to a microtiter plate. The mimicking pVII epitope was identified as a 15-mer linear peptide epitope (indicated within the rectangle in Panels A and B). Panel A shows binding of anti-PF4 IgG purified from serum samples from three patients with VITT, and Panel B shows binding of human recombinant anti-PF4 antibody CR22046, derived from the serum of one patient with VITT, and its counterpart back-mutated to germline (E31K-CR22046). (Amino acid sequences of these overlapping pVII peptides are shown in Fig. S2.) Panel C shows the identified pVII epitope (peptide 32, shaded in gray), which is highly conserved, with nearly identical amino acid sequences in pVII of ChAdOx1 and Ad26. (The two amino acids that differ are highlighted in red.) Accordingly, as shown in Panel D, anti-PF4 antibodies purified from VITT serum bind with similar strength to both peptides from different adenovirus species, regardless of whether VITT occurred after vaccination with ChAdOx1-S (VITT1) or Ad26.COV2.S (VITT38 and VITT40). Boxes indicate the means, and I bars indicate the standard deviations. Figure S8 shows binding of the recombinant antibody CR23004 and its counterpart back-mutated to germline E31K-CR23004, against PF4, ChAdOx1 pVII, and the pVII peptides Ad26 pVII and ChAdOx1 pVII.

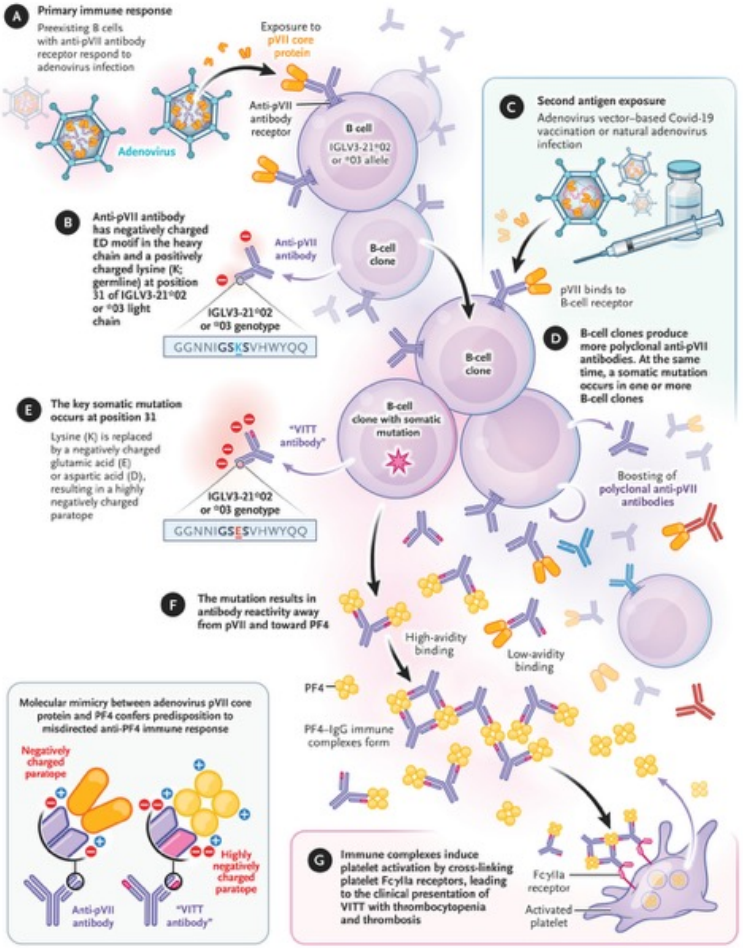

Immunopathophysiology of VITT.

Molecular mimicry between the adenoviral core protein pVII and PF4, combined with a specific somatic hypermutation transforming an anti-pVII immune response into a misdirected anti-PF4 immune response, is a fundamental pathobiologic mechanism of VITT. The primary antigen exposure occurs when a patient with the genetic predisposition conferred by allele IGLV3-21*02 or *03 encoding the hypervariable region of the immunoglobulin light chain comes into contact with numerous viral proteins, including pVII, during adenovirus infection. The resulting anti-pVII antibodies have the germline sequence of the IGLV3-21*02 or *03 genotype, with a positively charged lysine at position 31 and a negatively charged ED binding motif of the heavy-chain hypervariable region. The second antigen exposure occurs at the time of adenovirus vector–based Covid-19 vaccination (or natural adenovirus infection [not shown]). The vaccine contains adenoviral proteins, including pVII; pVII binds to the preexisting B-cell receptor and boosts antibody production. Boosting causes several B-cell clones to produce polyclonal anti-pVII antibodies. At the same time, a rare somatic mutation (or mutations) in one or a few B-cell clones occurs (alternatively, a preexisting low-level anti-pVII antibody clone harboring the K31E mutation rapidly expands after vaccination [not shown]). The key somatic mutation occurs at position 31 — a positively charged lysine is replaced by a negatively charged glutamic acid or aspartic acid, which results in a highly negatively charged paratope. This mutation results in antibody reactivity away from pVII and toward PF4. These cross-reacting anti-PF4 antibodies ("VITT antibodies") now bind with high avidity to PF4, forming large PF4–IgG immune complexes, while binding to pVII remains low-avidity. These immune complexes induce platelet activation by cross-linking platelet FcγIIa receptors, which leads to the typical clinical presentation of VITT with thrombocytopenia and thrombosis at unusual sites. This model explains the clinical features of VITT that include the apparent secondary (boosted) immune response with explosive onset of IgG anti-PF4 antibodies as early as 5 days after vaccination; the very low frequency of VITT (much rarer than heparin-induced thrombocytopenia) is due to the requirement of a specific somatic mutation in a B cell specific for a restricted epitope (reflected by the sequence RYARAKSRRRRIARR) on the background of a specific IGLV haplotype.

Discussion

Molecular mimicry between the adenoviral core protein pVII and PF4, combined with somatic hypermutation transforming an anti-pVII immune response to a misdirected anti-PF4 immune response, is a fundamental pathobiologic mechanism of VITT. Immune cross-reactivity between pVII and PF4 results from shared, highly positively charged epitopes with structural similarity in the alpha helixes of both proteins. Nonetheless, production of pathogenic, high-avidity anti-PF4 reactive antibodies requires additional specific genetic features. The first prerequisite is a genetic predisposition conferred by allele IGLV3-21*02 or *03 in the gene encoding the hypervariable region of the immunoglobulin light chain. This is supported by our finding that the allele was present in 99 of 100 patients with VITT (as compared with the expected background frequency of 20 to 60%, depending on the ethnic group). The second prerequisite is a somatic hypermutation that changes a positively charged lysine to a negatively charged glutamic acid at position 31 of the light-chain hypervariable region of the anti-pVII antibodies. We confirmed this previously described typical fingerprint of the hypervariable IgG regions in all 21 patients with VITT in our study. The results of this study are relevant for strategies to make adenovirus vector–based vaccines safer. This vaccination platform has major advantages — for example, affordability for health care systems in low- and middle-income countries and enabling of rapid vaccine provision in the case of a new pandemic. Identification of molecular mimicry between pVII and PF4 as a fundamental upstream immune mechanism of VITT may now pave the way for developing safer adenoviral vector–based vaccines — ones in which pVII is replaced by analogues that do not activate B cells specific for the epitope on pVII that has structural similarities to PF4.

Before EPO, iron overload in dialysis patients was common.
Mucormycosis in dialysis patients is a rare but highly fatal (up to 86% mortality) opportunistic fungal infection, often linked to iron overload treatment (deferoxamine) rather than just immunocompromise. It commonly presents as disseminated (44%) or rhinocerebral (31%) disease. Rapid diagnosis and treatment with liposomal Amphotericin B are critical.

Key Findings & Risks

- **Deferoxamine Connection:** Roughly 78% of reported dialysis-related cases were associated with the use of deferoxamine to treat aluminum toxicity. The drug creates iron-rich conditions favoring *Rhizopus* fungi.
- **High Mortality:** Diagnosis is often delayed, with 61% of cases only confirmed at autopsy.
- **Types:** Primarily disseminated (spread throughout the body) and rhinocerebral (nose/brain), though gastrointestinal cases occur, particularly in peritoneal dialysis patients.
- **Symptoms:** Fever, abdominal pain/bloody stool (GI), or nasal/eye symptoms (rhinocerebral).

Damals entwickelten Dialysepatienten Eisenüberlastung von Transfusionen; EPO gab es nicht. Nach Deferoxamin gab es Mucormyokose

Mucormycosis

Summary

Mucormycosis is a rapidly progressive, invasive fungal infection that affects patients who are severely immunocompromised, as well as patients with diabetes and persons with immunocompetence who have major trauma. Mucormycosis manifests in several clinical forms, including sino-orbital, rhinocerebral, sinopulmonary, gastrointestinal, cutaneous, musculoskeletal, osteoarticular, and disseminated mucormycosis, as well as single-organ disease. Although mucormycosis is often lethal, early intervention reduces mortality. Successful treatment depends on early detection and staging of the disease, timely initiation of antifungal therapy, surgical resection of infected tissue, reversal of immunodeficiencies, and correction of metabolic abnormalities. Liposomal amphotericin B is the preferred agent for initial antifungal therapy, with oral triazoles as alternative agents. Research on rapid molecular diagnostic strategies, new antifungal agents, host-directed immune augmentation, antivirulence immune therapeutics, and risk-based stratification to inform management of disease may substantially improve outcomes in patients with this highly destructive mycosis.

KEY POINTS

Mucormycosis

- Mucormycosis is a rapidly progressive and often lethal invasive fungal infection that affects patients who are severely immunocompromised, as well as patients with diabetes and persons with immunocompetence who have major trauma.
- Mucormycosis manifests in several clinical forms, including sino-orbital, rhinocerebral, sinopulmonary, gastrointestinal, cutaneous, musculoskeletal, osteoarticular, and disseminated mucormycosis, as well as single-organ disease.
- A high index of suspicion in the appropriate clinical context and subsequent microbiologic or histopathological confirmation are necessary for early intervention, which reduces mortality.
- Successful treatment depends on five pillars of intervention: early detection and staging of the disease, timely initiation of antifungal therapy, surgical resection of infected tissue, reversal of immunodeficiencies, and correction of metabolic abnormalities.
- Liposomal amphotericin B is the preferred agent for initial antifungal therapy. Oral triazoles (i.e., isavuconazole and posaconazole) are alternative agents, especially for step-down therapy.
- Research on rapid molecular diagnostic strategies, new antifungal agents, host-directed immune augmentation, antivirulence immune therapeutics, and risk-based stratification to inform management of disease may substantially improve outcomes in patients with this highly destructive mycosis.

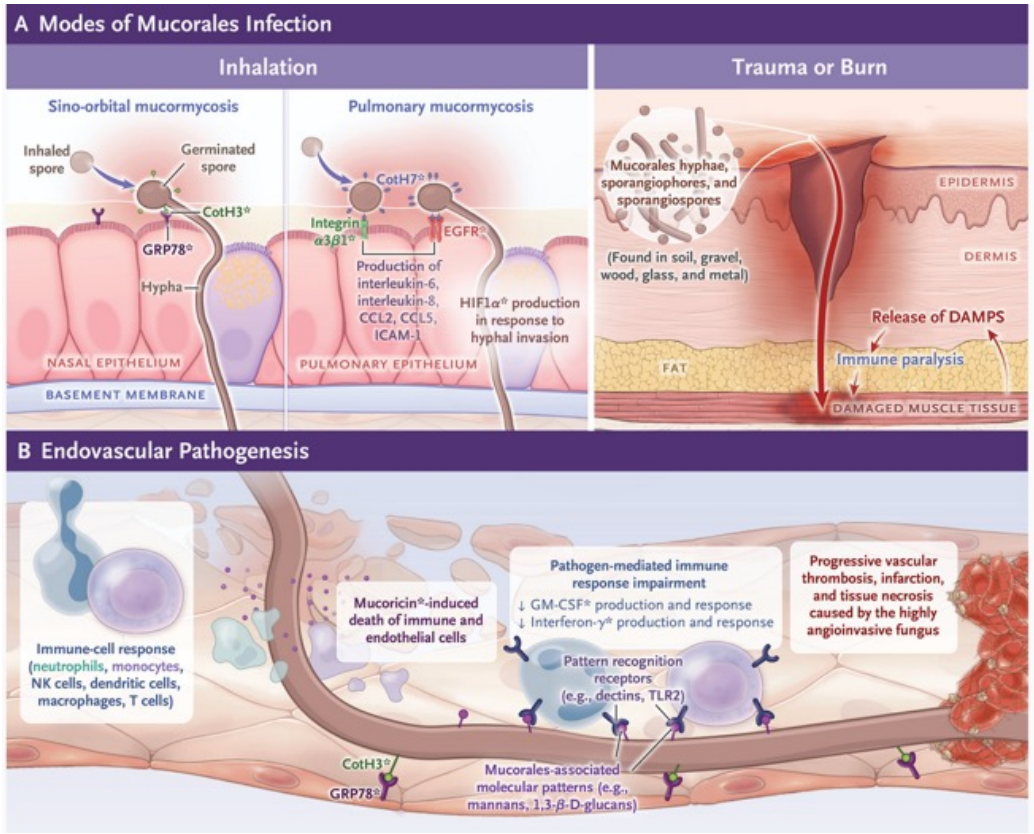

Pathogenesis of Mucormycosis, Host Defenses, and Potential Future Therapeutic Targets.

Mucorales sporangiospores released into the air from sporangia are inhaled, and the sporangiospore coat protein CotH3 binds to glucose-regulated protein 78 (GRP78) on the pseudostratified columnar epithelial cells of the upper respiratory tract, where the sporangiospores may germinate into hyphae to invade nasal airways and sinuses (Panel A). Sporangiospores, by means of another coat adhesin (CotH7), also bind to epidermal growth factor receptor (EGFR) and integrin α3β1 receptor on pulmonary alveolar epithelial cells of the lower respiratory tract, which triggers a downstream transcriptional response involving cytokines (interleukin-6 and interleukin-8), chemokines (CCL2 and CCL5), and intercellular adhesion molecule 1 (ICAM-1). Hyphal invasion also triggers production of hypoxia-inducible factor 1α (HIF1α) and release of proinflammatory cytokines. In wound-related mucormycosis, traumatic inoculation of fungal elements (found on the surfaces of rocks, wood, glass, and metal) into damaged tissue allows for the development of infection in a host with immune paralysis due to trauma. The release of endogenous host-derived molecules known as damage-associated molecular patterns (DAMPs) reduces phagocytosis, impairs chemotaxis, and induces immune paralysis. Mucoricin released by the invading hyphae induces death of immune and endothelial cells, which results in tissue necrosis and accelerates endovascular thrombosis, ischemia, and infarction (Panel B).

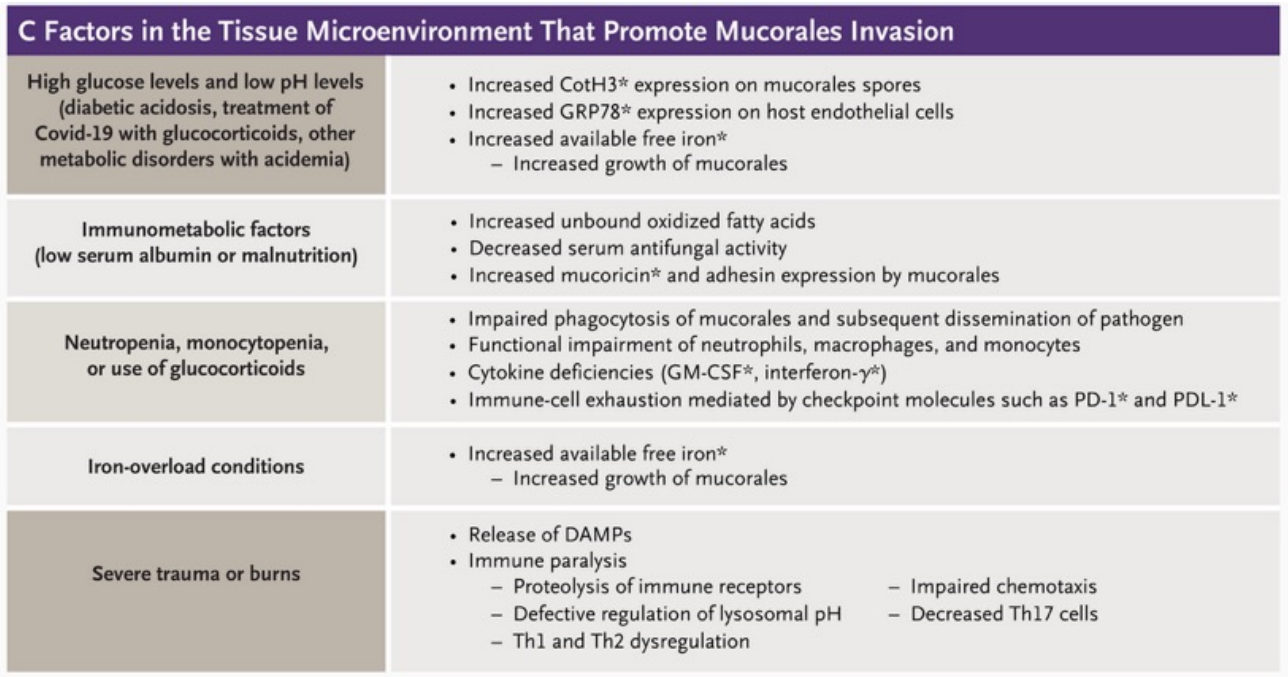

C Factors in the Tissue Microenvironment That Promote Mucorales Invasion	
High glucose levels and low pH levels (diabetic acidosis, treatment of Covid-19 with glucocorticoids, other metabolic disorders with acidemia)	• Increased CotH3* expression on mucorales spores • Increased GRP78* expression on host endothelial cells • Increased available free iron* – Increased growth of mucorales
Immunometabolic factors (low serum albumin or malnutrition)	• Increased unbound oxidized fatty acids • Decreased serum antifungal activity • Increased mucoricin* and adhesin expression by mucorales
Neutropenia, monocytopenia, or use of glucocorticoids	• Impaired phagocytosis of mucorales and subsequent dissemination of pathogen • Functional impairment of neutrophils, macrophages, and monocytes • Cytokine deficiencies (GM-CSF*, interferon-γ*) • Immune-cell exhaustion mediated by checkpoint molecules such as PD-1* and PDL-1*
Iron-overload conditions	• Increased available free iron* – Increased growth of mucorales
Severe trauma or burns	• Release of DAMPs • Immune paralysis – Proteolysis of immune receptors – Defective regulation of lysosomal pH – Th1 and Th2 dysregulation – Impaired chemotaxis – Decreased Th17 cells

Polymorphonuclear neutrophils and monocytes recognize early germinated sporangiospores by means of pattern recognition receptors (e.g., toll-like receptor 2 [TLR2]) that detect mucorales-associated molecular patterns (e.g., 1,3-β-d-glucans exposed on hyphal structures). Intrinsic host colony-stimulating factors such as granulocyte–macrophage colony-stimulating factor (GM-CSF) and interferon-*γ* further contribute to augmentation of innate host defenses against the invading hyphae, which in turn dampen immune responses. Factors in the tissue microenvironment that increase susceptibility to mucorales invasion are listed with the predominant mechanisms associated (Panel C). Asterisks indicate potential future therapeutic targets. Covid-19 denotes coronavirus disease 2019, NK natural killer, PD-1 programmed cell death protein 1, PD-L1 programmed death ligand 1, Th1 type 1 helper T, Th2 type 2 helper T, and Th17 type 17 helper T.

Risk Factors for Mucormycosis and Clinical Manifestations of Disease.

Clinical Form	Common Risk Factors	Symptoms	Clinical Features and Findings on Diagnostic Imaging	Comments
Sino-orbital[26,27]	Diabetes† Hematologic cancers Hematopoietic-cell transplantation Solid-organ transplantation Severe aplastic anemia Covid-19‡ Prolonged use of high-dose glucocorticoids	Congestion Localized sinus pain Odontogenic pain in cases of maxillary-sinus infection Nasal discharge Headache	Infection of nasal turbinates: ulcerations, eschars Maxillary-sinus infection: palatal ischemia or necrosis and involvement of the molars and premolars Ethmoid-sinus infection: hyposmia or anosmia; extension through the lamina papyracea bone into the orbit with entrapment of the medial rectus muscle and other extraocular muscles and progression to orbital apex syndrome	Sphenoidal mucormycosis may manifest with referred pain in the vertex of the skull. Sino-orbital mucormycosis is a medical and surgical emergency. Early examination and reexamination with imaging and otolaryngologic evaluation are important.
Rhinocerebral[26,27]	Diabetes† Hematologic cancers Hematopoietic-cell transplantation Solid-organ transplantation Severe aplastic anemia Covid-19‡ Prolonged use of high-dose glucocorticoids	Diplopia related to cranial nerve deficits Seizures	Focal neurologic deficits Extension from ethmoid sinuses and frontal sinuses into veins draining into the cavernous sinus, with damage to cranial nerves III, IV, V1, V2, and VI and the internal carotid artery	Frontal sinus mucormycosis may be complicated by direct extension into frontal lobes, which is indicated by meningeal enhancement of tissue invasion. Rhinocerebral mucormycosis is a medical and surgical emergency. Early examination and reexamination with imaging and otolaryngologic evaluation are important.
Sinopulmonary[28-31]	Hematopoietic-cell transplantation Solid-organ transplantation Severe aplastic anemia Covid-19‡ Prolonged use of high-dose glucocorticoids	Cough Dyspnea Pleuritic pain	Persistent fever refractory to empirical antibacterial therapy Hemoptysis Multiple pulmonary nodules with the halo sign or reversed halo sign on CT scan Intrathoracic extension of disease into the pleura, ribs, diaphragm, mediastinum, and pericardium	Angioinvasive properties lead to necrotizing pneumonia with pulmonary infarction and hemorrhage. Tracheobronchitis, bronchial obstruction, severe or fatal hemoptysis, and cavitary fungus ball are rare manifestations. The presence of a reversed halo sign is more highly suggestive of pulmonary mucormycosis than the conventional halo sign, which is associated with pulmonary aspergillosis and infection with other angioinvasive molds in patients with hematologic cancer.
Cutaneous and musculoskeletal[32-34]	Trauma Burns Blast injuries Severe natural disasters (e.g., tornadoes, tsunamis, floods, earthquakes) Premature birth Immunosuppression	Local pain at the site of injury	Cutaneous ulcerations Brown-black eschars with firm, woody consistency and deep necrotizing extension into fascia, tendon, and muscle	This form occurs in infants who are born prematurely and exposed to contaminated bed linens; it also occurs in patients who are immunocompromised, especially during neutropenia, as the result of cutaneous inoculation from soil or plant sources. CT scans, MRI, and surgical exploration typically show that the degree of subcutaneous infection is much deeper and more extensive than what can be detected on physical examination. The differential diagnosis includes cutaneous aspergillosis, fusariosis, and ecthyma gangrenosum caused by *Pseudomonas aeruginosa* and other gram-negative bacilli.
Osteoarticular[35]	Severe trauma Blast injuries Intravenous drug use Immunosuppression	Local pain at the site of injury Tenderness Erythema Limited range of motion	Tenderness with overlying cellulitis Lytic bone destruction at the site of direct or hematogenous inoculation	Infection of bone and joints may occur as a result of direct traumatic inoculation after severe trauma, blast injuries, or intravenous drug use. Osteoarticular mucormycosis also occurs in patients who are immunocompromised by means of direct extension from infected foci or hematogenous dissemination. In view of the broad differential diagnosis, which includes cancer and several other infectious entities, bone biopsy and cultures are indicated.
Gastrointestinal[36,37]	Premature birth Severe malnutrition Immunosuppression Pica	Abdominal pain Nausea Vomiting Hematemesis Abdominal tenderness Hematochezia Melena Abdominal distension	Gastrointestinal hemorrhage, obstruction, perforation, or infarction Intraabdominal dissemination	Gastrointestinal mucormycosis should be distinguished from gastrointestinal basidiobolomycosis.¶ Patients who are immunocompromised may become infected after ingesting contaminated food or herbal medicinal products containing mucorales species. This form is commonly diagnosed post mortem.
Disseminated[38]	Hematologic cancers Hematopoietic-cell transplantation Solid-organ transplantation Severe aplastic anemia Endocarditis (may be associated with illicit drug use)	Focal seizures	Focal neurologic deficits arising from involvement of the central nervous system	Involvement of the central nervous system is common. Other affected sites (alone or in combination with other organs) may include the lungs, spleen, kidneys, and thyroid. Dissemination most commonly arises from the lung but may also arise from a cutaneous lesion.
Early manifestations	High pretest probability that mucormycosis will develop	Diplopia	Periorbital cellulitis Focal palatal necrosis Necrotic wounds (consistent with angioinvasion)	These early sentinel clinical manifestations call for urgent assessment.

Laboratory Tools for Diagnosis of Mucormycosis.

Laboratory Method	Description
Direct examination[45,46]	On direct microscopic examination of a wet mount with potassium hydroxide or fluorescence staining, such as calcofluor or Blankophor, mucorales species typically have ribbonlike, nonseptated (coenocytic) or sparsely septated hyphae that are broad (7 to 15 μm in diameter) with nondichotomous branching. These features help narrow the differential diagnosis by ruling out infection with other pathogenic molds, including *Aspergillus* spp., *Fusarium* spp., and *Scedosporium* spp., which typically appear as slender, dichotomously branching, septated hyphae.
Culture[45-47]	Mucorales species typically grow rapidly to fill the petri dish as a floccose colony on Sabouraud's glucose agar at 25 to 37°C. Recovery of organisms may be enhanced by culturing at 37°C. *Lichtheimia corymbifera* (formerly known as *Absidia corymbifera*) and the most frequently encountered *Rhizopus* spp. and *Mucor* spp. have microscopically distinctive patterns of sporangiophores, sporangia, sporangiospores, and rhizoids (if present). *Cunninghamella* spp. have characteristic denticles and sporangiola instead of sporangiospores.
Antifungal susceptibility testing[48]	Because there are currently no established interpretive breakpoints by which to assess susceptibility, the value of minimum inhibitory concentrations in the management of mucormycosis is limited. Data from in vitro, preclinical animal models and clinical correlation indicate that echinocandins, flucytosine, fluconazole, itraconazole, and voriconazole are not active against mucorales species. Amphotericin B, isavuconazole, and posaconazole are active against the medically important mucorales species in vivo and clinically.
Histopathological analysis[49-51]	Detection of the characteristic ribbonlike, nonseptated or sparsely septate hyphae of the mucorales species in tissue samples with periodic acid–Schiff and Grocott–Gomori methenamine silver stains unequivocally establishes a diagnosis of mucormycosis in the corresponding site. Delays in time to detection may result from formalin fixation, paraffin embedding, sectioning, and staining. Immunohistochemical techniques and fluorescence in situ hybridization further establish a microbiologic diagnosis.
MALDI-TOF MS[52,53]	Recovery of an organism allows rapid molecular identification by MALDI-TOF MS. The informatics database of the MALDI-TOF MS instrument allows clinical laboratories to identify a wide range of medically important mucorales species.
Nucleic acid amplification testing[54-58]	Molecular detection of mucormycosis may be performed with whole blood or BAL fluid. Quantitive PCR assays with primer–probe sets that target the 18S ribosomal RNA have been shown to have the ability to detect *Rhizopus arrhizus*, *Mucor circinelloides*, *L. corymbifera*, and *Cunninghamella bertholletiae* in BAL fluid, plasma, and serum. Nucleic acid amplification assays that are commercially available in Europe, as well as proprietary assays, detect circulating mucorales DNA from BAL fluid, serum, and whole blood. Analysis of cell-free DNA from plasma or serum with the use of a PCR assay offers a new strategy that improves analytical sensitivity over that obtained with traditional whole-blood extractions.
Metagenomic analysis[59,60]	The usefulness of metagenomic analysis of cell-free DNA for the diagnosis of mucormycosis is not well defined. In a recent prospective, multicenter, observational study that involved patients with suspected pneumonia who were immunocompromised and underwent bronchoscopy for evaluation of pneumonic infiltrates of unknown cause, the use of plasma microbial cell-free DNA sequencing significantly increased diagnostic yield as compared with standard-care testing. Among the six fungal pathogens detected only by metagenomic sequencing, two mucorales species were identified.

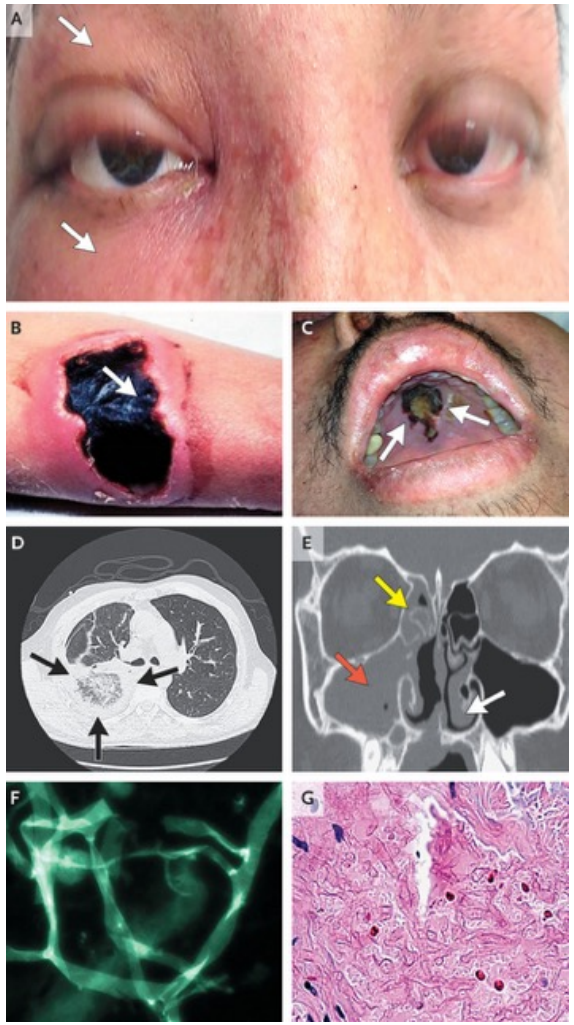

Direct Examination and CT Imaging in Mucormycosis. Sino-orbital mucormycosis is associated with right periorbital cellulitis (Panel A, arrows) and ophthalmoplegia. Cutaneous mucormycosis is characterized by blackened, raised eschars (Panel B, arrow). Lesions due to palatal mucormycosis are shown (Panel C, arrows). In pulmonary mucormycosis, a large reversed halo sign (Panel D, arrows) in the right lower lobe is characterized by a pulmonary infiltrate with a central ground-glass opacity that is circumscribed by denser air-space opacities. (Photo used with permission from Dr. Genovefa Papanicolaou.) Examples of imaging results in mucormycosis of the right maxillary sinus (Panel E, red arrow), right ethmoid sinus (yellow arrow), and left nasal turbinates (white arrow) are shown. Direct examination of sinus aspirate under fluorescence microscopy with calcofluor staining shows broad, ribbonlike hyphae with nondichotomous right-angled branching typical of rhizopus (Panel F). Histopathological analysis of infected tissue with periodic acid–Schiff staining also shows broad, ribbonlike hyphae with nondichotomous right-angled branching (Panel G).

Future Directions in Mucormycosis Research.

Epidemiology	Performance of national and multinational prospective, population-based studies to investigate the incidence of mucormycosis and regional differences in disease Development of multicenter registries of mucormycosis cases to characterize evolving patient-specific risk factors, including diabetes, hematologic cancer, transplantation, trauma, receipt of critical care, and age, as well as outcomes Characterization of immunogenetic risk factors
Laboratory diagnosis	Development of new culture-independent biomarkers with the use of mucorales-specific PCR, cell-free DNA, metagenomics, and volatolomics Further characterization of existing molecular biomarkers for early detection of mucormycosis and correlation of fungal burden with outcome Development of point-of-care diagnostic tools for mucormycosis
Treatment	Development of biomarkers and functional imaging techniques (e.g., PET-CT) for determination of intensity and duration of antifungal therapy Development of new first-in-class antifungal agents Exploration of combination antifungal therapy Harnessing of host-directed immune therapeutics against mucormycosis Development of antivirulence-based therapeutics Elucidation of the effects of metabolic control on risk of mucormycosis and outcomes Characterization of the mechanisms of hyperbaric oxygen therapy and its potential role in treatment of mucormycosis Clarification of the timing and extent of surgery Assessment of the role of local administration (by nebulization or retrobulbar or topical application) of antifungal agents Development of new regulatory pathways and adaptive clinical trials
Outcomes	Definition of the role of diagnostic imaging and biomarkers in outcomes Delineation of the role of coexisting conditions in risk stratification for outcomes Incorporation of patient-reported outcomes into clinical-trial assessments of outcomes Incorporation of desirability-of-outcome ranking into clinical-trial end points

New Directions for Improving Outcomes

Variables that influence outcomes in mucormycosis include the stage or location of disease, early diagnosis of invasive disease, timely initiation of antifungal therapy, surgical resection of tissue with medically intractable infection, occurrence of relapsed leukemia, allogeneic hematopoietic-cell transplantation, dissemination of infection, the involvement of the central nervous system, and reversal of immunodeficiencies, which involves remission of underlying hematologic cancers when present. The future research agenda in mucormycosis will be driven by exciting new developments in early diagnosis, new antifungal compounds, virulence targets, and host-directed immune adjunctive therapy Laboratory diagnosis of mucormycosis may be improved by expanded availability and use of new culture-independent techniques and tools, including polymerase-chain-reaction analysis of cell-free DNA, metagenomic analysis, new antigen assays, and point-of-care devices, such as loop-mediated isothermal amplification assays. In cases of mucormycotic wound infection, topical therapy may be beneficial. Dakin's solution (0.025% sodium hypochlorite) is recommended for topical treatment of mucormycotic combat wounds, but therapeutic advances may be possible with new clinically relevant murine models of musculocutaneous mucormycosis and blast injury.

Polyclonal antibodies that target CotH3 proteins protect neutropenic and diabetic ketoacidotic mice from mucormycosis. Polyclonal antibodies against mucoricin prolong survival in mice with experimental mucormycosis. The future promises to bring combinatorial strategies of early detection in conjunction with the use of antivirulence, antifungal, and immunomodulatory agents, all in concert with efforts to reverse underlying immunodeficiencies and metabolic abnormalities.

Pulmonary Mucormycosis

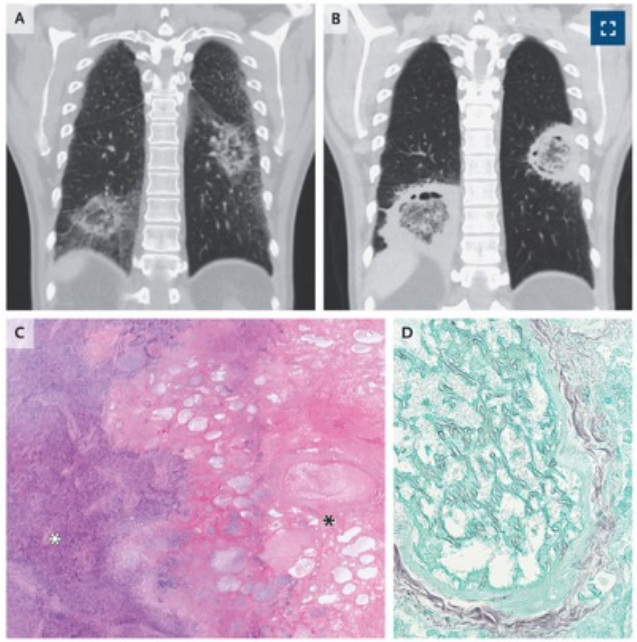

A 49-year-old man with acute myeloid leukemia who had been admitted to the hospital for induction chemotherapy was evaluated for prolonged neutropenic fever. On physical examination, crackles were heard at the lung bases. Computed tomography (CT) of the chest revealed rounded opacities with central ground-glass attenuation and ringlike peripheral consolidation in both lungs (Panel A, coronal view) — a finding known as the reversed halo sign that can occur with invasive fungal infections. Treatment with amphotericin B was started. A polymerase-chain-reaction (PCR) assay for mucorales species in bronchoalveolar lavage fluid was positive. After 2 weeks of treatment, repeat CT of the chest revealed increased attenuation of the ringlike peripheral consolidations and central cavitation of the opacities (Panel B, coronal view), findings consistent with neutrophil recovery. Surgical resection was performed. Histopathological analysis of the resected lung tissue showed central necrosis (Panel C, black asterisk; hematoxylin and eosin stain) surrounded by organizing pneumonia (Panel C, white asterisk). Intravascular hyphae were also seen (Panel D, Grocott's methenamine silver stain). PCR analysis of the resected tissue identified *Rhizomucor pusillus*, which confirmed the diagnosis of pulmonary mucormycosis. One week after surgery, the patient was discharged home with a prescription for isavuconazole for secondary prophylaxis. Two weeks later, he underwent allogeneic hematopoietic stem-cell transplantation.

Hepatic Angiosarcoma

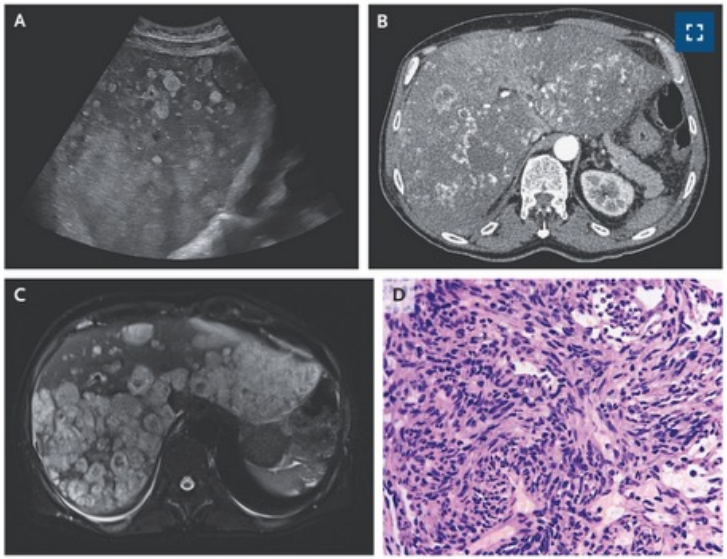

A 60-year-old man presented with a 15-day history of generalized weakness and right upper abdominal pain. A physical examination was notable for tender hepatomegaly. Laboratory testing showed mild elevations in aspartate aminotransferase and alanine aminotransferase levels. Abdominal ultrasonography revealed an enlarged liver with multiple hyperechoic nodules, resulting in diffuse disruption of the hepatic architecture (Panel A); these findings suggested an infiltrative vascular process. Computed tomography of the abdomen, performed after the administration of intravenous contrast material, revealed innumerable heterogeneous nodules and areas of necrosis and hemorrhage, which produced a mosaic pattern of enhancement (Panel B, arterial phase, axial view). Magnetic resonance imaging of the liver revealed multiple lesions with high signal intensity on the T2-weighted sequence (Panel C, axial view), a finding consistent with a vascular neoplasm. Histopathological examination of a needle-biopsy specimen of the liver showed proliferation of vasoformative and spindle-shaped cells (Panel D, hematoxylin and eosin stain). Immunohistochemical testing was strongly positive for endothelial markers ERG and CD31. A diagnosis of hepatic angiosarcoma — a rare, highly aggressive primary malignant vascular tumor of the liver — was made. Hepatic angiosarcoma is associated with exposure to vinyl chloride, arsenic, or anabolic steroids, which this patient did not have. One month after diagnosis, the patient died from rapidly progressive liver failure.

Case 5-2026: An 18-Year-Old Woman with Headache and Hypertension

An 18-year-old woman presented to the emergency department of this hospital because of worsening headache and hypertension. The patient had been in her usual state of health until 6 years before this presentation, when she began to note intermittent headaches, which her primary care physician diagnosed as both tension and migraine headaches. The headaches resolved after the administration of nonsteroidal antiinflammatory drugs (NSAIDs).

One year before, the patient had worsening daily headaches that usually occurred in the morning and, at times, woke her up from sleep. The headaches were described as bitemporal pain and throbbing with associated nausea, photophobia, and scintillating scotoma. The patient was referred to the pediatric neurology clinic of this hospital for evaluation. In the neurology clinic her blood pressure was 164/100 mm Hg, which was attributed to a headache at the time of the blood pressure reading. The gait and mental status were normal, and no motor or sensory deficits were present. The funduscopic examination showed sharp optic disks in both eyes; however, given the patient's medical history, increased intracranial pressure was clinically suspected. Magnetic resonance imaging (MRI) of the head was ordered, and a formal ophthalmologic examination was recommended, but neither was pursued at that time. Treatment with propranolol was initiated and helped to alleviate her symptoms, but it was discontinued after 2 months owing to insomnia and depression. Amitriptyline was prescribed, which also provided partial relief.

MRI of the head, performed after the administration of intravenous gadolinium-based contrast material, showed no evidence of infarction, thrombosis, hemorrhage, masses, or elevation of the optic nerve head. However, a funduscopic examination, performed after pupillary dilation at a local eye clinic, reportedly revealed papilledema. The patient subsequently underwent a lumbar puncture, which was notable for an opening pressure of 36 cm of water (normal range, 10 to 20) and a closing pressure of 10 cm of water after removal of 10 ml of cerebrospinal fluid (CSF). Analysis of the CSF showed normal cell counts and a normal total protein level. A diagnosis of idiopathic intracranial hypertension was made, and treatment was switched from topiramate to acetazolamide. A few days later, the patient presented to the pediatric emergency department of this hospital with an intensifying and debilitating headache. The headache was bitemporal with crushing pain and associated nausea and photophobia, and it was refractory to the administration of sumatriptan, ondansetron, and naproxen. The blood pressure was 207/143 mm Hg. An anteroposterior chest radiograph showed prominence of the perihilar vasculature with perihilar opacities in both lungs and peribronchial cuffing consistent with pulmonary edema. Treatment with lactated Ringer's solution, intravenous magnesium sulfate, and acetaminophen was initiated, and the headache abated. Owing to severe hypertension, a continuous infusion of nicardipine was initiated, and invasive hemodynamic monitoring was performed with the use of an intraarterial catheter placed in the left radial artery. The patient was admitted to the pediatric intensive care unit.

The oral temperature was 36.1°C, the blood pressure 170/74 mm Hg, the heart rate 102 beats per minute, the respiratory rate 22 breaths per minute, and the oxygen saturation 96%.

The plasma potassium level was 2.0 mmol per liter (normal range, 3.4 to 5.0), and the initial plasma creatinine level was 1.19 mg per deciliter (105 µmol per liter; reference range, 0.50 to 1.50 mg per deciliter [53 to 133 µmol per liter]), with improvement to 0.87 mg per deciliter (77 µmol per liter) after the administration of intravenous fluids; the baseline value had been reported at 0.60 mg per deciliter. Urinalysis showed 2+ proteinuria and a specific gravity of 1.001, with 640 mg of total protein excreted over 24 hours. The thyrotropin level was mildly elevated at 5.99 mIU per liter (reference range, 0.40 to 5.00), with normal free thyroxine levels. The plasma metanephrine and normetanephrine levels were within normal limits. The serum complement levels were normal, and antinuclear antibodies were not detected. Urine toxicology testing was negative for cocaine and amphetamines.

Variable	Reference Range, Adults†	On Initial Presentation
Hemoglobin (g/dl)	12.0–16.0	15.1
Hematocrit (%)	36.0–46.0	42.5
White-cell count (per µl)	4500–13,000	10,120
Platelet count (per µl)	150,000–450,000	350,000
Sodium (mmol/liter)	135–145	132
Potassium (mmol/liter)	3.4–5.0	2.0
Chloride (mmol/liter)	98–108	90
Carbon dioxide (mmol/liter)	23–32	26
Urea nitrogen (mg/dl)	8–25	16
Creatinine (mg/dl)	0.50–1.50	1.19
Aspartate aminotransferase (U/liter)	9–32	25
Alanine aminotransferase (U/liter)	7–33	23
Alkaline phosphatase (U/liter)	45–87	127
Total bilirubin (mg/dl)	<1.2	0.5
High-sensitivity troponin T (ng/liter)	0–9	43
Erythrocyte sedimentation rate (mm/hr)	0–19	48
C-reactive protein (mg/liter)	<8	44
Thyrotropin (mIU/ml)	0.4–5.0	5.99

Apparently acid-base balance was not so important. The hypokalemia was not further evaluated with urine studies.

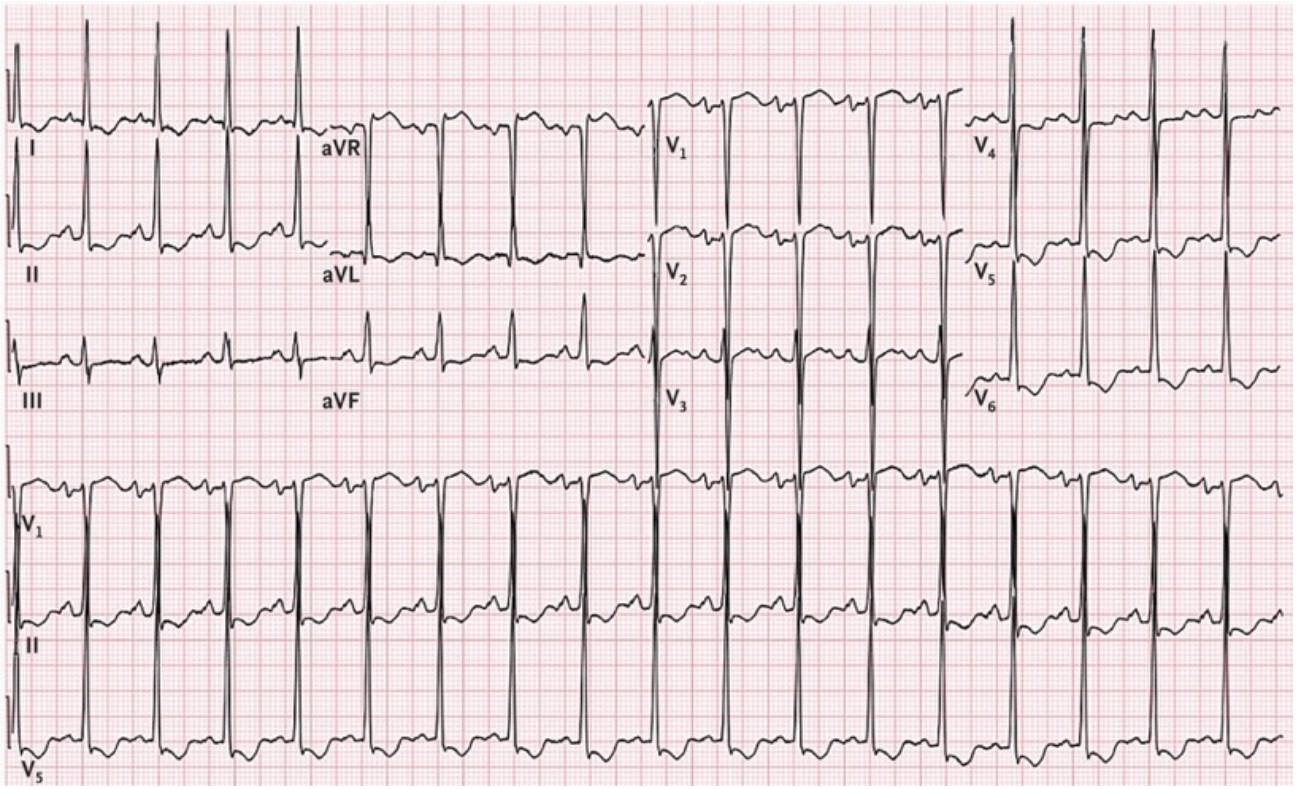

Electrocardiogram.

A 12-lead electrocardiogram shows sinus tachycardia with inferolateral ST-segment depressions and T-wave inversions, findings that indicate subendocardial ischemia or ventricular hypertrophy. Also visible is prominent R-wave amplitude in lead V_6, S-wave amplitude in lead V_1, and an R wave in aVL (>11 mm in amplitude), all of which are findings suggestive of left ventricular hypertrophy. The U waves noted in V_2, V_3, and V_4 are consistent with severe hypokalemia.

Differential Diagnosis

I participated in the care of this patient and am aware of the final diagnosis. This young woman presented with debilitating headaches, presumably due to refractory hypertension. The differential diagnosis for hypertension in an adolescent includes renal parenchymal disease, from both acute and chronic causes, and extrarenal conditions such as endocrine diseases, medication use, and congenital vascular anomalies.

Renal Parenchymal Diseases

Common causes of secondary hypertension in children and adolescents are acute kidney injury and chronic kidney disease. Possibilities include acute pyelonephritis, which can result from vesicoureteral reflux; glomerulonephritis, which can occur after streptococcal infection; and reflux nephropathy, which is kidney scarring that can be caused by any chronic renal parenchymal disease.

Extrarenal Diseases Associated with Hypertension

Extrarenal causes of secondary hypertension include primary hyperaldosteronism, which is one of the most common causes of treatment-resistant hypertension in children and adolescents. However, hypokalemia is present in only approximately one third of patients with primary hyperaldosteronism.

Toxins and Medications

This patient's urine toxicology screening showed no evidence of stimulant or cocaine use, and a medication history was notable for sparse use of NSAIDs and no use of over-the-counter decongestants, which are known culprits that can lead to hypertension.

Congenital Vascular Anomalies

Coarctation of the aorta should be considered in adolescents with hypertension. This patient had an echocardiogram that showed no evidence of coarctation of the aorta but was notable for left ventricular hypertrophy, a finding that suggests severe and long-standing hypertension.

At this point in the evaluation, most of the possible causes of this patient's refractory hypertension and hypokalemia had been ruled out, except for primary hyperaldosteronism or primary hyperreninemic hypertension. The latter could be the result of a rare primary tumor of the kidney, such as a reninoma. To rule out these possible diagnoses, we obtained abdominal and pelvic imaging and measured the plasma renin activity and aldosterone level.

Diagnostic Testing

CT angiography of the abdomen and pelvis showed no evidence of renal-artery stenosis. The patient had bilateral single renal arteries originating from the abdominal aorta without radiologically significant narrowing.

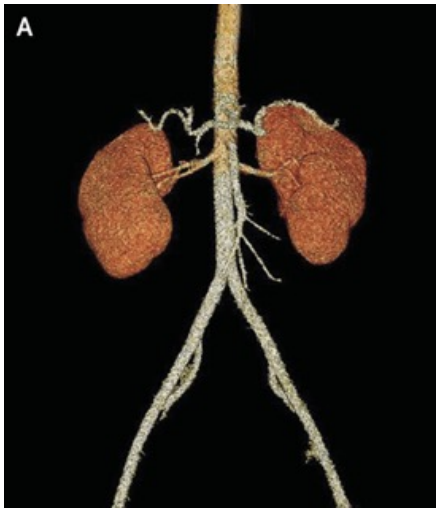

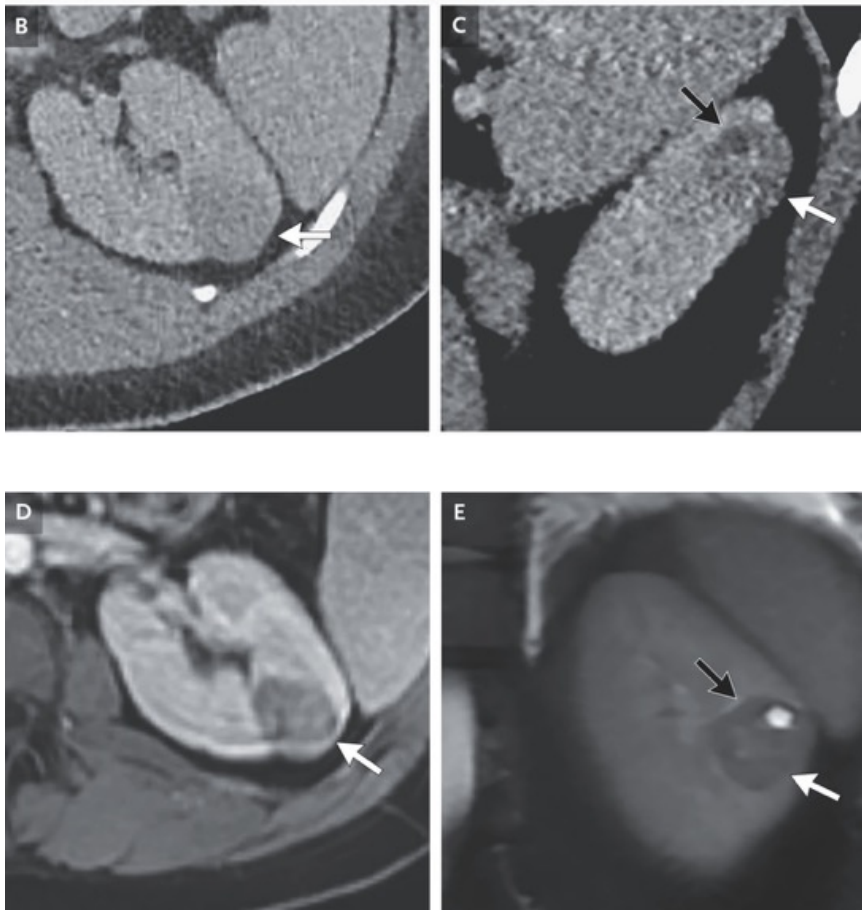

Imaging Studies of the Abdomen and Pelvis.

A three-dimensional volume-rendered image of the abdominal aorta and iliac arteries (Panel A) shows no evidence of stenosis or renal-artery abnormalities. An axial CT image, obtained in the portovenous phase after the administration of intravenous contrast material (Panel B), reveals a hypoenhancing, partially exophytic mass in the left kidney (arrow). A sagittal image obtained from contrast-enhanced CT in the portovenous phase (Panel C) shows the same lesion (white arrow), with a more hypodense focus along its superior margin (black arrow). An axial T1-weighted MRI, obtained after the administration of intravenous contrast material (Panel D), shows a hypointense, hypoenhancing lesion in the left kidney (arrow). A coronal T2-weighted MRI (Panel E) shows the lesion with predominantly hypointense signal (white arrow) and a small superior cystic component (black arrow).

On hospital day 4, the plasma level of renin was severely elevated at 150 ng per milliliter per hour (reference range, 1.2 to 2.4). The aldosterone level was 4.1 ng per deciliter (reference range, <21). The fact that this patient had an aldosterone level at the lower limit of the normal range was surprising. Given the high renin level, we expected the aldosterone level to be elevated as well, but it was not. At the time this testing was performed, the patient was not receiving an angiotensin-converting–enzyme (ACE) inhibitor or an angiotensin-receptor blocker; thus, a probable explanation for this result was an inaccurate result owing to interference with the assay or laboratory error. Furthermore, the presence of hyperreninemia also ruled out monogenic causes of hypertension, which are universally associated with very low plasma renin activity.

Given the extremely high plasma renin activity, refractory hypokalemia, and the presence of a single renal mass, we thought the most likely diagnosis was a reninoma. We consulted the urology service to evaluate this patient for possible surgical resection of the renal mass. Resection was scheduled to occur 6 weeks later to provide time to control this patient's refractory hypertension with medication.

Diagnosis

Hyperreninemic hypertension due to reninoma.

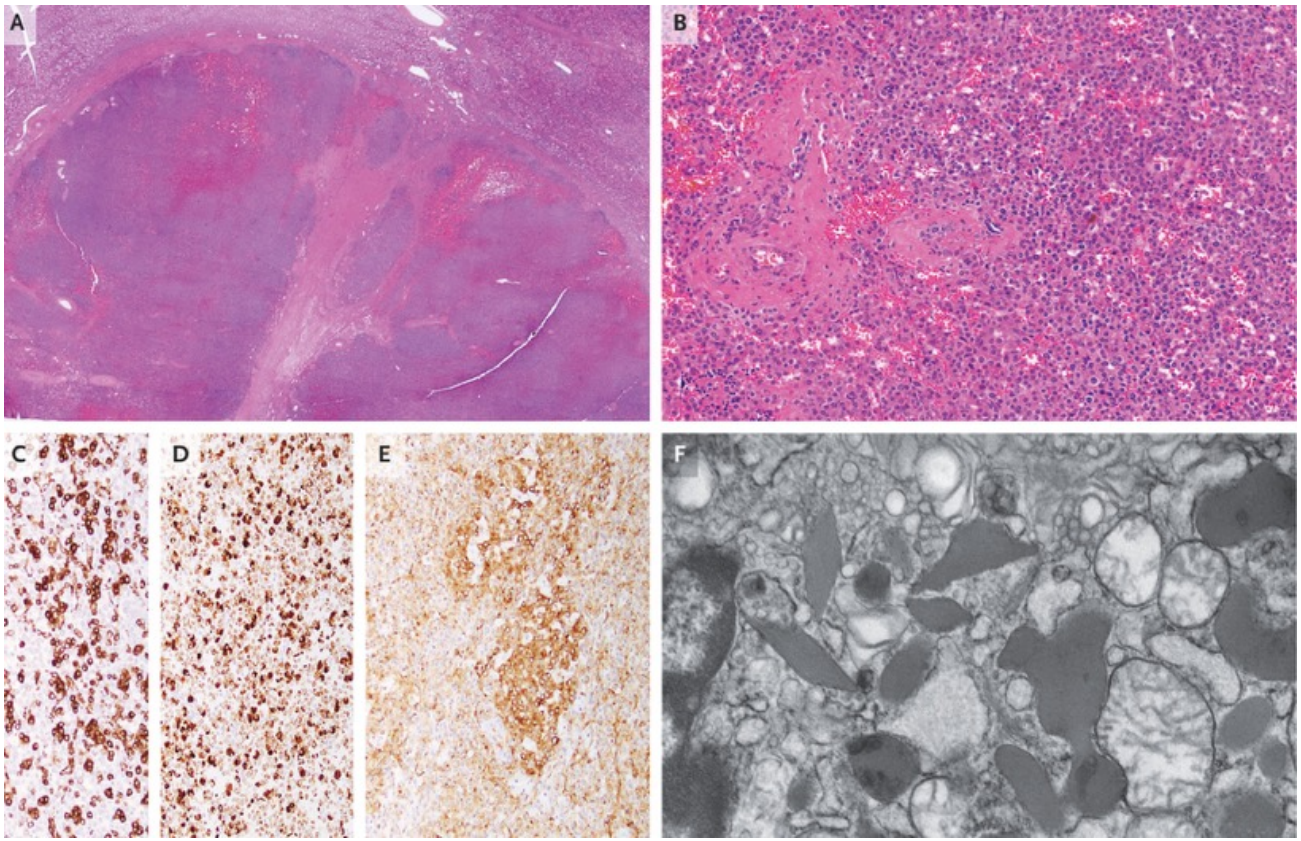

Excisional Biopsy Specimen of the Renal Mass.

Hematoxylin and eosin staining reveals a nodular, well-limited, and encapsulated lesion with fibrous scarring (Panel A) and, at a higher magnification, homogeneous proliferation of small cells with poorly visible cell borders and hyalinized blood vessels (Panel B). Immunostaining for smooth-muscle actin (Panel C), GATA3 (Panel D), and CD34 (Panel E) is positive, a finding that supports a diagnosis of reninoma. An image from electron microscopy (Panel F) reveals rhomboid renin crystals.

Final Diagnosis
Reninoma.

Ein Reninom, auch bekannt als juxtaglomerulärer Zelltumor, entsteht aus den Zellen des juxtaglomerulären Apparates der Niere. Diese Tumorzellen schütten große Mengen des Hormons Renin aus, was das Renin-Angiotensin-Aldosteron-System übermäßig aktiviert.

Klinische Merkmale

Die übermäßige Reninproduktion führt zu spezifischen Symptomen und Laborbefunden:

- **Schwere Hypertonie** (Bluthochdruck), die oft medikamentös schwer einzustellen ist.
- **Hypokaliämie** (niedriger Kaliumspiegel im Blut).
- **Metabolische Alkalose**.

Die Symptome treten meist bei Jugendlichen und jungen Erwachsenen auf, mit einer Häufung im zweiten und dritten Lebensjahrzehnt und einer Prädominanz bei Frauen.

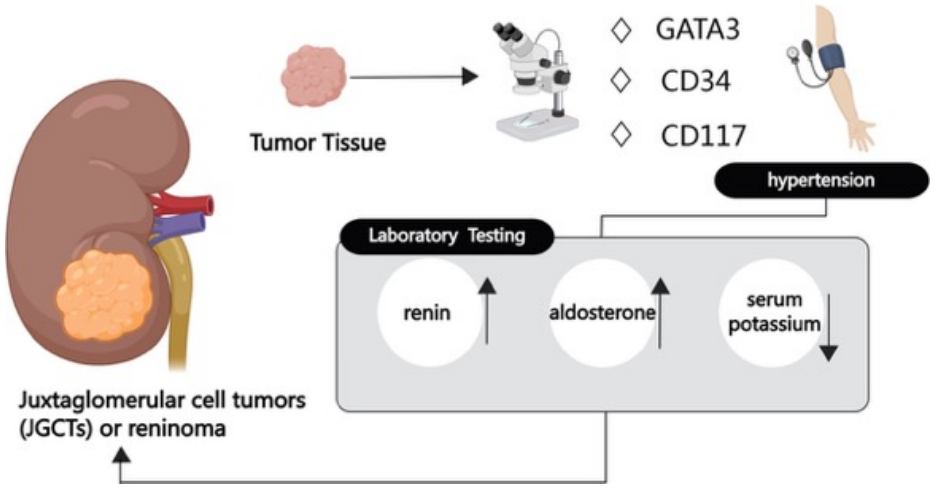

THE LANCET

Minocyclin ist ein verschreibungspflichtiges Breitbandantibiotikum aus der Gruppe der Tetracycline, das primär zur Behandlung mittelschwerer bis schwerer Akne, Rosacea sowie bakterieller Atemwegs- und Harnwegsinfektionen eingesetzt wird. Es wirkt bakteriostatisch (hemmt das Wachstum) und entzündungshemmend.

Minocyclin wird zur Verbesserung der Prognose nach einem akuten ischämischen Schlaganfall untersucht. Aufgrund seiner entzündungshemmenden und neuroprotektiven Eigenschaften kann es die Entzündungsreaktion im Gehirn reduzieren und die Funktionserholung geringfügig verbessern. Es gilt als sichere Begleittherapie zur Standardbehandlung.
Hier sind die wichtigsten Erkenntnisse im Überblick:

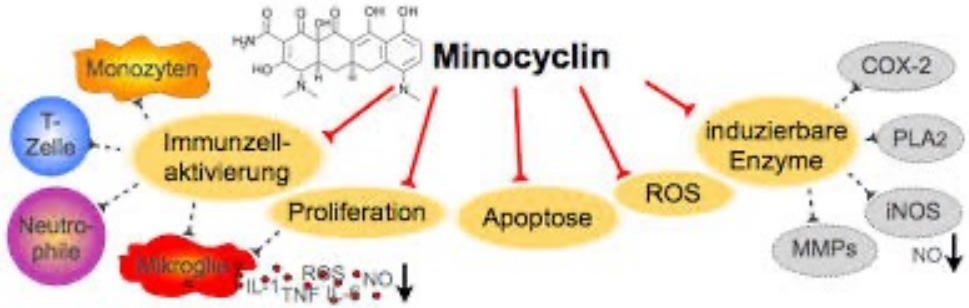

•**Wirkmechanismus:** Minocyclin wirkt als Mikroglia-Inhibitor, reduziert oxidativen Stress und schützt Nervenzellen vor Apoptose (Zelltod).

Efficacy and safety of minocycline in patients with acute ischaemic stroke (EMPHASIS): a multicentre, double-blind, randomised controlled trial

Summary

Background Minocycline has been reported as a multi-target anti-neuroinflammatory drug with potential benefits for ischaemic stroke in preclinical models and small-scale clinical studies. The EMPHASIS trial was designed to provide robust evidence regarding its efficacy and safety in patients with acute ischaemic stroke.

Methods A multicentre, double-blind, randomised, placebo-controlled trial was conducted at 58 hospitals across China. Patients who had an ischaemic stroke in the previous 72 h with a National Institutes of Health Stroke Scale (NIHSS) score ranging from 4 to 25 and a level of consciousness score (subscale 1a of the NIHSS) of 1 or less were randomly assigned in a 1:1 ratio to receive minocycline or placebo in addition to routine treatment. Minocycline (loading dose of 200 mg, followed by 100 mg every 12 h for the subsequent 4 days) or matching placebo was administered orally. Block randomisation with a fixed block size of four stratified by study site was done with a computer-generated randomisation sequence. All patients, treating clinicians, and investigators involved in the trial were fully masked to treatment allocation. The primary outcome was an excellent functional outcome at 90 days (with a modified Rankin Scale [mRS] score of 0–1) and was analysed in all patients who were randomised and received at least one dose of the study drug, without imputation for missing data. Safety outcomes were assessed in participants who received at least one dose of the study drug and had at least one safety evaluation and included symptomatic intracranial haemorrhage at 24 h and 6 days. This trial was registered with ClinicalTrials.gov (NCT05836740) and is now completed.

Findings Between May 19, 2023, and May 20, 2024, 1724 patients were randomly assigned to minocycline (n=862) or placebo (n=862) groups. Median age was 65 years (IQR 57–71). 1151 (66·8%) patients were male and 573 (33·2%) were female. Median NIHSS score at baseline was 5 (IQR 4–7). Four patients withdrew consent (three in the minocycline group and one in the placebo group) and 19 patients were lost to follow-up (nine in the minocycline group and ten in the placebo group). At 90 days, 447 (52·6%) of 850 patients with minocycline and 403 (47·4%) of 851 with placebo had an mRS score of 0–1 (adjusted risk ratio 1·11, 95% CI 1·03–1·20; p=0·0061). Ordinal analysis across the full range of mRS scores also favoured minocycline, with an adjusted common odds ratio of 1·19 (95% CI 1·03–1·38; p=0·018). The incidence of symptomatic intracranial haemorrhage was similar between the minocycline and placebo groups at 24 h (1/860 [0·1%] *vs* 0/861 [0%]) and 6 days (3/859 [0·3%] *vs* 0/861 [0%]). No significant differences were observed in other safety outcomes, including serious adverse events (40/862 [4·6%] in the minocycline group *vs* 51/862 [5·9%] in the placebo group; p=0·24).

Interpretation Minocycline therapy initiated within 72 h of acute ischaemic stroke provided a significant functional outcome benefit compared with placebo at 90 days, without safety concerns. Future studies are needed to confirm these findings and to establish whether the benefits extend to patients with more severe or minor strokes.

Funding National Natural Science Foundation of China, Beijing Healthunion Cardio-cerebrovascular Disease Prevention and Treatment Foundation, Noncommunicable Chronic Diseases—National Science and Technology Major Project, Beijing Municipal Science & Technology Commission, Chinese Institutes for Medical Research, Capital's Funds for Health Improvement and Research, and National Key R&D Program of China.

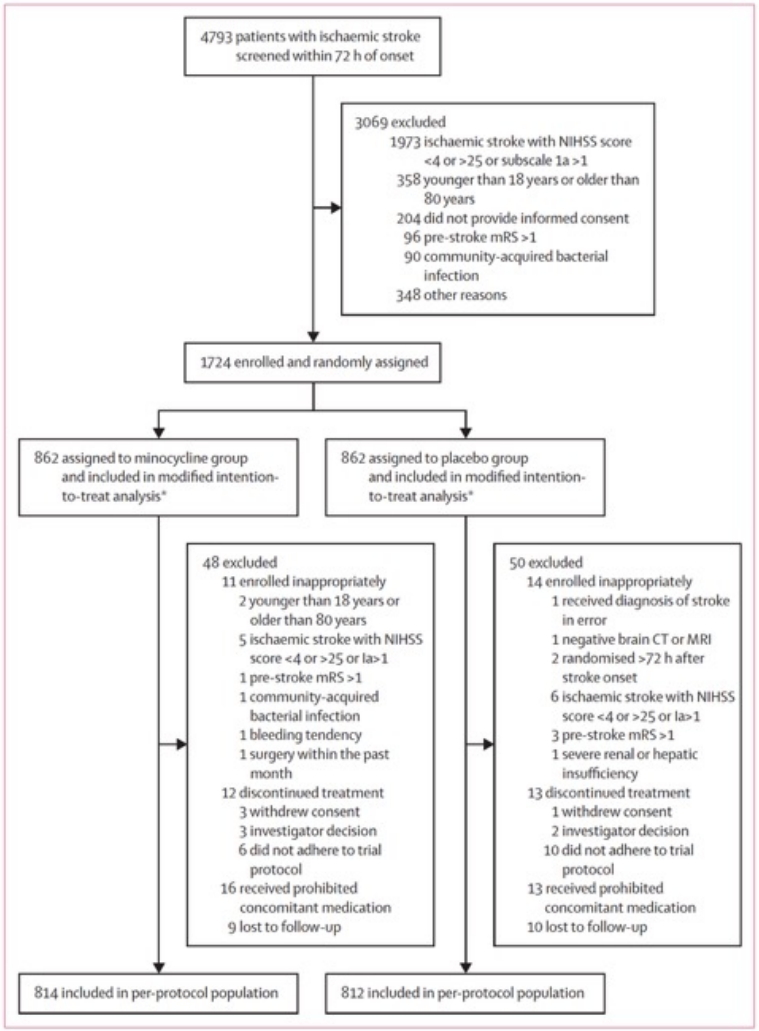

Figure 1: **Trial profile**
mRS=modified Rankin Scale. NIHSS=National Institutes of Health Stroke Scale. *850 participants in the minocycline group and 851 in the placebo group had mRS scores available at 90 days and were included in the primary outcome analysis without imputation of missing data.

	Minocycline (n=862)	Placebo (n=862)
Age, years	65·0 (57·0–72·0)	65·0 (57·0–71·0)
Sex		
Male	573 (66·5%)	578 (67·1%)
Female	289 (33·5%)	284 (32·9%)
BMI, kg/m²	24·8 (22·7–26·9)	24·5 (22·5–26·8)
Medical history		
Hypertension	554 (64·3%)	572 (66·4%)
Diabetes	286 (33·2%)	280 (32·5%)
Dyslipidaemia	378 (43·9%)	363 (42·1%)
Previous ischaemic stroke	238 (27·6%)	258 (29·9%)
Coronary heart disease	95 (11·0%)	114 (13·2%)
Heart failure	5 (0·6%)	6 (0·7%)
Atrial fibrillation	45 (5·2%)	39 (4·5%)
Ever smoker	325 (37·7%)	359 (41·6%)
Alcohol use	223 (25·9%)	241 (28·0%)
Medication within 1 month before stroke		
Antiplatelet agent	108 (12·5%)	122 (14·2%)
Anticoagulant agent	12 (1·4%)	13 (1·5%)
Statins	103 (11·9%)	97 (11·3%)
Antibiotics	2 (0·2%)	4 (0·5%)
Pre-stroke mRS score		
0	739 (85·7%)	744 (86·3%)
1	122 (14·2%)	115 (13·3%)
≥2	1 (0·1%)	3 (0·3%)
hs-CRP at baseline, mg/L*	2·0 (0·8–4·8)	2·0 (0·9–4·6)
NIHSS score at baseline	5·0 (4·0–7·0)	5·0 (4·0–7·0)
Stroke subtypes (TOAST classification)		
Large-artery atherosclerosis	388 (45·0%)	398 (46·2%)
Cardioembolism	49 (5·7%)	42 (4·9%)
Small vessel disease	340 (39·4%)	347 (40·3%)
Other determined aetiology	30 (3·5%)	22 (2·6%)
Undetermined aetiology	55 (6·4%)	53 (6·1%)
Time from stroke onset to treatment		
Median (IQR)	41·9 (26·1–52·8)	40·5 (26·5–52·0)
≤24 h	179 (20·8%)	175 (20·3%)
>24 to 48 h	375 (43·5%)	396 (45·9%)
>48 h	308 (35·7%)	291 (33·8%)
Reperfusion therapy	114 (13·2%)	130 (15·1%)

Data are n (%) or median (IQR). Percentages might not total 100 because of rounding. hs-CRP=high-sensitivity C-reactive protein. mRS=modified Rankin Scale. NIHSS=National Institutes of Health Stroke Scale. TOAST=Trial of Org 10172 in Acute Stroke Treatment. *hs-CRP data are missing for 96 patients in the minocycline group and 95 in the placebo group.

Table 1: **Baseline characteristics**

	Minocycline (n=862)	Placebo (n=862)	Adjusted treatment effect* (95% CI)	p value
mRS 0–1 at 90 days†	447/850 (52·6%)	403/851 (47·4%)	RR 1·11 (1·03–1·20)	0·0061
Ordinal mRS score at 90 days	..	..	cOR 1·19 (1·03–1·38)‡	0·018
0	195/850 (22·9%)	175/851 (20·6%)	..	..
1	252/850 (29·6%)	228/851 (26·8%)	..	..
2	168/850 (19·8%)	174/851 (20·4%)	..	..
3	140/850 (16·5%)	178/851 (20·9%)	..	..
4	58/850 (6·8%)	51/851 (6·0%)	..	..
5	23/850 (2·7%)	25/851 (2·9%)	..	..
6	14/850 (1·6%)	20/851 (2·4%)	..	..
mRS 0–2 at 90 days	615/850 (72·4%)	577/851 (67·8%)	RR 1·07 (1·02–1·12)	0·0056
mRS 0–3 at 90 days	755/850 (88·8%)	755/851 (88·7%)	RR 1·00 (0·97–1·03)	0·94
Change in NIHSS score from baseline to 24 h§	0 (0–0)	0 (0–0)	β –0·07 (–0·20 to 0·06)	0·32
Change in NIHSS score from baseline to 6 days¶	–2 (–3 to 0)	–1 (–3 to 0)	β –0·28 (–0·50 to –0·05)	0·015
Early neurological deterioration at 24 h‖	52/848 (6·1%)	54/854 (6·3%)	RR 0·97 (0·64–1·47)	0·89
Early neurological deterioration at 6 days**	56/842 (6·7%)	66/840 (7·9%)	RR 0·85 (0·59–1·21)	0·36
Change in hs-CRP from baseline to 6 days, mg/L††	0 (–1·20 to 1·97)	0·20 (–0·94 to 3·73)	β –2·72 (–5·64 to 0·19)	0·067
Stroke recurrence at 90 days	51/862 (5·9%)	47/862 (5·5%)	HR 1·09 (0·73–1·62)	0·68
Ischaemic stroke recurrence at 90 days	47/862 (5·5%)	43/862 (5·0%)	HR 1·09 (0·72–1·65)	0·67
Composite vascular events at 90 days	59/862 (6·8%)	52/862 (6·0%)	HR 1·14 (0·79–1·65)	0·49

Data are n/N (%), unless otherwise indicated. mRS=modified Rankin Scale. NIHSS=National Institutes of Health Stroke Scale. hs-CRP=high-sensitivity C-reactive protein. RR=risk ratio. cOR=common odds ratio. HR=hazard ratio. *Adjusted for pooled study centres using a mixed-effects model. †The mRS score is missing for 12 patients in the minocycline group versus 11 in the placebo group at 90 days. ‡A cOR >1 indicates a shift towards better mRS outcomes (ie, lower disability). §The NIHSS score is missing for 15 patients in the minocycline group versus 8 in the placebo group at 24 h. ¶The NIHSS score is missing for 21 patients in the minocycline group versus 23 in the placebo group at 6 days. ‖Early neurological deterioration at 24 h is missing for 14 patients in the minocycline group versus 8 in the placebo group. **Early neurological deterioration at 6 days is missing for 20 patients in the minocycline group versus 22 in the placebo group. ††Data on hs-CRP change from baseline to 6 days are missing for 172 patients in the minocycline group versus 184 in the placebo group.

Table 2: **Efficacy outcomes (in the modified intention-to-treat population)**

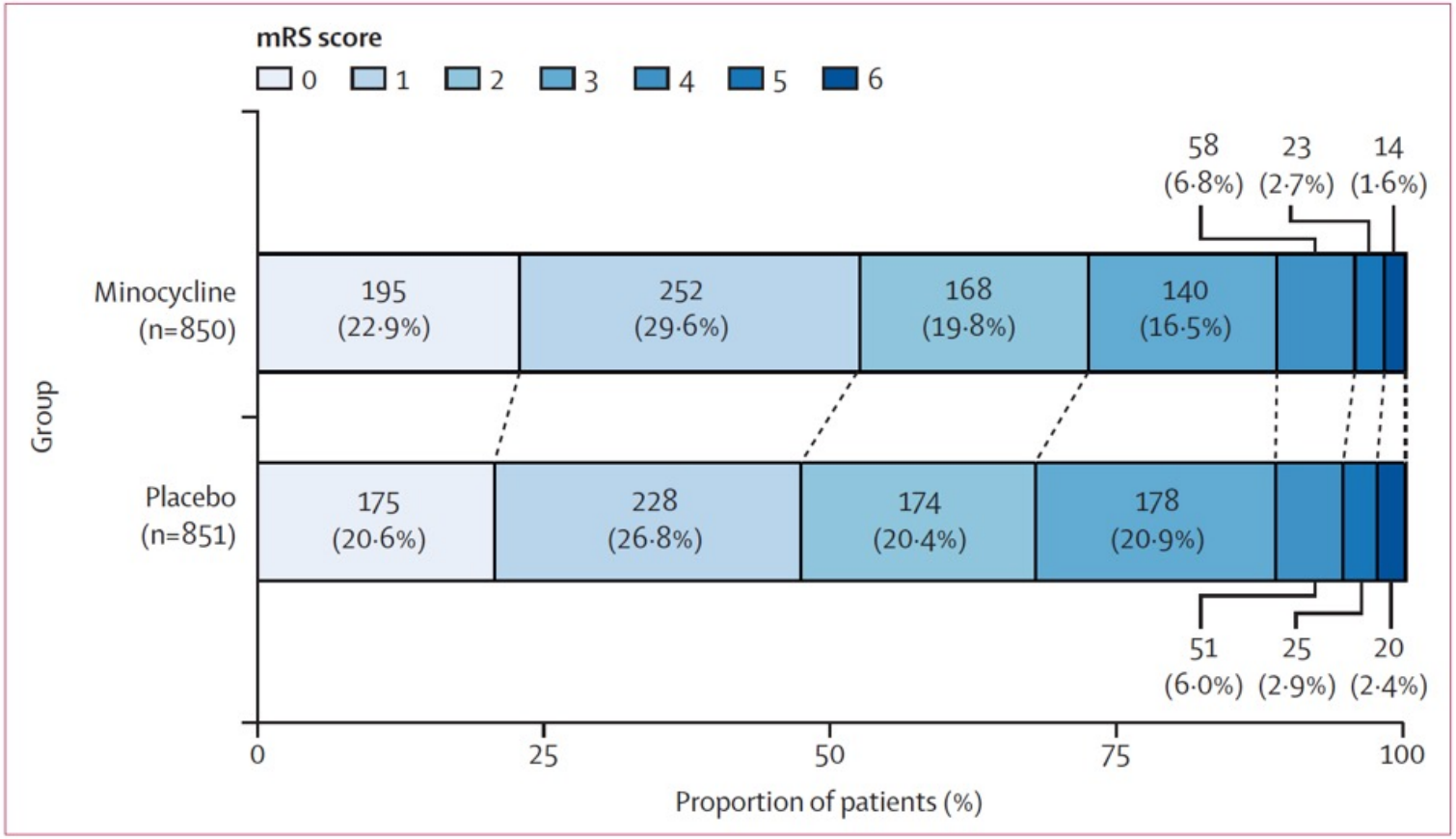

Figure 2: **Distribution of mRS scores at 90 days (modified intention-to-treat population)**
Percentages might not amount to 100% because of rounding. mRS=modified Rankin Scale.

	Minocycline (n=862)	Placebo (n=862)	Adjusted treatment effect (95% CI)*	p value
Symptomatic intracranial haemorrhage at 24 h†	1/860 (0·1%)	0/861 (0%)	..	..
Symptomatic intracranial haemorrhage at 6 days‡	3/859 (0·3%)	0/861 (0%)	..	..
Antibiotic-associated diarrhoea, enteritis, and constipation at 6 days‡	0/859 (0%)	2/861 (0·2%)	..	..
Any bleeding event at 90 days	63/862 (7·3%)	69/862 (8·0%)	HR 0·90 (0·64–1·27)	0·56
Minor bleeding§	56/862 (6·5%)	63/862 (7·3%)	HR 0·88 (0·61–1·26)	0·49
Moderate bleeding§	1/862 (0·1%)	2/862 (0·2%)	HR 0·50 (0·05–5·52)	0·57
Severe bleeding§	8/862 (0·9%)	6/862 (0·7%)	HR 1·34 (0·46–3·85)	0·59
Any bleeding event at 90 days¶	..	..	cOR 0·91 (0·64–1·30)||	0·60
None	799/862 (92·7%)	793/862 (92·0%)	..	..
Minor	54/862 (6·3%)	61/862 (7·1%)	..	..
Moderate	1/862 (0·1%)	2/862 (0·2%)	..	..
Severe	8/862 (0·9%)	6/862 (0·7%)	..	..
Vascular death at 90 days	10/862 (1·2%)	16/862 (1·9%)	HR 0·62 (0·28–1·36)	0·23
All-cause death at 90 days	14/862 (1·6%)	20/862 (2·3%)	HR 0·69 (0·35–1·36)	0·28

Data are n/N (%), unless otherwise indicated. HR=hazard ratio. cOR=common odds ratio. *Adjusted for pooled study centres using a mixed-effects model. †Data on symptomatic intracranial haemorrhage at 24 h are missing for two patients in the minocycline group and one in the placebo group. ‡Data on symptomatic intracranial haemorrhage and antibiotic-associated diarrhoea, enteritis, and constipation at 6 days are missing for three patients in the minocycline group and one in the placebo group. §In patients with multiple bleeding events of differing severity, the earliest event for each severity category (ie, minor, moderate, and severe) was included in the analysis. ¶In patients with multiple bleeding events, the highest severity was used for analysis. ||A cOR >1 indicates a shift towards more bleeding and bleeding of greater severity.

Table 3: **Safety outcomes (in the safety population)**

Research in context

Evidence before this study

We searched PubMed from database inception to May 31, 2025, for randomised trials assessing the efficacy of minocycline in patients with acute ischaemic stroke, using the terms "minocycline" AND "stroke", with no language restrictions. This literature search identified four small-scale, single-blind randomised controlled trials (RCTs) with inconsistent findings. Three RCTs enrolled patients with acute ischaemic stroke (National Institutes of Health Stroke Scale [NIHSS] score >4 or 5) within 6–24 h of onset and reported that a 5-day oral minocycline regimen improved functional outcomes at 90 days, as measured with the modified Rankin Scale (mRS) or NIHSS. By contrast, the remaining trial recruited patients with any measurable neurological deficit within 24 h of onset, administered five doses of intravenous minocycline (over 2·5 days), and found no significant benefit on 90-day mRS scores.

A meta-analysis of three RCTs suggested that minocycline significantly improved functional independence (mRS 0–2; risk ratio 1·59, 95% CI 1·19 to 2·12; p=0·002) and reduced mRS scores (mean difference −0·67, 95% CI −1·31 to −0·03; p=0·04) at 90 days. A supplementary search of ClinicalTrials.gov identified three ongoing RCTs investigating the efficacy of minocycline in this context. Overall, minocycline could offer potential therapeutic benefits in patients with acute ischaemic stroke; however, the available clinical evidence remains scarce and inconclusive.

Added value of this study

The EMPHASIS study is the first large-scale, double-blind, randomised controlled trial to evaluate the efficacy and safety of a 4·5-day course of oral minocycline in patients with acute ischaemic stroke treated within 72 h of symptom onset. We found that patients treated with minocycline in addition to routine therapy were more likely to reach an excellent functional outcome (mRS 0–1) and a more favourable overall distribution of mRS scores than those who received placebo and routine therapy at 90 days. Moreover, minocycline did not appear to increase all safety outcomes compared with placebo. Therefore, minocycline could be implemented with routine medical therapy to reduce the risk of disability and improve neurological function in patients with acute ischaemic stroke.

Implications of all the available evidence

The EMPHASIS trial showed the benefit of minocycline on functional outcomes at 90 days in patients with acute ischaemic stroke. These findings add to the growing body of evidence supporting the possible role of minocycline as an effective and safe drug that can be used on top of routine medical therapy in acute ischaemic stroke. Our results invite more research into the area of assessing the neuroprotective effects of anti-neuroinflammatory agents and their possible use in ischaemic stroke.

Die meisten Anwender vertragen Statine sehr gut, doch wie bei jedem Medikament können Nebenwirkungen auftreten.
Eine große Übersichtsarbeit im Lancet (Februar 2026) weist jedoch darauf hin, dass viele berichtete Symptome oft nicht direkt durch das Medikament, sondern durch den sogenannten **Nocebo-Effekt** (Erwartung negativer Effekte) verursacht werden.

Mostly nonesense!

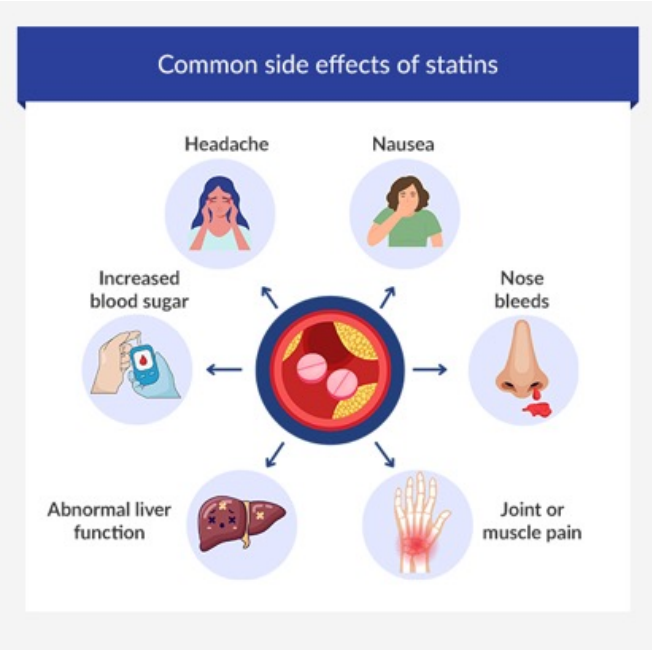

Häufige Nebenwirkungen
Diese treten meist zu Beginn der Therapie auf und sind oft mild:

- **Verdauungsbeschwerden:** Blähungen, Verstopfung, Durchfall oder Übelkeit.

- **Allgemeinsymptome:** Kopfschmerzen, Schwindel oder Schlafstörungen.

- **Muskelschmerzen (Myalgie):** Etwa 1–10 % der Patienten berichten über Muskelziehen oder -schwäche. Echte medikamentenbedingte Muskelschäden sind jedoch selten.

Assessment of adverse effects attributed to statin therapy in product labels: a meta-analysis of double-blind randomised controlled trials

Summary

Background Statin product labels (eg, Summaries of Product Characteristics [SmPCs]) list certain adverse outcomes as potential treatment-related effects based mainly on non-randomised and non-blinded studies, which might be subject to bias. We aimed to assess the evidence for such undesirable effects more reliably through a meta-analysis of individual participant data from large double-blind trials of statin therapy.

Methods In this meta-analysis of individual participant-level data from double-blind randomised controlled trials, we generated a list of all undesirable effect terms listed in statin SmPCs by searching an electronic medicines compendium for five statins (atorvastatin, fluvastatin, pravastatin, rosuvastatin, and simvastatin). Randomised trials were eligible for meta-analysis of these effects if they involved at least 1000 participants, had a scheduled treatment period of at least 2 years, and involved a double-blind comparison of statin versus placebo or of a more intensive versus a less intensive statin regimen. Event rate ratios (RRs) and 95% CIs were calculated with statistical significance assessed after controlling the false discovery rate (FDR) at 5%.

Findings 19 trials compared statin versus placebo (123 940 participants, median follow-up 4·5 years [IQR 3·1–5·4]). In addition to previously reported effects on muscle outcomes and diabetes, only four of 66 further undesirable outcomes that had been attributed to statins were FDR significant: abnormal liver transaminases (783 participants [0·30% per annum] allocated statin *vs* 556 [0·22% per annum] allocated placebo, RR 1·41 [95% CI 1·26–1·57]) and other liver function test abnormalities (651 participants [0·25% per annum] allocated statin *vs* 518 [0·20% per annum] allocated placebo, RR 1·26 [1·12–1·41]; absolute annual excess of 0·13% for combined liver function test abnormality), urinary composition alteration (556 [0·21% per annum] allocated statin *vs* 472 [0·18% per annum] allocated placebo, RR 1·18 [1·04–1·33]), and oedema (3495 [1·38% per annum] allocated statin *vs* 3299 [1·31% per annum] allocated placebo, RR 1·07 [1·02–1·12]). Analysis of the four trials of more intensive versus less intensive statin regimens also found significant excesses for abnormal liver transaminases and other liver function test abnormalities (supporting a dose-dependent effect), but no significant excess was found for urinary composition alteration or oedema.

Interpretation Adverse event data from blinded randomised trials do not support causal relationships between statin therapy and most of the conditions (including cognitive impairment, depression, sleep disturbance, and peripheral neuropathy) listed in product labels as potential undesirable effects. In light of these findings, such labelling and other official sources of health information should be revised so that patients and their doctors can make appropriately informed decisions regarding statin therapy.

Funding British Heart Foundation, UK Medical Research Council, and Australian National Health and Medical Research Council.

	Year of publication of primary results	Number of included participants*	Treatment regimen (mg/day)†	Follow-up (years)	LDL-C (mmol/L)	Age (years)	Women	Men	White participants‡	History of vascular disease	Medical history of diabetes	Timing of scheduled routine follow-up visits	Type of data principally collected
Statin *vs* placebo													
4S[30]	1994	4444	S20-40 *vs* placebo	5·4 (5·3–5·6)	4·9 (0·7)	59 (7)	827 (19%)	3617 (81%)	NA	4444 (100%)	202 (5%)	Every 1·5 months until 18 months, then every 6–48 months	All AEs
WOSCOPS[31]	1995	6595	P40 *vs* placebo	4·8 (4·3–5·3)	5·0 (0·5)	55 (6)	0	6595 (100%)	NA	1066 (16%)	77 (1%)	Every 3 months until final follow-up	All AEs
CARE[32]	1996	4159	P40 *vs* placebo	4·9 (4·4–5·5)	3·6 (0·4)	59 (9)	576 (14%)	3583 (86%)	3851 (93%)	4159 (100%)	586 (14%)	At 1·5 months, then every 3 months until 72 months	All AEs
AFCAPS/ TexCAPS[33]	1998	6605	L20-40 *vs* placebo	5·0 (4·7–5·8)	3·9 (0·4)	58 (7)	997 (15%)	5608 (85%)	5860 (89%)	0	155 (2%)	Every 1·5 months until 12 months, 15 months, 18 months then every 6 months until 60 months	All AEs
LIPID[34]	1998	9014	P40 *vs* placebo	5·9 (5·4–6·4)	3·9 (0·8)	61 (8)	1516 (17%)	7498 (83%)	NA	9014 (100%)	782 (9%)	At 3, 6, 9, 12 months, then annually until 72 months	SAEs
LIPS[35]	2002	1677	F80 *vs* placebo	4·0 (3·6–4·0)	3·4 (0·8)	60 (10)	271 (16%)	1406 (84%)	1650 (98%)	1677 (100%)	202 (12%)	At 1·5 and 6 months, then every ~6 months	All AEs
HPS[36]	2002	20 536	S40 *vs* placebo	5·2 (4·6–5·6)	3·4 (0·8)	64 (8)	5082 (25%)	15 454 (75%)	19 901 (97%)	17 386 (85%)	5963 (29%)	At 4, 8, and 12 months, then every 6 months until 60 months	SAEs + selected AEs
PROSPER[37]	2002	5804	P40 *vs* placebo	3·3 (3·0–3·5)	3·8 (0·8)	75 (3)	3000 (52%)	2804 (48%)	NA	2565 (44%)	623 (11%)	Every 3 months until final follow-up	All AEs
ASCOT-LLA[38]	2003	10 240	A10 *vs* placebo	3·3 (2·8–3·7)	3·4 (0·7)	63 (9)	1919 (19%)	8321 (81%)	9687 (95%)	1684 (16%)	2540 (25%)	At 1·5, 3, and 6 months, then every 6 months until 66 months or final follow-up	All AEs
ALERT[39]	2003	2102	F40-80 *vs* placebo	5·5 (5·2–5·6)	4·1 (1·0)	50 (11)	715 (34%)	1387 (66%)	2039 (97%)	409 (19%)	396 (19%)	At 1·5 months then every 6 months until 72 months	All AEs
CARDS[40]	2004	2838	A10 *vs* placebo	4·2 (3·4–4·9)	2·9 (0·8)	61 (8)	909 (32%)	1929 (68%)	2676 (94%)	106 (4%)	2838 (100%)	At 1, 2, 3, and 6 months, then every 6 months until 48 months	All AEs
4D[41]	2005	1255	A20 *vs* placebo	2·7 (1·7–4·0)	3·3 (0·8)	66 (8)	578 (46%)	677 (54%)	924 (74%)	1041 (83%)	1255 (100%)	At 1 and 6 months, then every 6 months until 48 months	All AEs
ASPEN[42]	2006	2410	A10 *vs* placebo	4·0 (2·9–4·5)	2·9 (0·7)	60 (8)	811 (34%)	1599 (66%)	2029 (84%)	747 (31%)	2410 (100%)	At 1, 2, 3, and 6 months, then every 6 months until 48 months	All AEs
SPARCL[43]	2006	4731	A80 *vs* placebo	4·9 (4·4–5·5)	3·5 (0·6)	63 (11)	1908 (40%)	2823 (60%)	4415 (93%)	4731 (100%)	794 (17%)	At 1, 3 and 6 months, then every 6 months until 78 months	All AEs
CORONA[44]	2007	4982	R10 *vs* placebo	2·7 (2·2–3·1)	3·6 (0·9)	72 (7)	1175 (24%)	3807 (76%)	NA	4982 (100%)	1473 (30%)	At 1·5 and 3 months, then every 3 months until 51 months or final follow-up	All AEs

(Table continues on next page)

	Year of publication of primary results	Number of included participants*	Treatment regimen (mg/day)†	Follow-up (years)	LDL-C (mmol/L)	Age (years)	Women	Men	White participants‡	History of vascular disease	Medical history of diabetes	Timing of routine follow-up visits	Type of data principally collected
(Continued from previous page)													
GISSI-HF[45]	2008	4574	R10 *vs* placebo	3·9 (3·0–4·4)	3·1 (0·9)	68 (11)	1032 (23%)	3542 (77%)	4574 (100%)	4574 (100%)	1196 (26%)	At 1, 3, and 6 months, then every 6 months until 60 months	SAEs + selected AEs
JUPITER[46]	2008	16 714	R20 *vs* placebo	1·9 (1·5–2·4)	2·7 (0·5)	65 (8)	6374 (38%)	10 340 (62%)	NA	0	44 (<1%)	At 3 and 6 months, then every 6 months until 36 months, close out	All AEs
AURORA[47]	2009	2555	R10 *vs* placebo	3·9 (2·2–4·6)	2·6 (0·9)	64 (9)	969 (38%)	1586 (62%)	NA	1025 (40%)	658 (26%)	At 3 and 6 months, then every 6 months until 42 months	All AEs
HOPE-3[48]	2016	12 705	R10 *vs* placebo	5·5 (5·1–6·2)	3·3 (0·9)	66 (6)	5874 (46%)	6831 (54%)	2546 (20%)	0	731 (6%)	At 1·5 and 6 months, then every 6 months until 96 months	SAEs + selected AEs
Subtotal (n=19 studies)	..	123 940	..	4·5 (3·1–5·4)	3·5 (0·9)	63 (9)	34 533 (28%)	89 407 (72%)	60 152 (81%)	59 610 (48%)	22 925 (18%)	..	..
More intensive *vs* less intensive statin (double blind)													
PROVE-IT[49]	2004	4162	A80 *vs* P40	2·1 (1·9–2·3)	2·6 (0·7)	58 (11)	911 (22%)	3251 (78%)	3776 (91%)	4162 (100%)	762 (18%)	At 0·5, 1, and 4 months, then every 4 months until 28 months	All AEs
A to Z[50]	2004	4497	S40 then S80 *vs* placebo then S20	2·0 (1·4–2·0)	2·1 (0·5)	60 (11)	1100 (24%)	3397 (76%)	3825 (85%)	4497 (100%)	1059 (24%)	At 1 and 4 months, then every 4 months until 24 months	SAEs + selected AEs
TNT[51]	2005	10 001	A80 *vs* A10	5·0 (4·8–5·3)	2·5 (0·5)	61 (9)	1902 (19%)	8099 (81%)	9410 (94%)	10 001 (100%)	1501 (15%)	At 3, 6, 9, and 12 months, then every 6 months until 72 months	All AEs
SEARCH[52]	2010	12 064	S80 *vs* S20	7·0 (6·5–7·5)	2·5 (0·6)	64 (9)	2052 (17%)	10 012 (83%)	11 854 (98%)	12 064 (100%)	1267 (11%)	At 2, 4, 8, and 12 months, then every 6 months until 84 months	SAEs + selected AEs
Subtotal (n=4 studies)	..	30 724	..	5·0 (2·3–6·6)	2·5 (0·6)	62 (10)	5965 (19%)	24 759 (81%)	28 865 (94%)	30 724 (100%)	4589 (15%)	..	..
All trials (n=23 studies)	..	154 664	..	4·7 (3·0–5·5)	3·3 (1·0)	63 (9)	40 498 (26%)	114 166 (74%)	89 017 (85%)	90 334 (58%)	27 514 (18%)	..	..

Data are median (IQR), mean (SD), or n (%) unless otherwise stated. All participants were randomly assigned in a 1:1 allocation. Overall totals and subtotals are calculated across all included trials. AURORA, CORONA, and JUPITER studies supplied age in categorical bands, and so the midpoint of each categorical band was used as a surrogate for baseline age in all analyses. Medical history of diabetes is defined as participants with a history of diabetes and does not include those retrospectively defined as having diabetes at baseline on the basis of adverse events, glucose-lowering medication, or glucose or HbA1c measurements at the time of assignment to a treatment group. Details for collection of adverse events represents the planned data collection timetable. However, not all data were available or could be used (eg, because only provided as summary-level data). 4S=Scandinavian Simvastatin Survival Study. WOSCOPS=West of Scotland Coronary Prevention Study. CARE=Cholesterol And Recurrent Events. AFCAPS/TexCAPS=Air Force–Texas Coronary Atherosclerosis Prevention Study. LIPID=Long-term Intervention with Pravastatin in Ischaemic Disease. LIPS=Lescol Intervention Prevention Study. HPS=Heart Protection Study. PROSPER=PROspective Study of Pravastatin in the Elderly at Risk. ASCOT-LLA=Anglo-Scandinavian Cardiac Outcomes Trial–Lipid Lowering Arm. ALERT=Assessment of Lescol in Renal Transplantation. CARDS=Collaborative Atorvastatin Diabetes Study. 4D=Die Deutsche Diabetes Dialyse Studie. ASPEN=Atorvastatin Study for Prevention of Coronary Heart Disease Endpoints in Non-Insulin-Dependent Diabetes Mellitus. SPARCL=Stroke Prevention by Aggressive Reduction in Cholesterol Levels. CORONA=Controlled Rosuvastatin Multinational Trial in Heart Failure. GISSI-HF=Gruppo Italiano per lo Studio della Sopravvivenza nell'Insufficienza Cardiaca. JUPITER=Justification for the Use of Statins in Prevention: an Intervention Trial Evaluating Rosuvastatin. AURORA=A Study to Evaluate the Use of Rosuvastatin in Subjects on Regular Hemodialysis: an Assessment of Survival and Cardiovascular Events. HOPE-3=Heart Outcomes Prevention Evaluation-3 trial. PROVE-IT=Pravastatin or Atorvastatin Evaluation and Infection Therapy. A to Z=Aggrastat to Zocor. TNT=Treating to New Targets. SEARCH=Study of the Effectiveness of Additional Reductions in Cholesterol and Homocysteine. NA=not available. ..=not applicable. *A small number of participants in the AURORA (n=218), CORONA (n=27), and JUPITER (n=1088) trials withdrew consent for use of their data post-trial, and hence data from these participants are excluded. The ASCOT-LLA trial excludes 65 participants for whom data were not available because of protocol violations. †S indicates simvastatin, P indicates pravastatin, F indicates fluvastatin, A indicates atorvastatin, R indicates rosuvastatin, and L indicates lovastatin; numbers following abbreviation indicate statin daily dose in mg. ‡Percentages were calculated after excluding the seven trials where information on race and ethnicity was not provided (the relevant denominators are therefore 73 832 for all trials of statin *vs* placebo and 104 556 for all trials).

Table: **Participant characteristics**

Statins versus placebo

Figure 1: Effect of statin versus placebo on events listed in statin SmPCs, subdivided by component parts
Results for two outcomes with fewer than ten events are not shown in the figure, but are included in the appendix. FDR=false discovery rate. LFT=liver function test. RBC=red blood cell. RR=rate ratio. SmPC=Summary of Product Characteristics. *FDR significant at the 5% level; RR for results FDR-significant at the 5% level are indicated by black circles and RR for results not FDR-significant at the 5% level indicated by grey circles. †Excluded from FDR testing; RR for results excluded from FDR testing indicated by white circles.

Statins low-dose versus high-dose

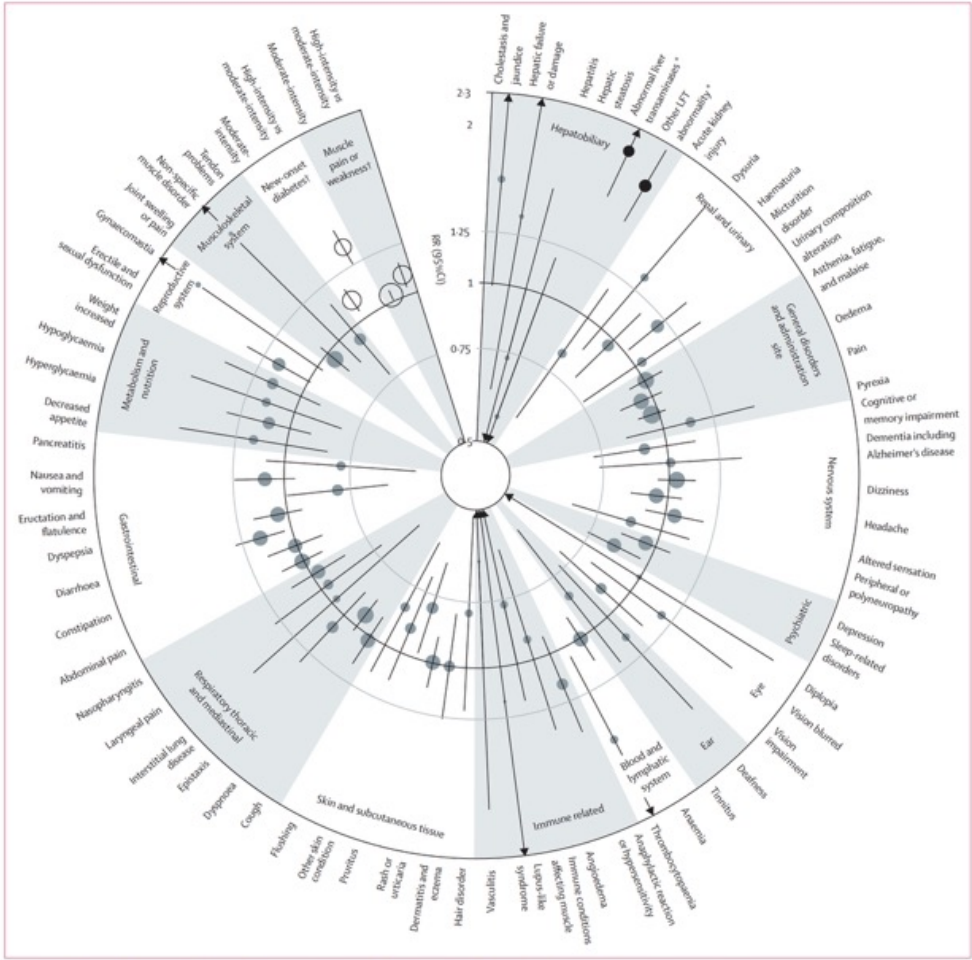

Figure 2: Effect of more intensive statin therapy versus less intensive statin therapy on events listed in statin SmPCs, subdivided by component parts
Results for three outcomes with fewer than ten events are not shown in the figure, but are included in the appendix. FDR=false discovery rate. LFT=liver function test. RBC=red blood cell. RR=rate ratio. SmPC=Summary of Product Characteristics. *FDR significant at the 5% level; RR for results FDR significant at the 5% level indicated by black circles and RR for results not FDR-significant at the 5% level indicated by grey circles. †Excluded from FDR testing; RR for results excluded from FDR testing indicated by white circles.

Research in context

Evidence before this study

We searched Ovid MEDLINE, Ovid Embase, and the Cochrane Database of Systematic Reviews from their date of inception to Dec 15, 2025 for meta-analyses and review articles, published in any language, which specifically assessed the effects of statin regimens on all outcomes listed as undesirable effects in statin product labels (Summaries of Product Characteristics [SmPC]). We searched using a combination of appropriate MeSH terms for meta-analyses and review articles (eg, "meta-analysis" or "systematic review" or "scoping review" or "network meta-analysis"), statins (eg, "statins" or "Hydroxymethylglutaryl-CoA Reductase Inhibitors"), and terms related to product information documents (eg, "Summary of Product Characteristics" or "SmPC" or "Patient Information Leaflet" or "Package insert" or "pil" or "Product Information" or "USPI" or "United States prescribing information" or "product insert"). Although some articles described the effect of statin therapy on a range of potential undesirable effects, no comprehensive assessment of all such terms appears to have been undertaken previously. Data from randomised controlled trials have shown that statin therapy can, rarely, cause substantial muscle damage or, in a more severe form, rhabdomyolysis as indicated by muscle symptoms accompanied by related biochemical changes (eg, multifold rises in creatine kinase). Recent individual participant data meta-analyses have also shown that statin therapy causes a small relative increase in less severe muscle symptoms largely confined to the first year of treatment. Individual participant data meta-analyses have also shown a moderate dose-dependent increase in new diagnoses of diabetes, the majority occurring in individuals with glycaemic markers already close to the diagnostic threshold for diabetes at the time of initiation of statin treatment. Statin SmPCs also list numerous other adverse (ie, undesirable) outcomes as possible effects of statin therapy. However, these attributions typically derive from case reports or observational studies, which can be subject to bias and confounding. Therefore, robust evidence is needed to clarify the possible effects of statin therapy on these outcomes to support informed decision-making by patients and clinicians.

Added value of this study

We aimed to minimise the risk of biases by restricting our analyses to large-scale, randomised, double-blind trials of statin therapy in which there was systematic and unbiased event reporting. We obtained details of all adverse events recorded in each individual trial participant, and coded them using standard nosology (from the Medical Dictionary for Regulatory Activities). The availability of individual participant data permitted assessment of any causal effects of statin therapy on health outcomes currently listed as possible undesirable effects in statin labelling. A false discovery rate (FDR) multiple-testing method was used to control for the number of health outcomes investigated. Results from randomised placebo-controlled double-blind trials showed that, after controlling for multiple testing using the FDR method, statin therapy was associated with a significant excess risk for only four of 66 prespecified outcomes: abnormal liver transaminases, other liver function test abnormalities, urinary composition alteration, and oedema. The absolute annual excesses for each of these outcomes was very small (<0·1%). The effect on liver function tests appeared to be related to statin intensity because a similar excess was also observed in trials comparing more intensive with less intensive statin therapy; however, this association was not seen for alteration in urinary composition nor for oedema. No significant excess risk was observed for any other hepatobiliary outcomes, nor for any of the other 62 prespecified outcomes including cognitive impairment, depression, sleep disturbance, erectile and sexual dysfunction, peripheral neuropathy, acute kidney injury, and interstitial lung disease.

Implications of all the available evidence

These findings indicate that, in addition to the previously reported adverse effects of statin therapy on muscle outcomes and diabetes, statins are associated only with small absolute increases in abnormal liver biochemistry, and possible adverse effects of unknown clinical relevance on urinary composition and oedema, but not with any other outcomes listed in statin SmPCs. Consequently, the undesirable effect sections of statin product labels might overstate risks and mislead clinicians and patients, and should be revised to better support informed, evidence-based decision making.

"KI-Stethoskope" (Künstliche-Intelligenz-Stethoskope) sind **digitale Stethoskope**, die Herz- und Lungengeräusche aufzeichnen und mithilfe von Algorithmen der maschinellen Lernens auswerten, um Ärzten bei der Erkennung von Herzerkrankungen zu helfen.

Verfügbare Produkte

KI-gestützte Stethoskope sind auf dem Markt erhältlich, oft als digitale Modelle, die mit entsprechender Software oder Apps verbunden sind.

- **3M™ Littmann® CORE Digital Stethoscope**
  - Dies ist ein beliebtes digitales Stethoskop, das in Zusammenarbeit mit Eko Health entwickelt wurde.
  - Es wandelt akustische Schallwellen in elektrische Signale um, um Geräusche zu verstärken und ermöglicht die Verbindung mit Software zur Visualisierung und, bei Nutzung der Eko-Plattform, potenzieller KI-gestützter Analyse.
  - Littmann-Stethoskope werden laut der Hersteller-Website für ihre Langlebigkeit und hervorragende Akustik gelobt.

Eko Core 500 angeschlossenes und verstärktes digitales Stethoskop mit EKG-Funktion

Hauptmerkmale

- Bis zu 40-fache Klangverstärkung mit TrueSound™-Technologie: ideal für medizinisches Fachpersonal mit Hörverlust
- 8-fache Umgebungsgeräuschunterdrückung für klares Hören auch in lauten Umgebungen
- **1-Kanal-EKG**-Anzeige auf integriertem Farb-LCD-Bildschirm
- **3-Kanal-EKG** über die Eko App (kostenlos und für Android und iOS verfügbar) für eine umfassende Beurteilung
- 3 intelligente Audiofilter: Kardio, Pulmonal, Weitwinkel
- Echtzeit-Herzfrequenzmessung
- Aufzeichnen, Anzeigen, Teilen und Exportieren von Geräuschen und EKG-Kurven über die Eko App
- **Bluetooth-kompatibel:** Kopfhörer, Hörgeräte, verbundene Geräte (unterstützt Bluetooth Low Energy (BLE) 4.2 und BLE 5.0 Kommunikation)
- Optional: Eko+ AI (Abonnement in der App): Automatische Erkennung von Herzgeräuschen und Vorhofflimmern
- Geeignet für Erwachsene und Kinder
- Automatische Abschaltung zur Batterieschonung

Triple cardiovascular disease detection with an artificial intelligence-enabled stethoscope (TRICORDER) in the UK: a cluster-randomised controlled implementation trial

Summary

Background Early detection of cardiovascular disease is a global public health priority. Artificial intelligence (AI)-enabled stethoscopes offer robust performance characteristics in point-of-care detection of heart failure, atrial fibrillation, and valvular heart disease (VHD). We conducted a pragmatic, cluster-randomised controlled implementation trial to determine the real-world effect and implementation challenges of AI-stethoscopes.

Methods UK primary care practices were cluster randomised 1:1 to intervention (training and implementation in use of AI-stethoscopes in routine care) or control (routine care). Given the nature of the intervention, masking of participants (practices, clinicians, and patients) was not feasible. During cardiac examinations, the AI stethoscope recorded 15 s of single-lead electrocardiogram and phonocardiogram signals for input to three AI algorithms that returned binary predictions for the presence or absence of reduced left ventricular ejection fraction (≤40%), atrial fibrillation, and VHD (all with regulatory approval). The primary endpoint was incidence of any newly coded diagnosis of heart failure (all subtypes), expressed per 1000 patient-years (incidence rate ratio [IRR]), derived from a UK National Health Service Secure Data Environment. A coprimary endpoint stratified detection of heart failure by place of diagnosis (community-based *vs* via hospital admission). Secondary endpoints included atrial fibrillation and VHD detection rates, performance characteristics of the AI-stethoscope, use rates, and clinician-reported implementation barriers and enablers.

Heart failure (HFrEF), Atrial fibrillation, and Valvular heart disease

Findings Between Oct 30, 2023, and May 22, 2024, 205 practices were randomly assigned (96 to the intervention arm [701 933 registered patients] and 109 to the control arm [851 242 registered patients]). Intervention practices recorded 12 725 patient examinations with the AI-stethoscope, across 972 clinical users. Intention-to-treat analysis found heart failure detection did not differ between groups (IRR 0·94 [95% CI 0·86–1·02]); with no difference in community-based or hospital-based diagnoses (p>0·05).

Interpretation Implementation of an AI stethoscope in routine primary care did not significantly increase detection of heart failure or increase community-based diagnosis after 12 months of implementation. AI stethoscope use was independently associated with significantly higher detection rates of heart failure, as well as atrial fibrillation and VHD. This randomised controlled implementation trial establishes a pragmatic design with randomisation that generates real-world data essential for understanding and overcoming the barriers to implementation of innovation in health care.

Funding National Institute for Health and Care Research, British Heart Foundation, and Imperial Health Charity.

Procedures

Primary care practices randomised to the intervention arm received a single, 1 h onboarding visit delivered by the research team. This visit (detailed in the published protocol[20]) covered delivery, setup, and how to use the AI stethoscope (Eko DUO, Eko Health Inc, Emeryville, CA, USA). In summary, this workflow involved turning on the AI-stethoscope, which then automatically connected via Bluetooth to an app for live ECG and phonocardiogram visualisation. After placing the device over the pulmonic position for cardiac auscultation, the user then activated a 15 s waveform recording via the app. Cellular or WiFi connectivity enabled access to three cloud-based AI algorithms, which, based on waveform analysis, returned real-time binary predictions (yes or no) corresponding to the three target conditions (appendix p 2).

Up to six AI-stethoscopes were provided per practice, donated by Imperial College London (study sponsor; ie, they could keep the devices beyond study completion). The hardware was user-agnostic and accessed via individual accounts within the app. No patient data were physically stored on the stethoscope or smartphone, but instead immediately saved to the manufacturer's secure cloud-based platform. Clinical users were encouraged, but not mandated, to label recordings using the patient's unique NHS identifier, in accordance with Good Medical Practice.[23] Use of the AI stethoscope was discretionary and not integrated with electronic health records (EHRs), requiring manual entry of results where clinically indicated.

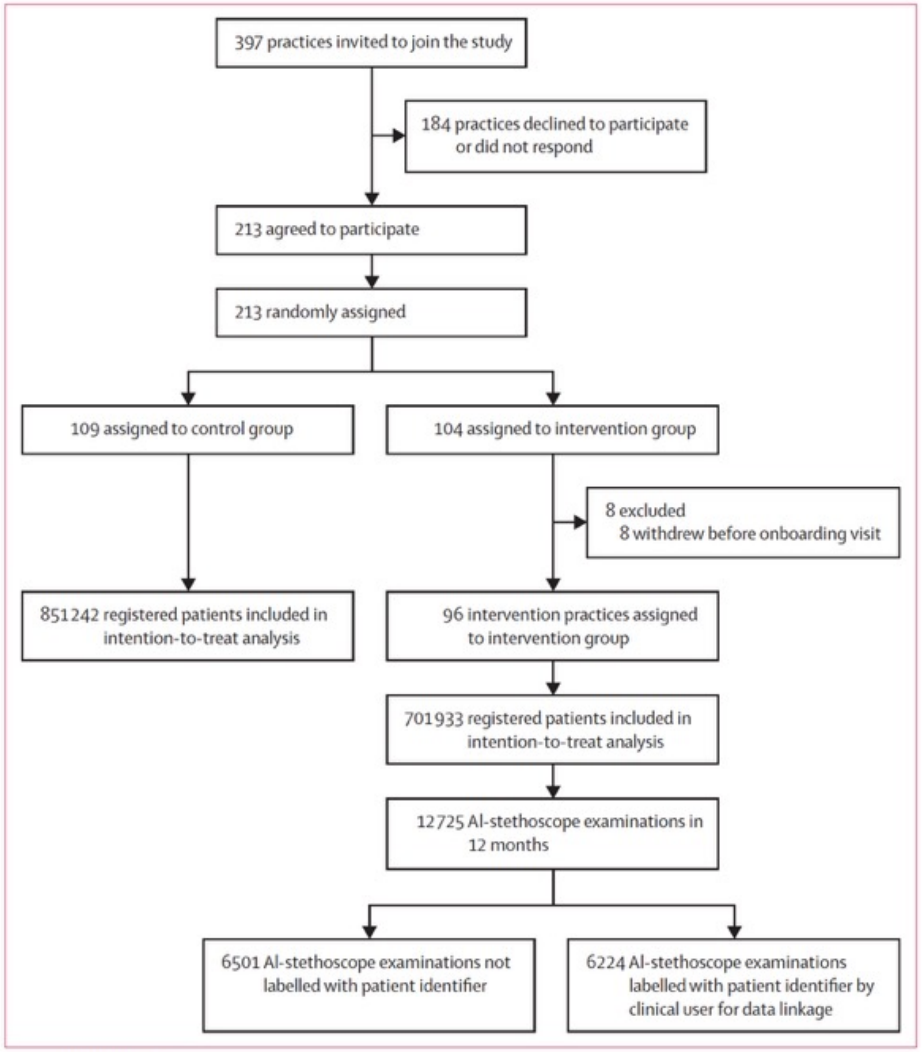

Figure 1: **Trial profile**
AI=artificial intelligence.

	Intervention (n=701 933)	Control (n=851 242)	Standardised mean difference (95% CI)
Adult registered list size per practice	7164·4 (3278·1)	7776·4 (9515·8)	0·085 (0·080 to 0·090)
Age, years	44·5 (17·2)	43·5 (17·5)	−0·060 (−0·070 to −0·051)
Sex	..	..	0·018 (0·018 to 0·020)
Female	343 044 (48·9%)	408 244 (47·9%)	..
Male	358 889 (51·1%)	443 828 (52·1%)	..
Ethnic group	..	..	0·10 (0·10 to 0·10)
Asian or Asian British	199 487 (28·4%)	271 685 (31·9%)	..
Black or Black British	65 978 (9·4%)	69 578 (8·2%)	..
Mixed	24 340 (3·5%)	28 192 (3·3%)	..
Other ethnic groups	96 651 (13·8%)	112 406 (13·2%)	..
White	299 042 (42·6%)	340 895 (40·0%)	..
Not recorded	16 481 (2·3%)	27 436 (3·2%)	..
IMD decile	..	..	0·14 (0·14 to 0·14)
1 (most deprived)	15 933 (2·3%)	20 479 (2·4%)	..
2	73 355 (10·5%)	83 263 (9·8%)	..
3	120 396 (17·2%)	121 485 (14·3%)	..
4	126 764 (18·1%)	129 490 (15·2%)	..
5	121 893 (17·4%)	125 204 (15·2%)	..
6	87 729 (12·5%)	116 483 (13·7%)	..
7	57 827 (8·2%)	82 396 (9·7%)	..
8	51 137 (7·3%)	72 474 (8·5%)	..
9	30 529 (4·3%)	49 545 (5·8%)	..
10 (least deprived)	15 888 (2·3%)	23 028 (2·7%)	..
Comorbidities	..	..	..
Cancer	24 057 (3·4%)	28 466 (3·3%)	0·0048 (0·0030 to 0·014)
Coronary artery disease	19 591 (2·8%)	23 429 (2·8%)	0·0019 (−0·0020 to 0·0061)
Chronic kidney disease	21 324 (3·0%)	24 757 (2·9%)	0·0084 (0·0022 to 0·014)
Diabetes	64 452 (9·2%)	78 453 (9·2%)	0·014 (0·010 to 0·019)
Hypertension	106 081 (15·1%)	123 799 (14·5%)	0·024 (0·020 to 0·028)
Stroke or transient ischaemic attack	11 571 (1·6%)	13 413 (1·6%)	0·0060 (0·0020 to 0·010)
Heart failure prevalence	1·42%	1·36%	..
Heart failure incidence per 1000 patient-years	2·39	2·46	..
Atrial fibrillation prevalence	1·67%	1·61%	..
Atrial fibrillation incidence per 1000 patient-years	2·26	2·06	..
Valvular heart disease prevalence	0·65%	0·62%	..
Valvular heart disease incidence per 1000 patient-years	1·16	1·24	..

Data are mean (SD) or n (%). IMD=Index of Multiple Deprivation.

Table 1: **Baseline characteristics of the intention-to-treat practice and patient population**

	Sensitivity	Specificity	Positive predictive value	Negative predictive value	Positive likelihood ratio	Negative likelihood ratio	F1 score
Heart failure	0·39 (0·34–0·43)	0·92 (0·92–0·93)	0·30 (0·26–0·34)	0·95 (0·94–0·95)	5·06 (4·33–5·93)	0·67 (0·62–0·72)	0·34
Atrial fibrillation	0·44 (0·39–0·49)	0·98 (0·98–0·98)	0·64 (0·58–0·70)	0·96 (0·95–0·96)	21·69 (17·30–27·20)	0·57 (0·52–0·62)	0·52
Valvular heart disease	0·24 (0·17–0·31)	0·947 (0·94–0·95)	0·10 (0·07–0·14)	0·98 (0·98–0·98)	4·43 (3·19–6·16)	0·81 (0·74–0·89)	0·14

Table 3: **Performance characteristics of the AI algorithms**

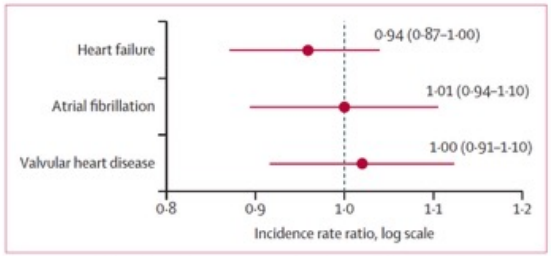

Figure 2: **Unadjusted incidence rate ratios for heart failure, atrial fibrillation, and VHD at 12 months**

	Events (intervention)	Events (control)	Event rate per 1000 patient-years (intervention/control)	Adjusted IRR (95% CI)	p value
Community	594	884	1·14/1·23	0·90 (0·75–1·08)	0·25
Hospital	867	1250	1·67/1·74	0·92 (0·79–1·07)	0·29

IRR=incidence rate ratio.

Table 2: **Incidence of heart failure by place of diagnosis**

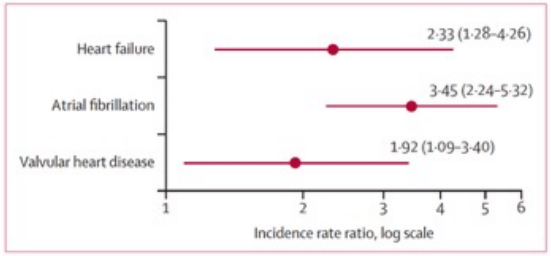

Figure 3: **Per-protocol adjusted incidence rate ratios for heart failure, atrial fibrillation, and VHD at 12 months**

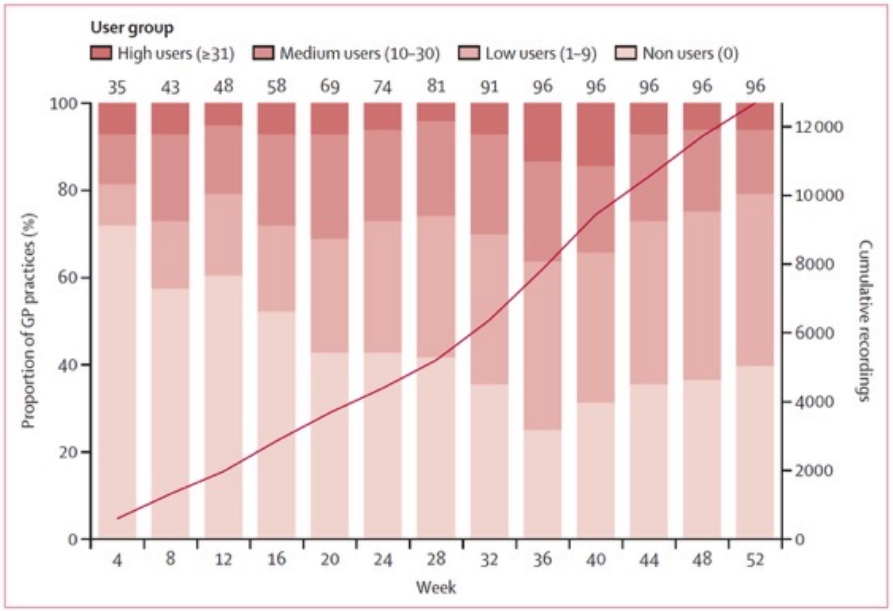

***Figure 4:* AI stethoscope use in the first year**

Use of AI stethoscope examinations (cardiac waveform recordings for AI interpretation) among recruited GP practices in the intervention group (n=96) during the first 12 months of implementation. Stacked bars represent the number of practices (y-axis, left) stratified by usage intensity category: high users (≥31 uses per month), medium users (10–30 uses per month), low users (<10 uses per month), and non-users (0 uses per month). Darker shades within each bar denote higher usage categories, with high users shown in the darkest shade. The overlaid line graph indicates cumulative number of AI stethoscope examinations (y-axis, right) over 12 months, with numbers above each bar denoting the total number of onboarded practices at that timepoint. AI=artificial intelligence. GP=general practitioner.

Research in context

Evidence before this study

We searched PubMed on Oct 1, 2023, using the terms "artificial intelligence" AND "randomised controlled trial" AND "implementation study" AND "real world evidence" AND "primary care". We included peer-reviewed articles published in English in the last 10 years. No published studies were identified that had prospectively evaluated an artificial intelligence (AI) technology using pragmatic trial methodology incorporating both clinical effectiveness and contextual implementation outcomes, particularly within primary care settings. A separate search using the terms "artificial intelligence" AND ("cardiovascular" OR "heart failure" OR "atrial fibrillation" OR "valve disease") AND "point-of-care" AND "electrocardiogram" AND "prospective" also returned no studies that implemented waveform-recording hardware with integrated AI—such as AI stethoscopes—in health-care settings at scale. The closest comparator was the EAGLE study, a cluster-randomised study across 45 US primary care clinics, which showed improved detection of low left ventricular ejection fraction (≤50%) through augmentation of 12-lead electrocardiogram reports with an AI-derived probability. We updated the literature search on July 21, 2025, and found no new evidence altering these conclusions.

Added value of this study

To our knowledge, TRICORDER is the first cluster-randomised controlled implementation trial of a clinical AI technology, and the first at scale in a national primary care system. The trial involved 205 UK National Health Service (NHS) primary care practices—an under-represented setting for AI research. The randomised controlled implementation trial methodology addressed key gaps in existing research: moving beyond algorithm validation to evaluate real-world algorithm performance, diagnostic effect, adoption patterns, and contextual implementation barriers. The AI stethoscope under investigation in TRICORDER integrates three distinct algorithms for heart failure, atrial fibrillation, and valvular heart disease—conditions that are frequently underdiagnosed in primary care. Outcomes were measured through novel access to an NHS Secure Data Environment (real-world data), enriched with AI stethoscope data for patient-level analyses. We showed across 972 clinical users and 12 872 patient examinations that improving detection rates of each of the three conditions was not achieved at population scale—despite robust algorithmic performance—but was dependent upon use, having revealed substantial challenges that need to be overcome in real-world adoption, including low uptake and related workflow misalignment.

Implications of all the available evidence

TRICORDER's study of a point-of-care AI technology highlights the potential for enhancing detection of cardiovascular disease in primary care, where clinical effect is closely tied to real-world adoption and integration into workflows. This randomised controlled implementation trial establishes the importance of study design embedding implementation science alongside pragmatic effectiveness research to ensure effective deployment and subsequent impact of AI technologies in health-care systems.

Der wesentliche Unterschied zwischen Tetanustoxin und Botulinumtoxin liegt in ihrer Wirkung auf das Nervensystem und den daraus resultierenden Symptomen: Tetanustoxin verursacht eine **spastische Lähmung** (Muskelkrampf), während Botulinumtoxin eine **schlaffe Lähmung** hervorruft. Beide stammen zwar von *Clostridien*-Bakterien, wirken jedoch an unterschiedlichen Stellen und gegensätzlich.

Hier sind die Unterschiede im Detail:

- **Tetanustoxin (Tetanusspasmin):**
  - **Wirkung:** Führt zu unkontrollierten, schmerzhaften Muskelverkrampfungen (Spastik), da es die Hemmung der Muskelkontraktion im Zentralnervensystem blockiert.
  - **Ort:** Wirkt im zentralen Nervensystem (Rückenmark).
  - **Quelle:** Wird in der Regel von *Clostridium tetani* nach einer Wundinfektion gebildet.
- **Botulinumtoxin (BoNT):**
  - **Wirkung:** Führt zu einer schlaffen Lähmung, da es die Freisetzung von Acetylcholin an der peripheren Nerven-Muskel-Verbindung blockiert.
  - **Ort:** Wirkt im peripheren Nervensystem.
  - **Quelle:** Wird meist von *Clostridium botulinum* extrakorporal gebildet (z. B. in verdorbenen Lebensmitteln) und dann aufgenommen.

Beide Gifte gehören zu den stärksten bekannten Toxinen und können ohne Behandlung tödlich verlaufen. Während Botulinumtoxin jedoch auch therapeutisch zur Muskelentspannung eingesetzt wird, ist Tetanustoxin ausschließlich hochgefährlich.

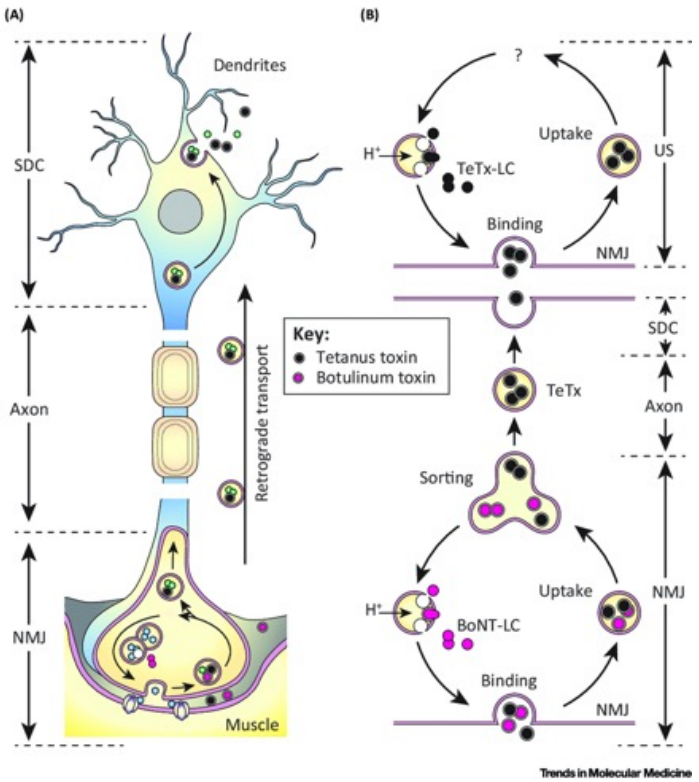

Tetanus

Tetanus, although preventable by a highly effective vaccine, continues to cause 30 000–50 000 deaths annually. Global mortality has fallen substantially since the 1980s due to widespread vaccination efforts, yet adult disease persists, especially among those with weakened immune response, diabetes, and people who inject drugs. Diagnosis is still clinical, and management combines wound debridement, antibiotics, and antitoxin. However, key questions about prevention, diagnosis, and management remain unanswered. Recent trials suggest human and equine antitoxin perform equally, but shortages and high costs persist. Autonomic instability, once thought a late stage complication, is now defined early in the disease course, affecting the prognosis. Due to patients being in intensive care, complications such as nosocomial infections can increase the burden of the disease, reinforcing that vaccination, surveillance, equitable access, and new therapy options are vital.

Tetanus toxoid vaccine is nearly 100% effective at preventing tetanus, a severe and often fatal disease. A complete primary series of shots, followed by boosters every 10 years, provides long-lasting immunity. It is highly effective in preventing neonatal tetanus, reducing deaths by 95% in the last 30 years. 10-Year Booster Schedule: The Centers for Disease Control and Prevention (CDC) recommends that adults get a tetanus booster (Td or Tdap) every 10 years.

Incidence

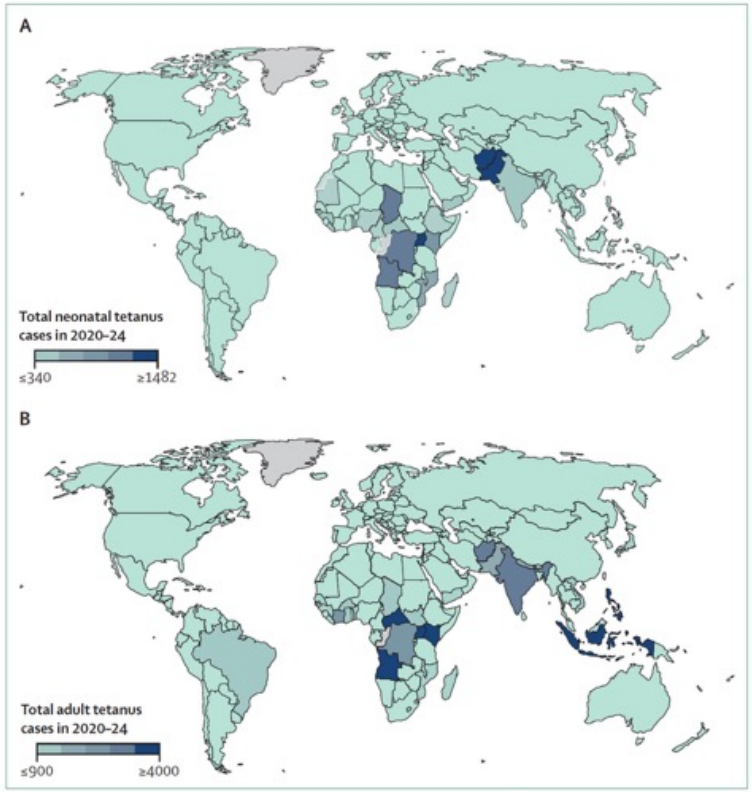

Figure 1: **Global incidence of adult and neonatal tetanus cases from 2020 to 2024**
Incidence rates are based on the total confirmed cases aggregated across 2020–24, expressed as neonatal cases per 1000 live births or total tetanus cases per 1 000 000 population (calculated with UN Department of Economic and Social Affairs World Population Prospects 2024 data[3]). Only reporting countries are included, so denominators vary. Data come from national authorities via the WHO/UNICEF Joint Reporting Form on Immunization[2] and may be affected by under-reporting and surveillance changes. Grey denotes no reported data available or countries with no tetanus surveillance systems.

Vaccine coverage

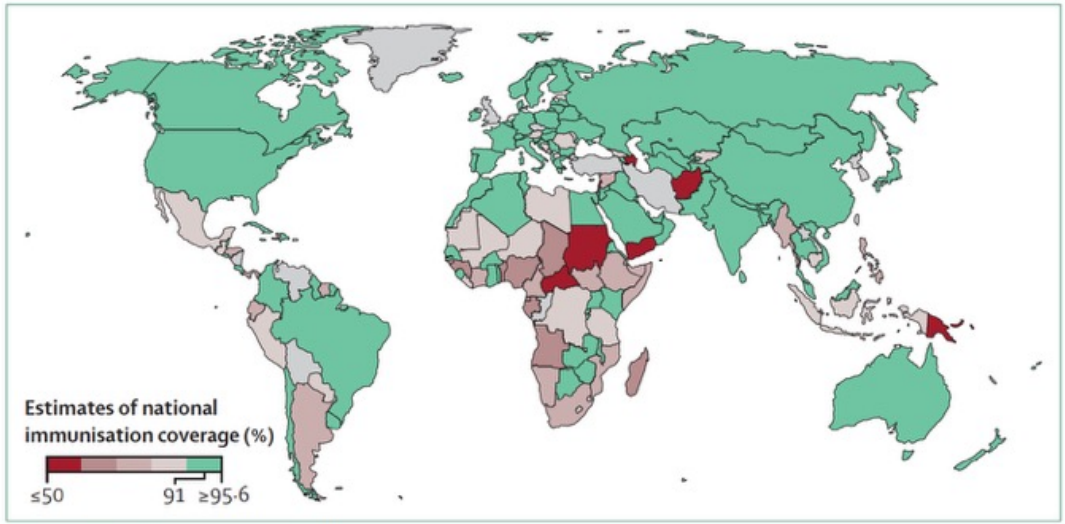

Figure 2: **DTPCV3 coverage globally in 2024**
Estimates of the percentage of infants receiving DTPCV3 in 2024. Grey countries indicate missing or non-reported data. Global and regional coverage uses WHO/UNICEF estimates of national immunisation coverage weighted by UN World Population Prospects target populations; see the official website for methods.[5] DTPCV3=three-dose diphtheria, tetanus toxoid, and pertussis vaccination.

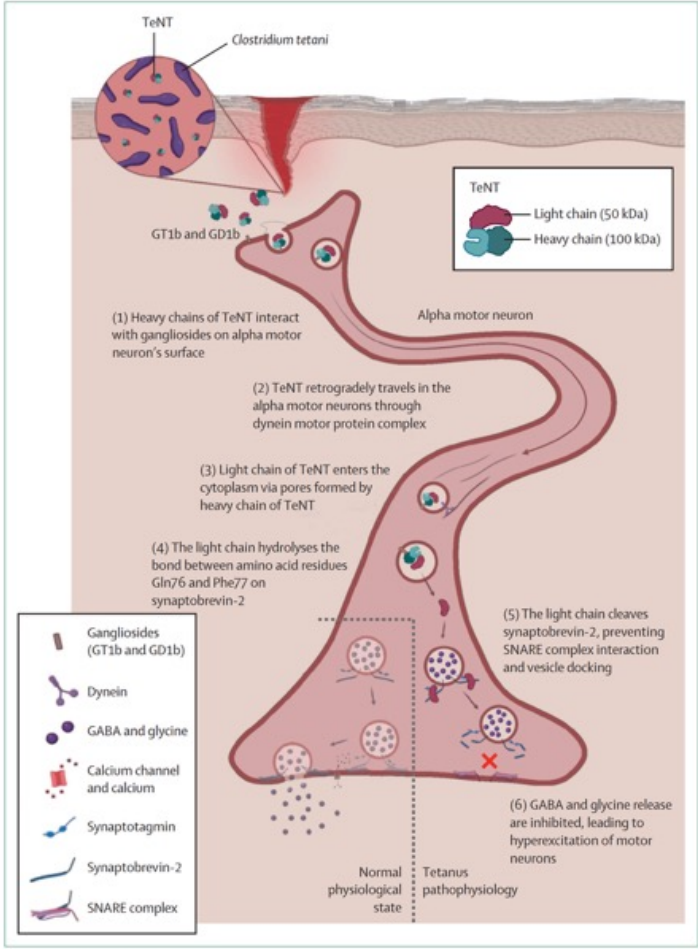

Figure 3: **Tetanus pathophysiology**
In the lower left part of the neuron, the normal physiology is depicted, where TeNT is not present, and vesicles containing neurotransmitters successfully dock and release inhibitory neurotransmitters, such as GABA and glycine, into the synaptic cleft. In the presence of TeNT this process is blocked. TeNT binds to gangliosides (GT1b and GD1b) on the cell surface, allowing entry. The heavy chain facilitates internalisation, while the light chain cleaves synaptobrevin-2, a key protein in the SNARE complex. This cleavage prevents vesicle docking, leading to a scarcity of inhibitory neurotransmitters in the synaptic cleft, which causes hyperexcitation of the following neuron and results in muscle rigidity and spasms. GABA=γ-aminobutyric-acid. TeNT=tetanus neurotoxin.

Differential diagnosis

	Clinical features		Diagnosis	
	Mimics tetanus	Uncommon in tetanus	Diagnostic tests	Clinical signs
Strychnine poisoning	Painful muscle spasms, opisthotonus, jaw tightness	Mydriasis, ocular proptosis, nystagmus, occurs more acutely than tetanus	Low serum calcium, thin-layer chromatography on gastric aspirate, and urine sample	History of illicit drug use within 8 h
Drug-induced dystonia	Muscle spasms, jaw stiffness, oromandibular dystonia, fever	Oculogyric crisis, spasmodic torticollis, twisting movements, spasms usually not painful	Discontinuation of medications, levodopa trial (if possible), imaging (MRI)	Change in the dose of first-generation antipsychotics, treatment with atypical antipsychotics, some antiemetics, lithium, stimulants, selective serotonin reuptake inhibitors, or tricyclic antidepressants
Malignant neuroleptic syndrome	Muscle rigidity, autonomic instability, fever, diaphoresis, less commonly trismus	Mental status change, stupor, automatisms, mutism, psychosis, catalepsy	None	Treatment with dopamine-receptor antagonist medications or rapid withdrawal of dopaminergic medications (within the past 1–4 weeks)
Stiff person syndrome	Painful muscle spasms, rigidity	Absence of trismus or facial spasms and rapid response to benzodiazepines, mydriasis, muscle spasms absent during sleep	EEG, anti-GAD or anti-GlyR antibodies in CSF (only highly positive), oligoclonal band might also be present in CSF	History of other autoimmune diseases
Progressive encephalomyelitis with rigidity and myoclonus (stiff person syndrome subtype)	Painful muscle spasms, muscle rigidity, dysphagia, myoclonus, hyperekplexia	Transient ocular flutter, eye movement paralysis, gaze paralysis, nystagmus and drooping eyelids, brainstem signs	EEG, anti-GAD or anti-GlyR antibodies in CSF, oligoclonal band might also be present in CSF	History of other autoimmune diseases
Hypocalcaemia	Muscle spasms, cramps, hyperexcitability	Perioral numbness, paraesthesia of the hands and feet	Low serum ionised calcium	Trousseau's and Chvostek's signs
Meningitis	Stiff neck, fever, photophobia, headache, trismus	Hypotonia, nausea, vomiting, disseminated rash	CSF culture, pleocytosis and leucocytosis in CSF	History taking, Kernig's sign, Brudzinski's sign
Black widow spider envenomation	Painful muscle cramping, autonomic dysfunction	Isolated diaphoresis around the port of bite, burning around the bite, vomiting, nausea, absence of trismus	Skin examination	Detailed history taking including port of entry, exposures, skin examination, response to anti-inflammatory medications and antihistamines
Dental abscess	Trismus, jaw stiffness, fever	Bad taste in the mouth, sensitivity to cold or hot food, erythema in the oral cavity, little symptom progression	Imaging (x-ray)	History of recent dental operation, poor oral hygiene
Cranial nerve palsies	Neck stiffness, dysphagia, trismus, drooping eyelids, weakened facial muscles	More than one cranial nerve can be affected at once	Detailed neurological examination, neuroimaging (primarily MRI and CT), and electrophysiological studies	Vascular risk factors (eg, diabetes, hypertension, hyperlipidaemia, coronary artery disease, previous stroke), sensory loss in the distribution of the affected nerve, and no history of recent wound, especially to the head or face
Stroke	Facial muscle weakness, dysarthria, dysphagia	Visual disturbances, numbness	Imaging (MRI or CT)	Lateralising findings, sensory deficits (eg, numbness, tingling) are more suggestive of stroke

CSF=cerebrospinal fluid. EEG=electroencephalogram. GAD=glutamic acid decarboxylase. GlyR=glycine receptors.

Table: **Differential diagnosis of tetanus**

Managing tetanus

***Panel*: Day-to-day management of tetanus: modified general outline for clinical practice[1]**

First presentation and admission

1 Patient suspected of tetanus: painful muscle spasms or muscle rigidity without a known explanation. Unexplained muscle weakness and cranial nerve palsies.
2 Ensure ventilation.
3 Complete the history about the port of entry, incubation period, period of onset, and immunisation.
4 Order the first laboratory tests in serum: complete blood count, electrolytes, blood urea nitrogen, creatinine, creatine kinase, C-reactive protein, and procalcitonin. In addition to these tests, uncommon symptom-tailored tests could be added accordingly (table). For instance, lumbar puncture if meningitis was suspected.
5 Use benzodiazepines intravenously to control spasms.
6 Place the patient in a quiet, darkened area in the intensive care unit.

First day of treatment

1 Administer 500 IU human tetanus immunoglobulin intramuscularly; if not available use equine tetanus immunoglobulin.
2 Administer adsorbed tetanus toxoid such as tetanus-diphtheria vaccine (0·5 mL) or diphtheria, tetanus toxoid, and pertussis vaccine (0·5 mL), intramuscularly.
3 Begin metronidazole, 500 mg intravenously every 6 h, for 10 days.
4 Debride the wound, if necessary.
5 Feed by a soft, small-bore nasal tube or a central venous catheter.
6 Adjust benzodiazepine dose to control spasms and produce sedation.
7 Initiate bedside physical therapy.

During hospitalisation

1 Treat sympathetic hyperactivity with magnesium sulfate or labetalol.
2 Control blood pressure. Place a pulmonary artery catheter and an arterial line, and administer fluids, dopamine, or norepinephrine as indicated.
3 Begin prophylactic heparin.
4 If the severity of spasms has diminished substantially, taper the benzodiazepine dose over 14–21 days.

Discharge and follow-up

1 When spasms are no longer present, begin physical therapy as early as possible.
2 Many patients require supportive psychotherapy.
3 Before discharge, administer another dose of tetanus-diphtheria vaccine or diphtheria-pertussis-tetanus vaccine.
4 Schedule a third dose of tetanus toxoid vaccine to be given 4 weeks after the second.

Conclusion

Tetanus remains a substantial global health concern, despite being a preventable disease. Effective vaccination programmes have drastically reduced its incidence in high-income countries, but it continues to pose a threat in regions with low access to health care, medical equipment including mechanical ventilators, and medications, especially among unvaccinated populations. Although the tetanus vaccine is highly effective, some tetanus cases have been reported in individuals who have completed the full course of vaccination. Cases of tetanus have been reported in vaccinated individuals due to waning immunity or other immunodeficiencies, underscoring the need for booster doses throughout adulthood to maintain immunity.[41] The challenges of neonatal and maternal tetanus in low-resource settings further emphasise the critical need for sustained immunisation efforts, improved access to care, and targeted public health interventions. Continued research into advanced treatment methods and vaccine development is essential to further reduce the burden of this life-threatening disease.

L-Carnitin ist eine körpereigene, aus Aminosäuren (Lysin, Methionin) hergestellte Verbindung, die als entscheidender Transporter langkettiger Fettsäuren in die Mitochondrien fungiert, um diese zu Energie zu verbrennen. Es wird vorwiegend zur Fettverbrennungsoptimierung, Leistungssteigerung im Sport und zur Linderung von Erschöpfungssyndromen eingesetzt. Eine Supplementierung (meist 500–3000 mg) kann besonders für Vegetarier/Veganer sinnvoll sein.

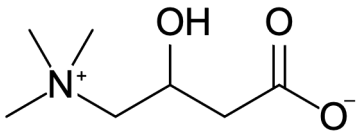

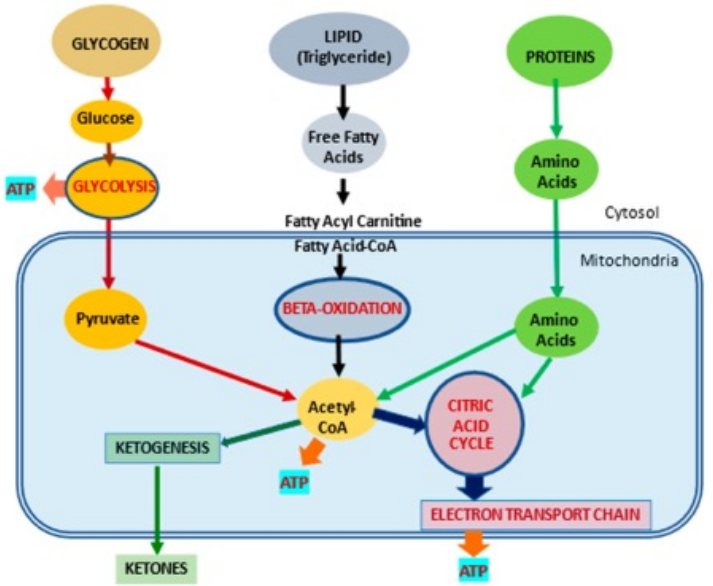

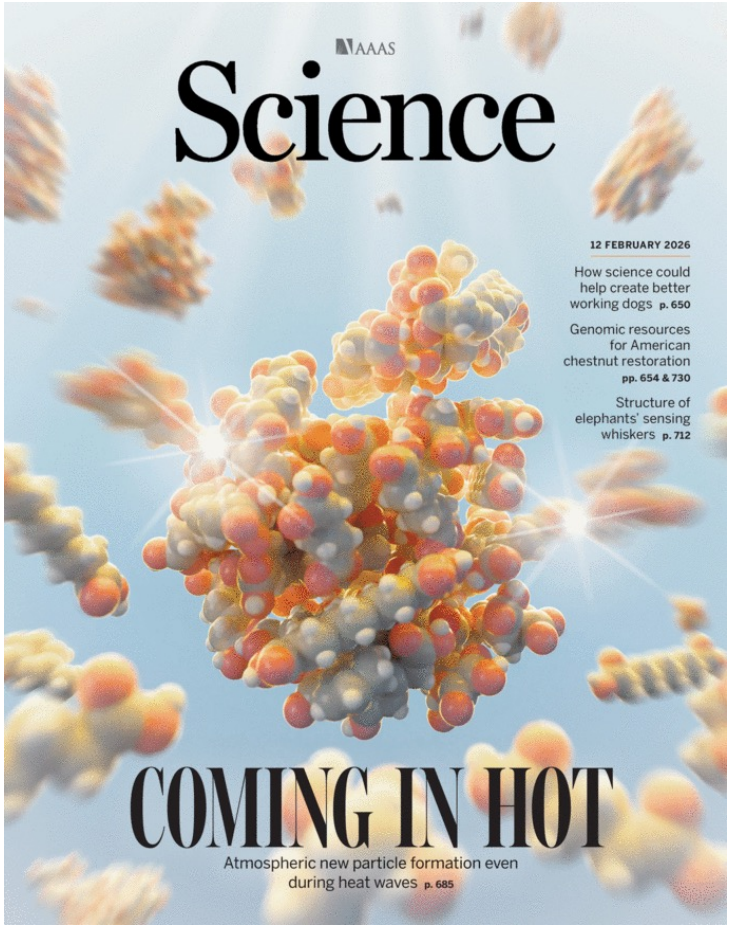

The bottleneck of fat burning

A mitochondrial transport protein promotes carnitine synthesis in mice when fat consumption is needed

L-Carnitine (the form of carnitine found in animals) transports long-chain fatty acids into mitochondria, where they go through b-oxidation, producing energy. This process occurs primarily in organs that use fat as energy, such as cardiac and skeletal muscles. For humans who eat meat, most carnitine is obtained from food. However, ~25% of the supply of carnitine in omnivorous humans relies on de novo synthesis, which reaches >90% among strict vegetarians or vegans. Endogenous carnitine is synthesized in the liver and kidneys from two methylated amino acids, lysine and methionine. This requires the transfer of trimethyllysine from the cytosol to the mitochondrial matrix (the innermost part of the mitochondria), for conversion into hydroxytrimethyllysine. Auger et al. report that a mitochondrial trimethyllysine transporter, SLC25A45, has a key role in fat consumption in mice. SLC25A45 is a member of the solute carrier 25 (SLC25) family of mitochondrial transporters. These proteins carry a variety of molecules—such as precursors for the synthesis of macromolecules, or metabolites for oxidative degradation and production of energy—between the cytosol and the mitochondrial matrix.

Auger et al. observed that in mice, SLC25A45 was required for de novo carnitine synthesis in response to fasting, which causes a switch between glucose (sugar) consumption and fat oxidation as an energy source (see the figure). The authors also uncovered a previously unknown role for SLC25A45 in lipid metabolism. They demonstrated that cold exposure, which boosts energy dissipation by burning fat to produce heat, increases the expression of SLC25A45 in the liver. When exposed to a low temperature (6°C), mice genetically engineered to lack the gene encoding SLC25A45 could not maintain their body temperature. However, exogenous carnitine supplements given to these mice before cold exposure prevented this effect. Furthermore, SLC25A45-deficient mice had low concentrations of several acylcarnitines in blood. In mammals, acylcarnitines are normally produced by the liver upon cold exposure and serve as fuel for heat production in brown adipose tissue. The findings of Auger et al. indicate that liver carnitine acts as a bottleneck for mobilization of fat from adipose tissues for multiple uses as an energy source.

Carnitine metabolism

In the liver and kidneys of mammals, the carrier SLC25A45 transfers TML into the mitochondrial matrix, where it is converted to HTML. In the cytosol, several enzymatic steps lead to the production of carnitine, which is released into the blood stream. Omnivorous animals obtain ~25% of their carnitine through this process, with 75% coming from their diet. When extra energy is needed or glucose availability is limited, fatty acids from adipose tissue are broken down in mitochondria through ß-oxidation, producing energy in the form of ATP and heat. Carnitine facilitates the transport of fatty acids into the mitochondria in the form of acyl-CoA. Cold exposure, fasting, physical exercise, or intake of GLP-1 receptor agonists create a need for more energy and stimulate the de novo synthesis of carnitine.

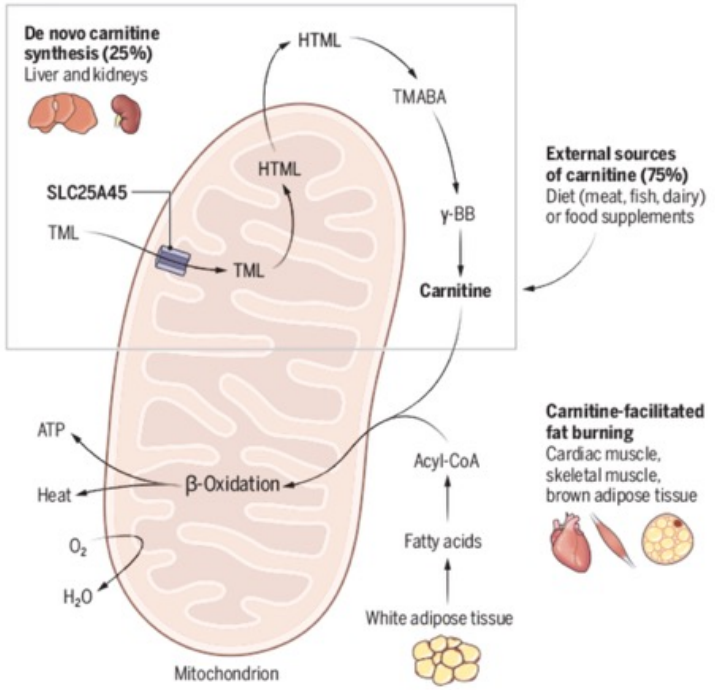

Acyl-CoA, acyl-coenzime A; ATP, adenosine triphosphate; γ-BB, trimethylammoniobutanoic acid, or γ-butyrobetaine; GLP-1, glucagon-like peptide-1; HTML, hydroxytrimethyllysine; TMABA, trimethylaminobutyraldehyde; TML, trimethyllysine.

Agonists for the receptor of glucagon-like peptide-1 (GLP-1), such as semaglutide, have been successfully used in patients with type 2 diabetes to achieve weight loss and combat obesity. To promote fat mobilization and expenditure, Auger et al. treated SLC25A45-deficient and control mice with semaglutide. In the absence of SLC25A45, the GLP-1 receptor agonist failed to induce weight loss. However, the effect of semaglutide was re-stored by the administration of exogenous carnitine, with no impact on food intake or blood glucose concentrations. These results indicate that the GLP-1 receptor agonist and carnitine act in combination to stimulate fat consumption.

Although the study of GLP-1 receptor agonists in the treatment of obesity has advanced substantially over the past decade, the reasons why individual responses to treatment vary are still poorly understood. The study of Auger et al. opens the route to investigating how the carnitine pathway could be modulated as part of antiobesity treatments involving GLP-1 receptor agonists. Dietary supplements of carnitine might support fat consumption in these cases, especially when the availability of carnitine (from endogenous or dietary sources) is limited. Such approaches could also be especially relevant in strict vegetarian or vegan patients, who rely mostly or solely on carnitine produced by de novo synthesis.

The identification of SLC25A45's ligand shows that de novo synthesis of carnitine is required for fat burning. Furthermore, the discovery that SLC25A45 has a role in the physiological adaptation of mice to increased fat consumption and energy expenditure raises new research questions, such as how this pathway is modulated by long-term fasting, intermediate feeding, physical exercise, or hormonal responses.

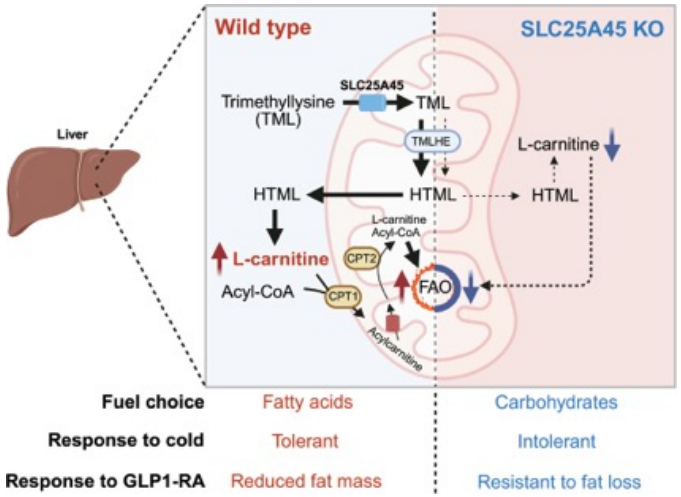

Sarah Schleper is 46 and in her seventh Olympics. Who's here with her? Her son.

The Mexican skier who used to compete for the United States is racing in Cortina while her son Lasse Gaxiola is skiing five hours away in Bormio.

CORTINA d'AMPEZZO, Italy — Here is Sarah Schleper's Olympics of logistics: ski in Thursday's women's super-G here, then tune her own skis for Sunday's giant slalom. She will, God willing, finish both runs of that race, pop off her ski boots, and hop in the car of a sponsor to begin the five-and-a-half-hour drive around the Dolomites to Bormio, the ski resort where the men's Alpine competition is being staged in these sprawling Milan Cortina Games.

"I'm thankful that my body's in good shape, that I can do it," Schleper said.

She was smiling. It was more than an hour after the super-G — in which she finished 26th of the 26 athletes who didn't wipe out — ended. The crowd had thinned. The Italian anthem — for champion Federica Brignone — had played. A majestic flyover of jets streaming smoke in the colors of the Italian flag — red, white and green — had long since roared into the mountains.

Sarah Schleper, who traveled with her son Lasse, competed for the United States with Julia Mancuso (left) and Lindsey Vonn (right) until she got her dual Mexican citizenship in 2014. (Giovanni Auletta/AP)

Schleper skied through the 2010 Vancouver Games — where Lindsey Vonn and Julia Mancuso shined for the U.S. women — and finished 16th in slalom and 14th in giant slalom. She completed the next World Cup season. When it was over — when she knew she was retiring from the U.S. ski team — she scooped up Lasse and skied with him down a slalom course.

From that moment, to this one?

“I never thought, ‘Oh, I want my kid to race the Olympics with me,’ ” Schleper said. “Once you set yourself on a trajectory, I think the universe lines up to make your life and your path — if you have a lot of passion — more spectacular than you can ever imagine.”

Lasse Gaxiola is representing Mexico and skiing in the men's giant slalom and the men's slalom. (Denis Balibouse/Reuters)

"I've been saying a bunch that I'm just very grateful to be able to give something back to her for showing me this wonderful sport and how to ski and being such an amazing mother," Lasse said on a podcast produced by the International Ski Federation. "And I feel very grateful to her for being able to show me how to ski — and how to ski fast, especially."

So they're doing it. But not without some difficulty. Federico, who serves as Schleper's coach, is instead in Bormio with Lasse. (In that sense, it's a shame that these Olympics have separate sites — separated by a mountain range and many hours — for male and female racers.) That leaves Schleper to tune her own skis, and Schleper to watch Lasse from afar.

That will happen first in Saturday's men's giant slalom in Bormio. That will be followed by Schleper's appearance in Sunday's giant slalom here. And then — the jump in the car, and the jet across Italy to catch Lasse in the men's slalom on Monday. In person.